



HOST UNIVERSITY: GHENT UNIVERSITY

FACULTY OF ENGINEERING AND ARCHITECTURE

DEPARTMENT OF STRUCTURAL ENGINEERING

Academic Year 2020-2021

STRATIFICATION AND BACK-LAYERING MODELLING FOR LONGITUDINAL VENTILATED TUNNELS

Ir. Arthur Rohaert

Supervisors: Prof. Dr. Ir. Bart Merci & Prof. Dr. Ir. Ruben Van Coile

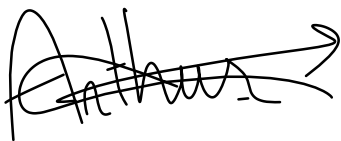
Master thesis submitted in the Erasmus+ Study Program:

International Master of Science in Fire Safety Engineering

Disclaimer

This thesis is submitted in partial fulfilment of the requirements for the degree of *The International Master of Science in Fire Safety Engineering (IMFSE)*. This thesis has never been submitted for any degree or examination to any other University/program. The author declares that this thesis is original work except where stated. This declaration constitutes an assertion that full and accurate references and citations have been included for all material, directly included, and indirectly contributing to the thesis. The author gives permission to make this master thesis available for consultation and to copy parts of this master thesis for personal use. In the case of any other use, the limitations of the copyright must be respected, in particular regarding the obligation to state expressly the source when quoting results from this master thesis. The thesis supervisor must be informed when data or results are used.

Read and approved,

A handwritten signature in black ink, appearing to read 'Arthur Rohaert', with a long horizontal stroke extending to the right.

Arthur Rohaert

Monday the 10th of May 2021

STRATIFICATION AND BACK-LAYERING MODELLING FOR LONGITUDINAL VENTILATED TUNNELS

Word count, body: 17.973

Word count, total: 26.393

Arthur Rohaert

Promotor: Prof. Dr. Ir. Bart Merci

Co-promotor: Prof. Dr. Ir. Ruben Van Coile

Industrial Supervisor: Dr. Ir. Matteo Pachera

Faculty of Engineering and Architecture
Department of Structural Engineering and Building Materials
Research Group of Fire Safety Science and Engineering

Dissertation submitted to Ghent University in partial fulfilment of the requirements for the degree of
Master in Fire Safety Engineering

Academic year: 2020 – 2021



ABSTRACT (EN)

Fires in tunnels can have severe consequences. Examples are the BAKU metro tunnel fire of 1995 (289 fatalities and 265 injuries), the Mont Blanc road tunnel fire of 1999 (all 39 occupants died) and the Daegu subway tunnel fire of 2003 (over 192 fatalities) [1]. Life safety is not naturally guaranteed in tunnels, neither is structural stability or traffic continuation. Therefore, a comprehensive risk assessment of existing and new designs is indispensable. Such a risk assessment requires a reasonably fast and accurate smoke behaviour model. One-dimensional, one-layer models provide fast simulations but are not able to predict stratification or back-layering phenomena.

A model is developed in Python 3.9. It considers the separation of a hot smoke layer and a cold fresh air layer. Analogue to the two-zone models for enclosures, it employs a plume correlation. In addition, a velocity correlation is used to simplify the fluid dynamics. Unlike simple empirical correlations, the model is not only able to predict the back-layering length, but also the temperature, velocity, and thickness profiles of the smoke layer. The model considers the tunnel's geometry, applied ventilation strategies and fire parameters. Moreover, it can be elaborated to consider changing cross-sections, slopes, thermal material properties, entrainment... Unlike complex three-dimensional CFD calculations, the results are obtained almost instantaneously.

The outcome of the simulations (critical velocity, temperature profiles and back-layering length) is compared to simple (semi-) empirical correlations and to small-scale and large-scale experimental data. In general, a satisfactory agreement is found. For high heat release rates, causing temperature rises above 1350 K, the model loses accuracy and requires further research. The effect of the deflected back-layering flow on the flow, downstream of the fire, also necessitates additional investigation.

Keywords: Tunnel fire safety • Smoke behaviour • Stratification • Back-layering • Critical velocity • Longitudinal ventilation • One-dimensional model • two-layer model

ABSTRACT (NL)

Branden in tunnels kunnen ernstige gevolgen hebben. Voorbeelden zijn de brand in de metrotunnel van Baku in 1995 (289 doden en 265 gewonden), de brand in de Mont Blanc-tunnel van 1999 (alle 39 aanwezigen stierven) en de brand in de metrotunnel van Daegu in 2003 (meer dan 192 doden) [1]. In tunnels is de levensveiligheid tijdens brand niet vanzelfsprekend en evenmin is de structurele stabiliteit of de verkeerscontinuïteit. Bijgevolg is een uitgebreide risicobeoordeling van bestaande en nieuwe ontwerpen onmisbaar. Een alomvattende risicobeoordeling vereist een schappelijk snel en nauwkeurig rookmodel. Eendimensionale modellen die één laag veronderstellen, verschaffen snelle simulaties maar zijn niet in staat om stratificatie of *backlayering* te voorspellen.

In dit rapport wordt een model voorgesteld (geschreven in Python 3.9) dat rekening houdt met de scheiding van een warme rooklaag en een koude luchtlaag. Analoog aan het twee-zones-model voor omsloten ruimtes, hanteert het model een rookpluim correlatie. Bovendien wordt een correlatie gebruikt voor de snelheid van de rooklaag om zo de berekeningen te vereenvoudigen. In tegenstelling tot eenvoudige empirische correlaties, kan het model niet alleen de lengte van de rooklaag voorspellen, maar ook het temperatuur-, snelheid- en hoogteprofiel van de rooklaag. Het model houdt rekening met de geometrie van de tunnel, toegepaste ventilatiestrategieën en brandparameters. Bovendien kan het worden uitgebreid om rekening te houden met wisselende dwarsdoorsneden, hellingen, thermische materiaaleigenschappen, vermenging... Anders dan de complexe driedimensionale CFD-berekeningen, worden de resultaten bijna ogenblikkelijk verkregen.

De uitkomst van de simulaties (kritische snelheid, temperatuurprofielen en de *backlayering* lengte) wordt vergeleken met eenvoudige (semi-) empirische correlaties en met data van kleinschalige en grootschalige experimenten. Over het algemeen wordt een bevredigende overeenkomst gevonden. Bij hoge warmteafgiftesnelheden, met temperatuurstijgingen van meer dan 1350 K, is het model minder nauwkeurig en vereist het verder onderzoek. Het effect van de terugkerende *backlayering* laag op de rooklaag stroomafwaards van de brand, behoeft ook nog bijkomend onderzoek.

Slutelwoorden: Tunnelbrandveiligheid • rookgedrag • stratificatie • *backlayering* • Kritische snelheid • Longitudinale ventilatie • eendimensionaal model • tweelagenmodel

ACKNOWLEDGEMENTS

I would like to thank several people for their help and support in the realization of this dissertation. Firstly, I wish to thank my promoters, Prof. Dr. Ir. Bart Merci and Prof. Dr. Ir. Ruben Van Coile. This thesis research allowed me to apply the knowledge and skills that I acquired over the last years, in an integral manner. I would especially like to thank my supervisor Dr. Ir. Matteo Pachera for the individual supervision and his sincere involvement. Without his persistent and constructive feedback, I would never have been able to present this dissertation in its current form.

Finally, I would also like to thank my family and friends. Thank you for the nice evenings that gave me the necessary courage to continue working the next day. Thanks for the entertainment, affinity, and support. Above all, I would like to thank Lucas for amusing me during the last months and for being there for me at any time of the day.

Arthur Rohaert

TABLE OF CONTENT

Abstract (EN)	I
Abstract (NL)	II
Acknowledgements	III
Table of Content	IV
List of Figures	V
List of Tables	V
List of symbols	V
1 Introduction	1
1.1 Problem statement.....	1
1.2 Existing risk assessment methods.....	2
1.3 Objective	5
1.4 Structure of the report.....	6
2 Stratification and back-layering	7
2.1 Introduction in stratification	7
2.2 Existing stratification predictions techniques	7
2.3 Introduction to back-layering.....	9
2.4 Existing critical velocity prediction techniques	10
2.5 Existing back-layering predictions techniques	12
3 One-dimensional models	15
3.1 Concept of one-dimensional models	15
3.2 Conservation equations for the one-layer model.....	15
3.3 Conservation equations for the two-layer model	16
3.4 Existing one-dimensional models	18
4 Methodology	19
4.1 Concept of the proposed model.....	19
4.2 Plume mass flow.....	21
4.3 Upstream and downstream distribution of the mass flow	24
4.4 Smoke propagation velocity.....	26
4.5 Heat loss rates	31
4.6 Solution schemes.....	32
5 Discussion of the results	36
5.1 Critical velocity	36
5.2 Flow profiles.....	39
5.3 Level of stratification	41
5.4 Back-layering length	42
5.5 Effective height and total height.....	45
5.6 Calculation time	45
6 Conclusion	47
References	49
Appendix A: Derivatives of the plume mass flows	55
Appendix B: Temperatures profiles downstream	56
Appendix C: Code of the proposed model	59
"" SEAT OF THE FIRE ""	59
"" UPSTREAM FLOW ""	63
"" DOWNSTREAM FLOW ""	65
"" RESULTS AND CURVES ""	66

LIST OF FIGURES

Figure 1: Tunnel meters for some countries (left) and human loss in tunnel fire incidents in Europe (right) [11].....	1
Figure 2: One-dimensional models assuming one layer (above) and two layers (below)	5
Figure 3: Stratification regions for a tunnel with a ventilation flow that moves to the right, redrawn from [35].	7
Figure 4: Illustration of the critical ventilation velocity its effect on back-layering	10
Figure 5: Critical velocity predictions for a six-meter-high and twelve-meter-wide tunnel.....	12
Figure 6: Back-layering length predictions for a fire of 5 MW in a six-meter-high and twelve-meter-wide tunnel. .	13
Figure 7: Schematic representation of the two-layer model.....	17
Figure 8: Flowchart of the proposed methodology.....	20
Figure 9: Comparison of different plume mass flow correlations	23
Figure 10: Total mass flow rate and upstream mass flow rate for different distributions	24
Figure 11: Back-layering length, employing different mass flow rate distributions.....	25
Figure 12: Lock-exchange problem	28
Figure 13: Modified lock-exchange problem with the low-density fluid released from a partial depth.....	29
Figure 14: The smoke propagation velocity as a function of the hot gas layer temperature	31
Figure 15: Radiative and convective heat transfer among two different perimeters	32
Figure 16: Mass flow at the seat of the fire	33
Figure 17: Heat balance of cell P0.....	34
Figure 18: Critical velocity as a function of the total heat release rate for EX1	36
Figure 19: Smoke layer height and plume mass flow rate in function of the heat release rate (EX1)	37
Figure 20: Dimensionless critical velocity, presented with experimental data from Li, Lei & Ingason [45].....	38
Figure 21: Sensitivity of the critical velocity for EX1 and EX2.....	38
Figure 22: Temperature, height, and velocity profiles of the smoke layer of EX1	39
Figure 23: Temperature, height, and velocity profiles of the smoke layer of EX2	40
Figure 24: Comparison between the constant heat loss coefficient and the proposed model (for EX1 and EX2) .	41
Figure 25: Downstream temperature profile for EX1, with a ventilation velocity of 1.5 m/s.	41
Figure 26: Back-layering length as a function of the ventilation velocity for EX1 ($Q = 5 MW$)	42
Figure 27: Back-layering length as a function of the ventilation velocity for EX2 ($Q = 60 MW$).....	43
Figure 28: Back-layering length as a function of the heat release rate, for EX1 ($u_0 = 1.5m/s$).....	44
Figure 29: Dimensionless back-layering length as a function of the dimensionless confinement velocity	44
Figure 30: Sensitivity of the back-layering length for EX1 and EX2.....	45
Figure 31: Calculation time in function of the simulated length for examples EX1 and EX2.....	46
Figure 32: Downstream temperature profile for EX1 with subcritical and supercritical ventilation flows	56
Figure 33: Downstream temperature profile for EX2 with subcritical and supercritical ventilation flows	57
Figure 34: Different assumption regarding the downstream mass flow rate and temperature	57
Figure 35: Corrected downstream temperature profile for EX1, considering the deflected back-layering flow	58
Figure 36: Corrected downstream temperature profile for EX2, considering the deflected back-layering flow	58

LIST OF TABLES

Table 1: Overview of the European risk assessment methods for tunnel fires, adopted from Ntzeremes et al. [11]	2
Table 2: Different Froude numbers as a limit of stratification region.....	9
Table 3: Parameters and values for the example problems EX1 and EX2	11
Table 4: Overview of one-dimensional models of tunnel fires.....	18
Table 5: Overview of different smoke propagation correlations	30
Table 6: Position of destratification (region RII) for EX1	42

LIST OF SYMBOLS

A	cross-section of the tunnel [m ²]
b_f	(virtual) radius of the seat of the fire
c	specific heat capacity of a solid material [kW/kg/K]
C_k	correction factor [-]
c_p	specific heat capacity of a gas under constant pressure [kW/kg/K]
d	smoke layer thickness [m]
$E_{gra}, \Delta E_{gra}$	gravitational potential energy, gain in gravitational potential energy [J]
$E_{kin}, \Delta E_{kin}$	kinetic energy, gain in kinetic energy [J]
Fr	Froude number [-]

g	gravitational constant [= 9.81 m/s ²]
H, H_{eff}	tunnel height [m], effective height of the tunnel, $H - h_f$, [m]
\bar{H}	hydraulic diameter of tunnel [m]
H_f	height of the flames [m]
h_c	convective heat loss coefficient [kW/m ² /K]
h_f	height of the seat of the fire [m]
h_t	total heat loss coefficient [kW/m ² /K]
K	momentum [kg·m/s]
k	velocity factor for the smoke propagation correlations [-]
L_b, L_s	back-layering length [m], length of stable stratification [m]
M	molar weight of air or of smoke [= 0.02897 kg/mol]
m	mass [kg]
Nu	Nusselt number
P	perimeter of the tunnel [m]
p	pressure [Pa] or ambient pressure [= 101325 Pa]
Pr	Prandtl number [-]
q, Q	heat release or heat transfer [kJ]
R	ideal gas constant [= 8.314472 J/K/mol]
Ri	Richard number [-]
Re	Reynolds number [-]
$T, \Delta T$	temperature, temperature rise [K]
t	time [s]
u	longitudinal velocity [m/s]
u_{ent}	entrainment velocity [m/s]
V^*	dimensionless ventilation velocity [-]
W	width of a rectangular tunnel [m]
w^*	characteristic plume velocity [m/s]
y	mass concentration of a species [-]
Y	mass of specie [kg]
z, z_{eff}	height [m], effective height [m]
$\alpha_1, \alpha_2, \beta$	entrainment factors [-]
γ, ϵ	parameters of the back-layering length correlation by Hu, Huo and Chow (2008) [-]
δ	upstream mass flow rate ratio, $\dot{m}_{up}/\dot{m}_{pl}$, [-]
ϵ	emissivity of a material surface [-]
λ	thermal conductivity [kW/m/K]
λ_t	friction loss coefficient [-]
ρ	density [kg/m ³]
σ	Stefan-Boltzmann constant [= 5.67·10 ⁻⁸ Wm ⁻² K ⁻⁴]
φ	section ratio, W/H [-]

Superscript

\dot{x}	parameter per unit time [original unit/s]
x', x''	parameter per unit length or unit surface [original unit/m, original unit/m ²]
x^*	dimensionless parameter [-]

Subscript

x_0	property of the ambient environment or the main flow before interaction with the fire
x_a, x_c	property of the (cold) air layer flow
x_{cr}	critical value of the parameter x
x_f	property directly downstream of the seat of the fire
x_h, x_s	property of the (hot) smoke layer flow
x_{pl}	property of the smoke plume
x_r	property of the (hot) smoke layer flow, relative to the (cold) air layer flow
x_w	property of the wall surface

1 INTRODUCTION

In this chapter, the problem statement is given, followed by a summary of existing risk assessment methods. Next, the objective of this dissertation is discussed, as well as the structure of the rest of this report.

1.1 Problem statement

Tunnel fire safety has been a growing concern over the last decades. The first reason is the increasing amount of tunnel constructions and their complexity. This can be seen in [Figure 1](#), which shows the tunnel meters for some member state of the European Union. Moreover, in the list of the ten longest road tunnels, eight have been finished after the turn of the century [2]. The same statement is valid for the list of railway tunnels and the list of continuous metro tunnels [2]. The second reason is a change in traffic. Traffic is becoming denser: in tunnels like the Mt Blanc Tunnel (1965) and the St Gotthard Tunnel (1981), the traffic flow has doubled in less than twenty years [3]. Moreover, the properties of the vehicles are changing. The use of plastic components has increased to an average of 150 kg per new passenger car in 2016 and continue to increase in a steady linear manner with about 3 kg every year [4]. These plastic components have a major contribution to the heat release rate of passenger cars in a fire. Moreover, the new energy carriers require special attention. In 2020, cars that use gasoline and diesel still make up 96% of all passenger cars in Belgium. However, due to environmental awareness and political support, the share of electric cars will increase significantly during the lifetime of new tunnels. In five years, all new company cars in Belgium will be electric [5]. Those company cars make up one-fifth of the passenger car fleet [6]. Other European countries plan to prohibit the sale of new fossil fuel cars entirely in the next two decades [7].

As a consequence of those trends, tunnel fire safety requires more attention. Although traffic accidents occur less frequently in road tunnels than on the open road, the consequences of a fire can be far more serious. Carvel and Marlair grounded this statement with a long list of accidents [1]. [Figure 1](#) shows the human losses in tunnel fire incidents in the European Union in a more concise manner. The lists and figures prove that life safety is not naturally guaranteed in tunnels, but neither is property protection or traffic continuity. This is well illustrated by the Mt Blanc tunnel fire of 1999, as it took three years before the tunnel could reopen [8] at a direct construction cost of approximately 206 million EUR [9].

The same insight came to the European Economic Community (EEC), which published the Directive 2004/54/EC on minimum safety requirements for tunnels in the Trans-European Road Network (TERN) [10]. Among other things, the EEC stated that a comprehensive risk assessment is required.

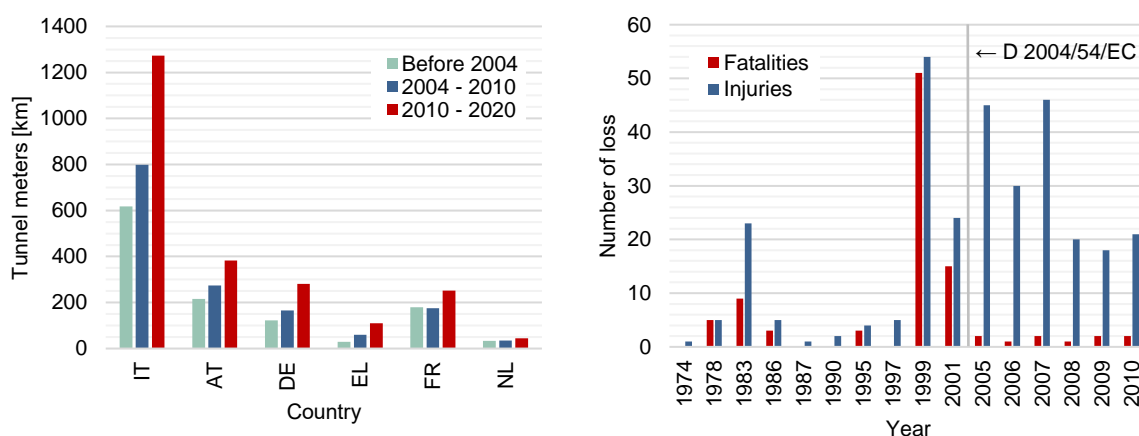


Figure 1: Tunnel meters for some countries (left) and human loss in tunnel fire incidents in Europe (right) [11]. The graphs are redrawn from Ntzeremes and Kirytopoulos [11] who used data from NTUA [12].

Nevertheless, no assessment framework has been developed in Belgium yet. Due to the current and future projects, such as the construction of the *Oosterweel verbinding* and the renovation of multiple TERN tunnels like the *Liefkenshoek tunnel*, Fire Engineered Solution Ghent (FESG) started to develop such a risk analysis framework [13].

1.2 Existing risk assessment methods

According to article 13 of Directive 2004/54/EC, a risk analysis is required at the design phase of new tunnels and the renewal of safety documentation of new and existing tunnels of the TERN (at least every six years). Every member state of the European Union has to ensure that a clearly described methodology is followed corresponding to the best practices known [10]. However, multiple authors like Beard [14], Ntzeremes and Kirytopoulos [11], [15], [16] and Bjelland [17] state that current assessment methods are not considering the knowledge available in literature sufficiently.

An evaluation of the tunnel risk assessment methods has been published by Ntzeremes and Kirytopoulos in 2019 [11]. The methods discussed in this study are shown in Table 1.

Table 1: Overview of the European risk assessment methods for tunnel fires, adopted from Ntzeremes et al. [11]

Member state	Name of the model	Type of risk approach	Type of transport	Type of method	Year of publication
Austria	TuRisMo	System-based	Non-dangerous goods	Quantitative	2007
	OECD/PIARC QRA	System-based	Dangerous goods	Quantitative	2007
France	SHI	Scenario-based	Non-dangerous goods	Quantitative	2003
	OECD/PIARC QRA	System-based	Dangerous goods	Quantitative	2005
Germany	BASt	Scenario-based	Non-dangerous goods	Quantitative	2010
	OECD/PIARC QRA	System-based	Dangerous goods	Quantitative	2006
Greece	SAM	Scenario-based	Non-dangerous goods	Quantitative	2011
	OECD/PIARC QRA	System-based	Dangerous goods	Quantitative	2011
The Netherlands	DSA	Scenario-based	Non-dangerous goods	Qualitative	2008
	RWS	System-based	Dangerous goods	Quantitative	2008
Italy	IRA	System-based	Both types of goods	Quantitative	2009

Some of the findings of the article are listed here:

- All methods treat the system parameters as deterministic values. None of them deals with the uncertainties of these input parameters, which do influence the obtained safety of the design.
- To determine the possible accident rate, all methods use statistical data. Most methods do not allow to take into account important aspects of the tunnel design (such as length, curvature, lightning...) to determine an accurate and specific accident rate. The same is true for preventive measures (such as imposed maximum speed, minimum distance...). Therefore, the methods do not facilitate to trade off preventive and mitigating measures, which is essential for an efficient risk reduction.
- The different methods lead to very different outcomes since they assume different scenarios and different standard fire behaviour. The obtained level of safety is very sensitive to some assumptions, among which the heat release rate curve. Moreover, some methods have sets of scenarios that fail to represent the complete risk properly.
- With exception of the SHI method and the SAM method, no information is given about the evacuation speed and its relation to the smoke concentration. Only the SAM method employs the principle of fractional effective dose.
- None of the methods can take into account the effect of FFFS. Although those systems are not common in Europe, they have shown some potential safety benefits in other countries, like Japan.
- The ease of use, the reliability and the cost of safety measures are not considered in any method.

It should be noted that some of the conclusions, made by the authors, do not consider the newest versions of the risk assessment methods. For instance, in the Netherlands, an update has been performed seven years before the release of this paper which replaces the two old methods. The intake of smoke gasses to determine the evacuation velocity and incapacitation are now considered [18]. The same is true for TuRisMo, which was updated five years before the release of this overview [19].

The World Road Association has reported on the 'Current Practice For Risk Evaluation For Road Tunnels' in 2013 [20], which can be consulted for a more extensive description. Unsurprisingly, some of the discussed models have been updated since this report.

In the following subsections, some methods are discussed in more detail.

TuRisMo

TuRisMo is the Austrian Tunnel Risk Model, which was published in 2008 as a response to the Directive 2004/54/EC and updated six years later. The model consists of a frequency analysis and a consequence analysis. [21]

The frequency analysis applies event trees to identify a set of characteristic incident scenarios (collisions and fires) and to calculate their frequencies. The consequence analysis consists of two parts: one for the direct consequences of a collision and one for the consequences of a fire. The collision consequence model provides standardized damage impacts for different collision categories based on a statistical study. The categories distinguish between bidirectional and unidirectional tunnels, single vehicle, rear-end and front-end collisions and different types of vehicles involved. [22]

For the fire consequence model, a standard or detailed model can be chosen. For the standard model, the damage impacts are included from premade calculations with standard tunnels. The values are only a valid approximation for a certain range of tunnels [22] but are obtained instantaneously. The extensive calculations for the detailed multi-scale model could be summarized in three main steps, performed for each scenario [19]:

- a one-dimensional flow simulation (in SPRINT)
- a three-dimensional CFD simulation (in FDS), using boundary conditions from SPRINT
- a one-dimensional evacuation simulation (in ODEM) is performed for each scenario

The evacuation simulation is one-dimensional in the sense that possible obstacles are not considered and that the travel path is approximated by the longitudinal distance. Separate agents represent the tunnel users, which start evacuation starting from a certain level of obscuration. Their evacuation speed and incapacitation are determined by the dose of gasses (CO, CO₂ and HCN) the agents are exposed to. The gas concentrations of the CO, CO₂ and HCN originate from the FDS and the SPRINT simulations.

A list of all parameters that are considered in the risk model is given on the website of the model [22] and more details about the model can also be found in [23], [24]. The following aspects are not explicitly considered:

- probability distributions of input parameters
- fixed firefighting systems (FFFS)
- new energy carriers
- structural damage, traffic effects or costs
- risks related to the transport of dangerous goods

ASTRA Bayesian network

Although Switzerland is not a member state of the European Union, it aims to fulfil the requirements of Directive 2004/54/EC [25]. The Federal Roads Office of Switzerland, ASTRA, developed a method that, just like the Italian method, employs a Bayesian approach [26] and is therefore substantially different from the other methods. The use of Bayesian networks in risk assessments is a recent, promising development that allows relatively accurate predictions. Moreover, the method provides clear graphical representations which can facilitate designers and authorities [27].

ASTRA applies two Bayesian networks: one network for the transport of non-dangerous goods and one for the transport of dangerous goods. These networks calculate the frequency of incidents and their consequences at once, using statistical data. The method can consider the uncertainties of the input data to estimate the uncertainty of the output data. [26], [28]

For projects that are still in the design phase, not all input parameters might be known, and general statistical distributions are applied. For projects with a final design, a detailed study is required, in which all general distributions are replaced by values specific to the tunnel. [28]

When known parameters are filled in, the network takes into account the conditions in the tunnel that deviate from the general statics and therefore decreases or increases the change of injuries and deaths due to car accidents and fire accidents. When parameters are not constant over the length of the tunnel, the tunnel is divided into homogenous segments (for instance, a straight segment and a curved segment). The method is then applied to the segments separately. [28]

A major drawback of this method is that it requires quantifying numerous conditional probabilities. Many of those conditional probabilities seem to be based on engineering judgment and are hardly ever accompanied by indisputable arguments in the background documentation. For instance, when a fire

occurs at a moment that the traffic is providing 150 GJ/km, there is a 99% chance of a 5MW and a 1% change of a 30MW fire. No explanation is offered.

However, to estimate the changes in injuries and deaths, a semi-empirical method is used. A set of simulations is performed in SPRINT and ODEM to generate response surfaces. These response surfaces allow ASTRA to make a fast and rough prediction of injuries and deaths, taken into account four parameters (inclination, fire load, distance between emergency exits and length of the tunnel). The applied ventilation is considered by choosing between five key ventilation strategies. To consider the effect of deviating strategies, an interpolation between the effect of the key strategies is applied. [19], [28]

Last, Bayesian methods complicate the anticipation of changes to the system. For example, the effect of new technologies, like lane assistance, electric cars or FFFS will only be taken into account when they are represented in the statistics or when a prior distribution is proposed, based on expert judgement.

RWS QRA-tunnels

QRA-tunnels 2.0 is a program developed by the Rijkswaterstaat (Directorate-General for Public Works and Water Management of the Netherlands) in 2012. It replaces the previous version, RWSQRA 1, which was published in 2006 [29]. The new version deals with risks related to NDG and DG traffic.

The model consists of an event tree analysis, in which the chance of each scenario is calculated, and a scenario tree analysis, in which the consequences of each scenario are calculated. The two analyses combine into a bow tie model, which describes the risk. [30]

The consequence analysis uses constant smoke velocities. For this purpose, sixty simulations are performed in FDS. In these simulations, two different lengths, two different ventilation methods and fifteen different heat release rates are considered. The premade simulations are used to predict the smoke velocity of the tunnel in question. The influence of length, ventilation and heat release rates are assumed to be linear [18]. In other words: a similar approach is applied as in the previous method, but now the 'response surfaces' are assumed to be linear. The resulting smoke velocities are then used in a simple one-directional evacuation model. Occupants of the tunnel will start evacuating when visibility is reduced (below 5m) or when the operator is demanding to do so. Their walking speed is influenced by the dose of gasses they breathe. Incapacitation is also considered [18].

The risks relating to dangerous goods and alternative fuels (CNG, LPG, H2) are considered in seven scenarios, among which vapour cloud explosions and boiling liquid expanding vapour explosions. The transport of nitrogen and carbon dioxide is also included in those scenarios since those gasses can endanger occupants once they are released into the tunnel's atmosphere. Electric battery fires are not considered [18], [31].

Just as with TuRisMo, probabilistic distributions, FFFS or electric cars are not taken into consideration. Structural damage, traffic continuity or other costs are overlooked as well since the goal of the method is to assess life safety only.

OECD/PIARC DG-QRA

The World Road Association (PIARC) and the Organisation for Economic Co-operation and Development (OECD) have developed a quantitative analysis method for risks related to the transport of dangerous goods. This method has been employed by many countries, including some member states of the European Union, to assess the risks of large fires, explosions and toxic releases. [32]

The method calculates the intrinsic risk of the tunnel and compares, if necessary, the risk of alternative routes. Both are calculated in a similar manner as in the RWS QRA method: a quantitative frequency analysis (which includes thirteen representative scenarios) and a quantitative consequence analysis are combined. The consequence analysis contains a one-dimensional and a two-dimensional tool to determine the events in the open air and another one-dimensional tool for events inside tunnels. [20]

1.3 Objective

The goal of the research project of FESG is to provide a holistic framework to assess the fire risk of tunnels in Belgium. The framework will allow designers, operators, and authorities to choose between different design options and trade off different safety measures. The framework will be called Fire Integrated Environment for Risk Comprehension and Evaluation (FIERCE) and will incorporate new knowledge from recent studies to go beyond the already existing risk assessment models for tunnel fires. The framework will include, among other things, the following features [13]:

- probabilistic distributions of input values to deal with the uncertainty of the input data.
- a one-dimensional fluid dynamics model to efficiently solve a high number of scenarios.
- a one-dimensional evacuation model which considers the influence of visibility and intoxication to determine the evacuation speed and incapacitation.
- a fire development model to implement the fire spread between different vehicles. Not only traditional vehicles, but also the so-called new energy carriers will be implemented (LPG, CNG, H₂, electric batteries...). The effect of active measures like sprinklers will be taken into account as well, just as the fire fighter intervention. Calculations will determine the time of activation and intervention, as well as their reliability.
- a traffic model that will determine the effect of the traffic on the fire (draft and piston effect) and the effect of the fire on the traffic (congestion upstream of the fire).
- a structural model to estimate the level of damage to the structure of the tunnel, considering the applied passive protection. Also direct (repair) and indirect (traffic discontinuity) costs will be estimated.

The development of this framework will be divided over the complete R&D department of FESG. This thesis will focus on one package of the framework: the one-dimensional fluid dynamics model. Currently, the one-dimensional model assumes that all flow properties (velocity, temperature, density, smoke concentration...) are uniform over the cross-section. However, a hot buoyant smoke layer might spread along with the ceiling and distinguish itself from the cold air layer below, as shown in [Figure 2](#).

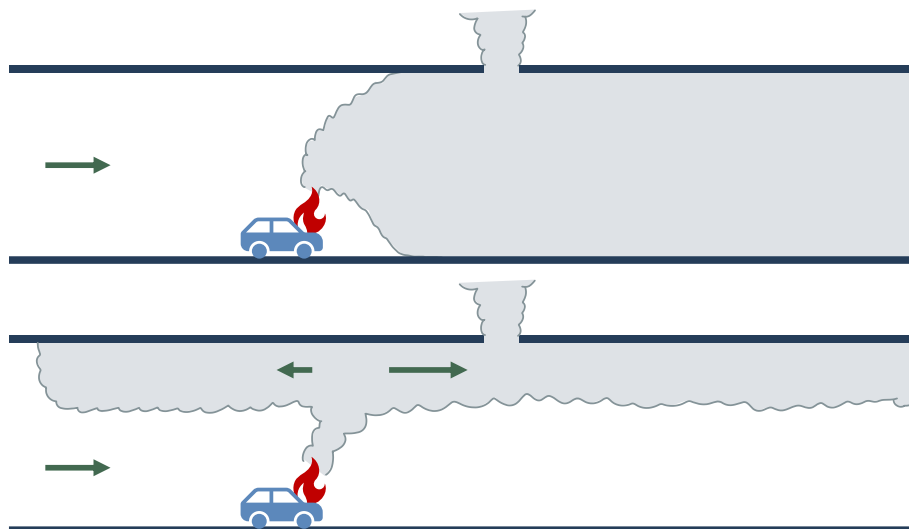


Figure 2: One-dimensional models assuming one layer (above) and two layers (below)

Therefore, the following research question will be treated to contribute to this model:

How can the back-layering effect upstream and stratification downstream of the fire seat be predicted by the one-dimensional fluid dynamics model in a fast and reliable manner, which is useful to evaluate life safety and structural stability?

More practically, the model will be developed in Python 3.9 that considers two layers: a cold air layer and a hot smoke layer. Both layers are still one-dimensional (uniform properties along the layers' cross-section). This model does require solving balances for mass, momentum, energy, and species, just like the one-layer model. Moreover, it requires some correlations to describe the interaction between the layers.

In order to evaluate life safety, the length, thickness, and temperature of these layers are of high importance. The entrainment of smoke in the fresh layer should also be considered. To evaluate the structural stability of the tunnel, the temperature close to the ceiling is the single most valuable property.

1.4 Structure of the report

The remainder of the report is divided into four chapters. In the following chapter, the phenomena of stratification and back-layering are described, and different prediction techniques are explored. Several correlations that predict the level of stratification, critical velocity, and back-layering length, are examined. Chapter 3 deals with one-dimensional models. The main concept is clarified, as well as the set of governing equations they require to describe the fluid dynamics. Existing models are briefly mentioned as well. The fourth chapter elaborates on the methodology of the proposed model. It also contains thorough discussions on the correlations that are employed by the model. The outcome and the sensitivity of the model are presented in Chapter 5, as well as a comparison with prediction techniques from the literature and experimental data. Last, a conclusion is drawn, and the references are given.

2 STRATIFICATION AND BACK-LAYERING

In this chapter, the concepts of smoke stratification and back-layering are described, as well as some correlations that allow for rough predictions of the level of stratification and the back-layering length.

2.1 Introduction in stratification

In this dissertation, the term stratification is used to describe the separation of the hot smoke layer and the cold air layer. During fires and other combustion processes, the chemical potential energy of the fuel is transformed to heat. For most fuels and fires, 60 to 80% of this heat releases as hot smoke (convection), the rest radiates towards the environment [33]. In tunnels, this hot smoke will rise to the ceiling and spread sideways. (see Figure 3, region I). This warm upper layer implies a risk for people underneath it as it radiates heat downwards and pollutes the cold lower layer with smoke gasses. Additionally, it can compromise the structural stability of the tunnel.

The stratification is reinforced by buoyancy (the difference in density of the two layers) and counteracted by turbulence [34]. Therefore, stratification will be most prominent close to the seat of the fire – where the smoke layer has its highest temperature – and decreases downstream as the smoke layer cools down (see Figure 3, region II and III). Moreover, high heat release will lead to more buoyancy and strengthen the stratification, while strong ventilation flows will intensify the turbulent mixing of the two layers and undermine the stratification.

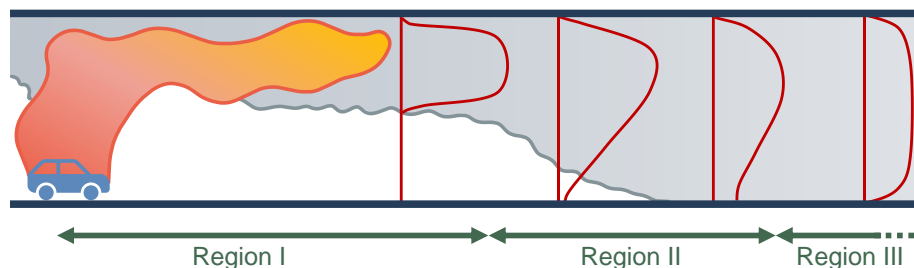


Figure 3: Stratification regions for a tunnel with a ventilation flow that moves to the right, redrawn from [35]. Temperature profiles are shown in red. Note that region I and region II might be absent in certain scenarios.

In the following section, some parameters are presented which can be used as an indicator of the level of stratification.

2.2 Existing stratification predictions techniques

Stratification and back-layering can easily be observed from experiments. However, experiments can only be performed after the construction and are financially costly and time-consuming, especially when a high number of scenarios needs to be evaluated or when the test fires cause damage. Therefore, this approach is not practicable for every tunnel nor every scenario.

Another way of accurately defining the stratification or back-layering, are three-dimensional computational fluid dynamics (CFD) simulations. During those simulations, the Navier-Stokes' equations are solved numerically to obtain the properties of the fluids in the domain. The results of CFD calculations are generally accepted as accurate when the simulation is set up properly. Unfortunately, a proper set-up still forms a stumbling block. Moreover, the calculations can be exceedingly computationally costly. This is especially true for large domains such as tunnels, even when the domain is reduced to the segment close to the seat of the fire. Such a method is used in the detailed consequence analysis of the Austrian TuRisMo (multi-scale simulations). However, it is inadequate for assessment methods that consider numerous scenarios, such as the probabilistic methods, like FIERCE.

One-dimensional models have much lower computation cost and can therefore be used in probabilistic risk assessments to simulate the smoke spread in numerous scenarios. One-dimensional models that consider two-layers, can employ empirical correlations to determine if a one-layer or a two-layer

assumption is the most appropriate. The model SpitFire, for instance, employs a densimetric Froude number as the threshold between the two assumptions [36].

Richardson number

In 1922, Richardson published a dimensionless number that expresses the ratio of buoyancy and flow shear as an indicator of the stability of stratification [37]. Although the number is originally meant for two-dimensional flows (atmospheric and oceanic flows), it can also be employed for one-dimensional flows as well.

For a tunnel where a hot smoke layer with density ρ_h and layer thickness d is located above a cold air layer with density ρ_c , the Richardson number is expressed as follows:

$$Ri = \frac{g(\rho_c - \rho_h)d}{\rho_h u_r^2} = \frac{g(T_h - T_c)d}{T_c u_r^2} \quad (2-1)$$

where u_r is the relative flow velocity of the two layers.

A low Richardson number indicates that the inertial forces dominate over the buoyancy forces. Some authors [38]–[40] came with limiting Richardson numbers which indicate the level of stratification. Since these limits are also expressed as Froude numbers, they are discussed below.

Froude number

In 1930, Weber defined the Froude number as the ratio of the inertial forces and the gravitational forces [41]:

$$Fr = \frac{u}{\sqrt{gd}} \quad (2-2)$$

However, in tunnel fire safety engineering, the literature often refers to the densimetric Froude number Fr_ρ . This number accounts for the specific gravity and therefore relates to the Richardson number:

$$Fr_\rho = \frac{u_r}{\sqrt{g'd}} = \frac{u_r}{\sqrt{g \frac{\rho_a - \rho_s}{\rho_a} d}} = \frac{1}{\sqrt{Ri}} \quad (2-3)$$

Just as a low Richardson number, a high Froude number indicates destratification. Newman defined three *stratification regions*, with different levels of stratification, as shown in Figure 3. In the first region (RI), clear stratification is present. In the second region (RII), stratification is less prominent and in the third region (RIII), it disappeared entirely. Newman suggests that clear stratification occurs for Froude numbers lower than 0.9, and that stratification practically disappears for Froude numbers above 10. However, he defined the Froude number slightly different. He replaces the relative velocity with the average velocity and the dimensionless density difference with a temperature difference between the ceiling and the floor. Moreover, the height of the smoke layer is replaced by the height of the tunnel. The formula is given below. [42]

$$Fr_N = \frac{u_{avg}}{\sqrt{g \frac{T_c - T_f}{T_{avg}} H}} \quad (2-4)$$

Nyman and Ingason compared formula (2-4) with small- and large-scale experiments and found that a Froude number of 3.2 represents the transition between region I and region II better [43]. Ever since, more research has been performed. Table 2 summarizes some proposed limits.

Table 2: Different Froude numbers as a limit of stratification region

Source	Data*	Froude number	RI ↔ RII	RII ↔ RIII
Newman (1984) [42]	S	Fr_N	0.9	10
Yang, Hu et al. (2010) [38]	S	Fr_p	1.02	2.4
Nyman and Ingason (2012) [34], [43]	S & L	Fr_N	0.9	3.2
Tang, Li et al. (2017) [39]	S	Fr_p	0.66	0.80
Tang, Zhao and Zhao (2020) [40]	S	Fr_p	0.44	1.05

*(S = small scale smoke experiments, L = large scale fire experiments, N = numerical experiments)

Stratification length correlation by Zeng, Xiong et al. (2018) [44]

Zeng, Xiong et al. performed small scale experiments and numerical experiments. They obtained a correlation for the dimensionless length over which stable stratification occurs in longitudinal ventilated tunnels. This correlation is given in equation (2-5).

$$L_s^* = \frac{L_s}{\bar{H}} = 10.79 \ln\left(\frac{Q^*}{u^{*3}}\right) - 4.06 \quad (2-5)$$

with

$$\bar{H} = \frac{4A}{P}, \quad Q^* = \frac{Q}{\rho_a c_p T_a \sqrt{g \bar{H}^5}}, \quad u^* = \frac{u}{\sqrt{g \bar{H}}}$$

This simple formula allows for stratification length predictions as a function of the dimensionless HRR and the dimensionless ventilation velocity. Unlike the technique with local Richardson numbers and Froude numbers, it does not allow to take into account the heat losses (towards the walls) or other modelled effects (entrainment, extraction, variable tunnel width...).

2.3 Introduction to back-layering

In tunnel tubes with one-directional traffic, the smoke is typically blown away in the same direction as the traffic to ensure that people can evacuate safely from the tunnel. This strategy rises from the assumption that people downstream left the tunnel in their vehicles quickly without any problem and that people upstream are stuck. To prevent smoke from spreading upstream, the critical ventilation velocity could be applied [45]. This is the minimum longitudinal ventilation velocity to prevent a reverse flow of smoke. When lower ventilation velocities are applied, some smoke will flow upstream along with the ceiling. Back-layering is defined as the development of this flow (the back-layering flow) reverse to the ventilation flow [45]. Figure 4 visualizes the concept.

In intense fires, the ventilation system might lack the capacity to produce the desired critical velocity. Moreover, subcritical velocities might even be preferred when there are people present downstream, for instance when traffic congestion occurs. Therefore, it is important to understand back-layering and to predict the layer properties when performing a risk analysis. In order to evaluate life safety, the length, thickness, and temperature of this layer are of high importance. The entrainment of smoke in the fresh air layer should also be considered. To evaluate the structural stability of the tunnel, the temperature is the single most valuable property.

The back-layering flow properties can easily be observed from experiments or three-dimensional computational fluid dynamics (CFD) simulations. However, as mentioned before, both approaches are undesirable for risk assessments. Therefore, back-layering predictions are sometimes limited to the use of rough empirical correlations. Many authors have researched back-layering length predictions but not all authors have validated their correlations against large scale experiments with high heat release rates. Hence, attention to the validity limitations and accuracy of the correlations is required.

In the next section, a few of the many correlations are mentioned to predict the critical velocity and the back-layering length. Note that all predictions are only established for the critical velocity and the back-layering length. No simple correlations exist to assess other essential properties, such as temperature and thickness of the back-layering flow.

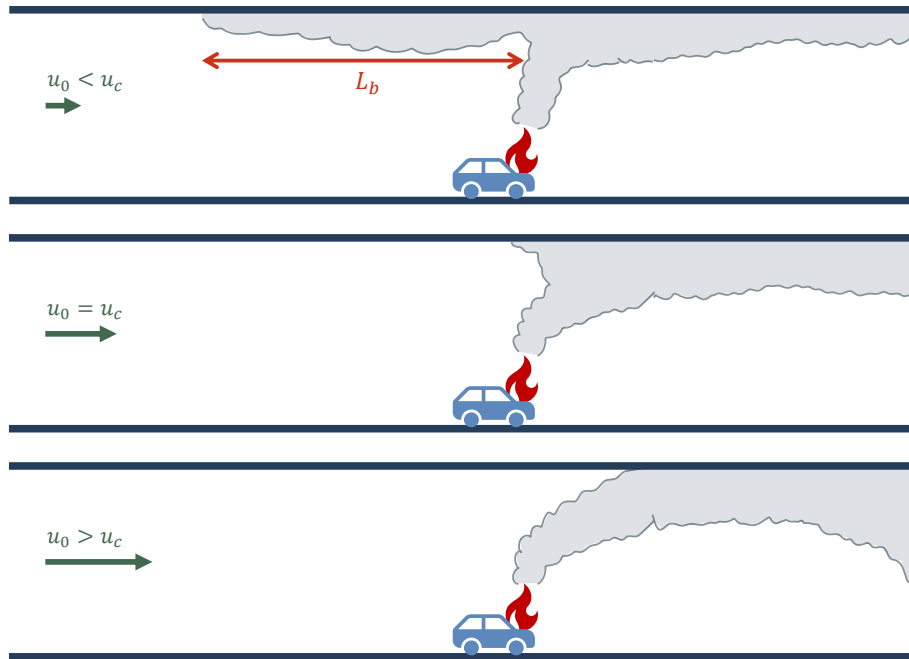


Figure 4: Illustration of the critical ventilation velocity its effect on back-layering

2.4 Existing critical velocity prediction techniques

In this section, a few critical velocity correlations are discussed. Many more can be found in the literature.

Critical velocity prediction by Thomas (1958) [46]

Thomas reasoned that back-layering would be prevented when the kinetic energy of the ventilation flow exceeds the kinetic energy of the hot smoke layer. The latter kinetic energy originates from the potential gravitational energy, without considering conversion losses. Both kinetic energies equate when the Richardson number (or the densimetric Froude number) is equal to 1. Moreover, he wrote the density difference as a function of the convective heat and the entire mass flow rate. Therefore, he implicitly assumes that at this critical velocity, no stratification will occur. The equation is given below [46]:

$$u_{cr} = \left(\frac{2gH\dot{Q}}{\rho_0 c_p T_f A} \right)^{\frac{1}{3}} \quad (2-6)$$

Critical velocity prediction by Danziger and Kennedy (1982) [47]

Danziger and Kennedy compared Thomas equation with the small scale experiments of Lee [48] and found that the critical densimetric Froude number varies between 4.5 and 6.7 and proposed to use 4.5 for predictions. To obtain the critical velocity and the smoke temperature, an iteration process is required. The formulae are given below [49].

$$\begin{cases} u_{cr} = \left(\frac{g\dot{Q}_c H}{\rho_0 c_p T_f A F r_{cr}} \right)^{\frac{1}{3}} \\ T_f = T_0 + \frac{\dot{Q}_c}{\rho_0 c_p A u_{cr}} \end{cases} \quad (2-7)$$

Critical velocity prediction by Wu and Bakar (2000) [50]

In 1995, Oka and Atkinson derived a formula starting from a dimension analysis and performed small scale experiments [51]. The same process was repeated by Wu and Bakar in 2000, who performed physical (small scale) and numerical experiments. They propose the correlation below:

$$u_{cr}^* = \frac{u_{cr}}{\sqrt{g\bar{H}}} = \begin{cases} 0.68(Q^*)^{\frac{1}{3}}, & Q^* \leq 0.20 \\ 0.40, & Q^* > 0.20 \end{cases} \quad (2-8)$$

with

$$Q^* = \frac{Q}{\rho_0 c_p T_0 g^{1/2} \bar{H}^{5/2}}$$

The diameter $\bar{H} = 4A/P$ is the hydraulic diameter of the tunnel section and should not be confused with the real tunnel height H which is used in the dimension analysis of Oka and Atkinson and the analysis of Li, Lei and Ingason.

Critical velocity prediction by Li, Lei and Ingason (2010 and 2017) [45]

The formula of Li, Lei and Ingason is also derived from a dimension analysis and is therefore of the same shape. The correlation was derived from small scale experiments and validated against large-scale experiments.

$$u_{cr}^* = \frac{u_{cr}}{\sqrt{g\bar{H}}} = \begin{cases} 0.81(Q^*)^{\frac{1}{3}}, & Q^* \leq 0.15 \\ 0.43, & Q^* > 0.15 \end{cases} \quad (2-9)$$

with

$$Q^* = \frac{Q}{\rho_0 c_p T_0 g^{1/2} H^{5/2}}$$

Due to the validation of large-scale experiments, this correlation is typically preferred over the previous correlations. Moreover, the correlation is easy to use as it does not require any iterations, nor does it contain parameters that are difficult to obtain.

However, in 2017, Li and Ingason published a new correlation for the critical velocity. The influence of the width W was incorporated through the section ratio $\varphi = W/H$ [52]:

$$u_{cr}^* = \frac{u_{cr}}{\sqrt{g\bar{H}}} = \begin{cases} 0.81(\varphi^{-1/4} Q^*)^{1/3}, & Q^* \leq 0.15\varphi^{1/4} \\ 0.43, & Q^* > 0.15\varphi^{1/4} \end{cases} \quad (2-10)$$

Comparison of different critical velocity correlations

The different correlations are compared by means of example EX1. The parameters and their corresponding values of this example are presented in Table 3. The same example is used to illustrate other correlations, such as back-layering predictions (section 2.5), plume entrainment (section 4.2) and smoke propagation (section 4.4). It represents a fire involving a single passenger car [53]. Table 3 also contains example EX2, which represents a fire involving two busses, a small lorry or a metro carriage [53].

Table 3: Parameters and values for the example problems EX1 and EX2

Parameter	Symbol	Value in EX1	Value for EX2	Unit
Tunnel height	H	6.00	6.00	m
Tunnel width	W	12.00	12.00	m
Heat release rate	\dot{Q}	5.00	60	MW
Convective heat release rate	\dot{Q}_c	3.75	45	MW
Heat release rate per unit area	\dot{q}''	1.00	1.00	MW/m ²
Fraction of convective heat	χ_c	0.75	0.75	-
Temperature of fresh air	T_0	288.15	288.15	K
Density of fresh air	ρ_0	1.2250	1.2250	kg/m ³
Specific heat capacity of smoke	c_p	1.0045	1.0045	kJ/kg/K
Radius of the seat of the fire	b_f	1.26	4.37	m
Height of the seat of the fire	h_f	1.00	1.00	m
Ventilation velocity	u_0	1.50	2.30	m/s

The graph below shows the critical velocity for the example problem in question, with varying heat release rates. High discrepancies can be noticed between the different correlations. Especially the correlation by Danziger and Kennedy seems to predict lower critical velocities. However, for greater heat release rates, it is the correlation by Thomas that outlies the others. This can easily be noticed after calculating the asymptotic values:

- Thomas (1958): $u_{cr}(\dot{Q} \rightarrow \infty) = \sqrt{2gH/\chi_c} = 12.53 \text{ m/s}$
- Danziger & Kennedy (1982): $u_{cr}(\dot{Q} \rightarrow \infty) = \sqrt{gH/Fr_{cr}} = 3.62 \text{ m/s}$
- Wu & Bakar (2000): $u_{cr}(\dot{Q} \rightarrow \infty) = 0.40\sqrt{gH} = 3.54 \text{ m/s}$
- Li, Lei and Ingason (2010): $u_{cr}(\dot{Q} \rightarrow \infty) = 0.43\sqrt{gH} = 3.30 \text{ m/s}$
- Li, Lei and Ingason (2017): $u_{cr}(\dot{Q} \rightarrow \infty) = 0.43\sqrt{gH} = 3.30 \text{ m/s}$

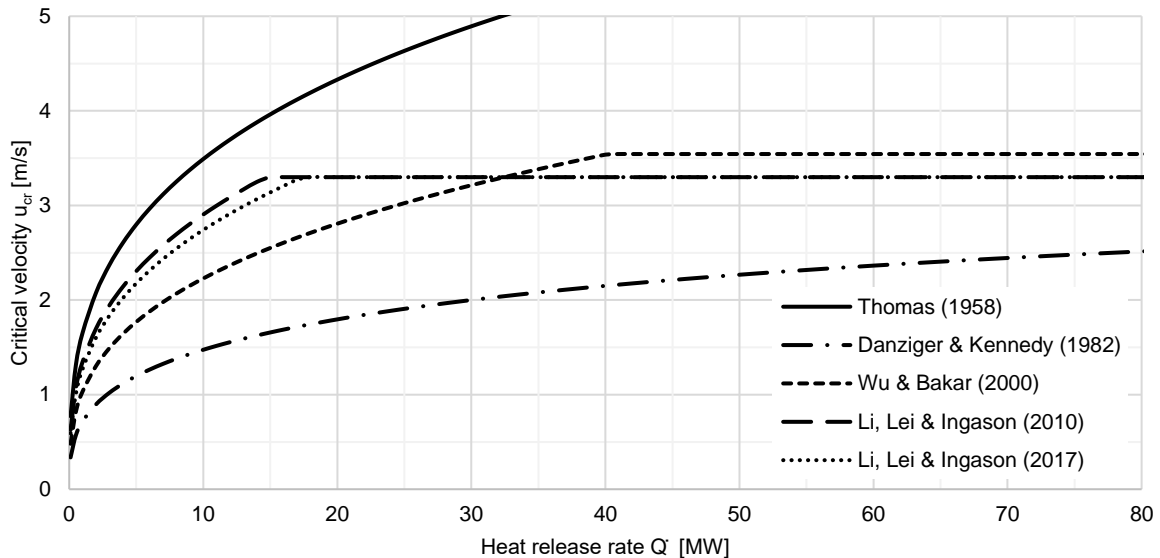


Figure 5: Critical velocity predictions for a six-meter-high and twelve-meter-wide tunnel

2.5 Existing back-layering predictions techniques

In this section, a few back-layering length correlations are discussed. Many more can be found in the literature.

Back-layering length correlation by Thomas (1958) [46]

The first attempt to predict the back-layering length was done by Thomas in 1958. He used the results of full-scale experiments in mining tunnels and conducted a small-scale experiment himself. The result is given in the formula below.

$$L_b = \left(0.6 \left(\frac{u_{cr}}{u_0} \right)^3 - 3 \right) H \quad (2-11)$$

Here, the critical velocity u_{cr} should be calculated in accordance with equation (2-6).

The details of the full-scale experiment are not published. Likely, the size and geometry of the mining tunnels do not differ significantly from those of typical road tunnels. Unfortunately, no details are given about the fire (fuel, heat release, size, location) either. Big fires might not have been part of the experiments.

Back-layering length correlation by Hu, Huo and Chow (2008) [54]

Hu, Huo and Chow published a correlation meant for small fires, of which the flames do not reach the ceiling. They stated that at the back-layering front, the buoyancy of the hot layer causes a static pressure

that is equal to the hydraulic pressure, applied by the ventilation velocity. Their correlation, given below, is based on four full-scale tests with fire intensities up to 3.2 MW.

$$L_b = \frac{1}{0.019} \ln \left(g\gamma \left(\frac{\dot{Q}^{*2/3}}{Fr^{1/3}} \right)^\epsilon \frac{C_k H}{u_0^2} \right) \quad (2-12)$$

where

$$Fr = \frac{u_0^2}{gH_{eff}}, \quad \dot{Q}^* = \frac{\dot{Q}}{\rho_0 c_p T_0 g^{1/2} H_{eff}^{5/2}}, \quad \begin{cases} \epsilon = 1.2, \gamma = 1.77, & \dot{Q}^{*2/3}/Fr^{1/3} < 1.35 \\ \epsilon = 0, \gamma = 2.54, & \dot{Q}^{*2/3}/Fr^{1/3} \geq 1.35 \end{cases}$$

The factor C_k varies in between 0.19 and 0.37. The average (0.28) is proposed to make predictions.

Back-layering length correlation by Li, Lei and Ingason (2010) [45]

As mentioned before, Li, Lei and Ingason performed a series of model-scale experiments. Their method and results can be seen as a continuation of the work of Oka and Atkinson [51] and Wu and Bakar [50]. The correlation, given below, corresponds well to multiple full-scale experiments [45]:

$$L_b^* = \frac{L_b}{H} = 18.5 \ln \left(\frac{u_{cr}^*}{u_0^*} \right) = 18.5 \ln \left(\frac{u_{cr}}{u_0} \right) \quad (2-13)$$

Here, the critical velocity is calculated in accordance with equation (2-9). The ventilation velocity u_0^* is multiplied with the same factor as the critical velocity to eliminate the dimensions ($u_0^* = u_0/\sqrt{gH}$).

This correlation is commonly used, due to its simplicity and good agreement with experiments. Moreover, later research (experimental and numerical), that takes into account other factors (see [below](#)) tend to confirm the validity.

Comparison of different back-layering length correlations

The figure below illustrates the back-layering length for example EX1 (see [Table 3](#)). The figure illustrates the great discrepancies between the different correlations. For this case study, the formula of Thomas leads to negative values (not shown in the figure) for velocities considerably smaller than the critical velocity proposed by the same author. The correlation of Hu, Huo and Chow also results in negative back-layering lengths.

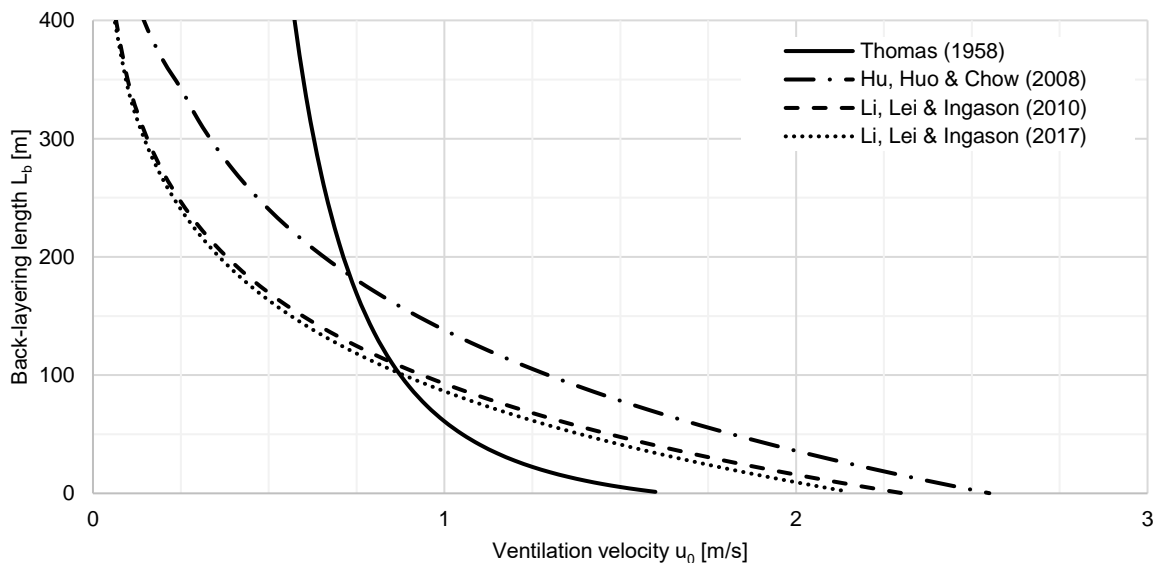


Figure 6: Back-layering length predictions for a fire of 5 MW in a six-meter-high and twelve-meter-wide tunnel.

Other parameters that influence the back-layering length

The correlations above are rough estimations that predict the back-layering length based on the heat release rate, the height of the tunnel, and the ventilation velocity. However, other parameters influence the length as well:

- **the width and/or the aspect ratio**

Wu and Bakar [50] performed small-scale experiments and noticed that for a range of width-height ratios (aspect ratios) going from 0.5 to 4, the influence on the critical velocity is small. Consequently, the effect on the back-layering length is often neglected. However, Li and Ingason found out that, for small fires, the critical velocity decreases for increasing widths and suggested a new correlation [52], with a relative weak dependency on the width (2-10). Tilley, Deckers and Merci [55] also obtained a correlation for car parks from numerical experiments. The critical velocity and therefore the back-layering length in the numerical car park simulations seemed to be relatively constant with different widths (but slightly higher for small widths). This confirms the finds of Li and Ingason.

- **the obstruction ratio**

When vehicles are present in the tunnel, the ventilation velocity is forced to increase locally. Therefore, the back-layering length will be lower than predicted. Li, Lei and Ingason [45] suggested a reduction of the critical velocity, equal to the obstruction ratio. A similar trend was noticed in a numerical study by Gannouni and Maad [56] for shorter obstruction located upstream (yet close to) the seat of the fire. Zhang, Yao, Zhu, Li, Zhang, Lu and Cheng [57] developed a method to estimate the back-layering length for long obstruction with a high blockage ratio. However, for road tunnels, the obstructions are usually small and discontinuous.

- **the slope**

Hot smoke rises due to buoyancy. Therefore, it is not surprising that critical velocity is higher for tunnels that decline in the direction of the ventilation flow. Ko, Kim and Ryou [58] developed a correlation, based upon small-scale experiments.

- **the curvature**

Wang, Wang, Carvel and Wang [59] performed numerical experiments to study the impact of the curvature of the road. Fires that occur among the convex tunnel wall are exposed to a lower local ventilation velocity and therefore, the back-layering flow is longer, compared to the same conditions in a straight tunnel. At the concave wall, the opposite is true.

3 ONE-DIMENSIONAL MODELS

As mentioned earlier, physical experiments and three-dimensional computational fluid dynamics simulations are often too expensive and time-consuming to predict the smoke spread of tunnel fires. When the smoke behaviour of many scenarios must be assessed, fast calculations are much more desirable. Empirical correlations can give a first rough estimation, but do not allow to obtain all important properties (such as smoke height and smoke temperature).

One-dimensional models offer a great compromise, as they provide simulations within seconds, whilst still being reasonably accurate. In this chapter, the concept of one-dimensional models is briefly discussed, as well as their governing equations.

3.1 Concept of one-dimensional models

Tunnels typically have one dimension that exceeds the others. Therefore, it can be assumed that properties (velocity, temperature, density, smoke concentration) of the flow only vary in one dimension. In other words, properties are uniform along a cross-section. This assumption is accurate for fresh air flows upstream and for smoke flows downstream, far from the seat of the fire. Near the seat, cold fresh air and hot smoke will separate due to buoyancy: back-layering and stratification might occur. To predict the smoke behaviour more accurately, a one-dimensional model can assume two layers with different properties, analogue to the two-zone models for enclosure fires.

For both methods, the flow properties can be calculated by solving the coupled conservation equations of mass, momentum, energy, and species. However, the two-layer model does require more submodels to assess the gains and losses in the second and third dimension (e.g., the amount of smoke entering the smoke layer through the smoke plume or the entrainment and detrainment at the interface of the layers).

In this chapter, the conservation equations are briefly described for both models. The required submodels, as well as the numerical techniques, are discussed in the next chapter.

In both models, some simplifications are typically made:

- The heat release rate is predefined.
- The mass of combustion products is negligible compared to the mass of the air flow (one-layer model) or compared to the mass of the entrained air (two-layer model).
- The pressure variations are small compared to the absolute pressure $p \approx p_{amb}$. The flows are assumed to be incompressible, and the density is only a function of the temperature. This assumption is reasonable when low Mach numbers are expected. This is the case for fire incidents, but not for explosions.
- Fresh air and smoke are assumed to behave as ideal gases with a molar mass of 28.97 g/mol.

3.2 Conservation equations for the one-layer model

The simplest version of a one-dimensional model only considers one layer and therefore, it does not describe back-layering nor stratification. This model is more accurate for supercritical ventilation flows and severe fires as they cause more turbulence.

Just as for three-dimensional simulations, the flow properties are calculated from the mass, momentum, energy, and species balance. Together, they form the set of governing equations:

$$\frac{\partial}{\partial t}(\rho A) + \frac{\partial}{\partial x}(\rho A u) = \dot{m}'_s \quad (3-1)$$

$$\frac{\partial}{\partial t}(\rho u) + \frac{\partial}{\partial x}(\rho u^2) = K' \quad (3-2)$$

$$\frac{\partial}{\partial t}(\rho A c_p T) + \frac{\partial}{\partial x}(\rho A c_p T u) = \dot{Q}'_s + \dot{Q}'_f - \dot{Q}'_w \quad (3-3)$$

$$\frac{\partial}{\partial t}(\rho Ay) + \frac{\partial}{\partial x}(\rho Ayu) = \dot{Y}'_s + \dot{Y}'_f \quad (3-4)$$

The following representations are used:

\dot{m}'_s The mass flow per running meter of imposed sources. In case of fire, the strategy is generally to cease all fresh air inlet flows and only extract smoke. For those extraction points, the mass flow rate is negative (as defined by the formula (3-1)). For the simulations, the inlet and outlet flows are typically predefined. In principle, those flows can also be triggered or adjusted during the simulation, depending on the situation.

K' The additional momentum per running meter. This additional momentum can be written as a pressure gradient over the length of the tunnel, which is caused by the meteorological difference between the two ports, the stack effect of the slope, the piston effect of the traffic, the jet fans, and the wall friction:

$$K' = -\frac{\partial p}{\partial x} = -\left(\frac{\partial p}{\partial x}\right)_{meteo} - \left(\frac{\partial p}{\partial x}\right)_{stack} - \left(\frac{\partial p}{\partial x}\right)_{traffic} - \left(\frac{\partial p}{\partial x}\right)_{ventilation} - \left(\frac{\partial p}{\partial x}\right)_{friction}$$

The formulae for these pressure gradients can be found in the literature (for example, in [60] and [61]). As explained in the next chapter, the proposed model assumes that the main velocity flow is known as a result of the overall momentum balance: the calculation of the pressure gradients is not incorporated.

\dot{Q}'_s The additional heat rate per running meter which comes with the additional mass flow \dot{m}'_s .

\dot{Q}'_f The heat release rate of the fire per running meter. \dot{Q}'_s and \dot{Q}'_f are typically predefined, although they could also be triggered or changed during the simulation, depending on the evolution of the fire.

\dot{Q}'_w The heat loss rate through the walls per running meter. This rate is assessed by means of a sub-model, which is discussed in the next chapter.

\dot{Y}'_s The additional species per running meter, which come with the additional mass flow \dot{m}'_s .

\dot{Y}'_f The combustion products of the fire, expressed per running meter as well.

3.3 Conservation equations for the two-layer model

In order to model stratification and back-layering, at least two layers need to be modelled. In those layers, the flow properties are uniform over the cross-section, analogue to the two-zone models for enclosure fires. Consequently, the conservation equations need to be solved for the two layers. In this section, the balances are briefly discussed, and an explanation is provided about why it is unfavourable to solve the set entirely.

The sources of mass, momentum, energy, and species need to be separated for the two layers. Interaction between the two layers also needs to be represented. Therefore, the following additional terms need to be considered (visualized in [Figure 7](#)):

\dot{m}'_{pl} Air is entrained from the lower layer by the plume and enters the upper layer as smoke.

$\dot{m}'_{a,s}$ Mass sources in the lower layer, such as supply fans. This mass source can also result in a heat source $\dot{Q}'_{a,s}$ and a species source $\dot{Y}'_{a,s}$.

$\dot{m}'_{sm,s}$ Mass sources in the upper layer, such as extraction fans. This mass source can also result in a heat source $\dot{Q}'_{sm,s}$ and a species source $\dot{Y}'_{sm,s}$.

\dot{m}'_{ent} Air entrainment by the upper layer. This mass exchange also results in an exchange of heat \dot{Q}'_{ent} and of species \dot{Y}'_{ent} .

- \dot{m}'_{det} Smoke entrainment by the lower layer (referred to as *detrainment*). This mass exchange also results in an exchange of heat \dot{Q}'_{det} and of species \dot{Y}'_{det} .
- $K'_{a,s}$ Pressure gradients in the lower layer due to effects, such as traffic and friction.
- $K'_{sm,s}$ Pressure gradients in the upper layer due to effects, such as ceiling jets and friction.
- \dot{Q}'_{cw} Heat losses in the lower layer towards the surrounding *cold walls*.
- \dot{Q}'_{hw} Heat losses in the upper layer towards the surrounding *hot walls*.
- \dot{Q}'_r Radiative heat losses of the upper layer towards the cold walls below.

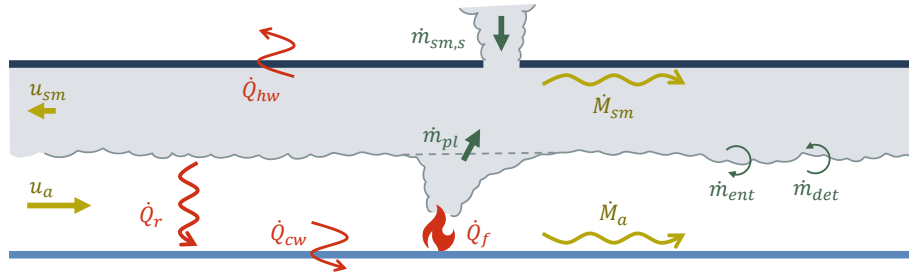


Figure 7: Schematic representation of the two-layer model

The formulae below embody the mass (3-5), momentum (3-6), energy (3-7), and specie balance (3-8) of the cold air layer.

$$\frac{\partial}{\partial t}(\rho_a A_a) + \frac{\partial}{\partial x}(\rho_a A_a u_a) = \dot{m}'_{a,s} - \dot{m}'_{pl} - \dot{m}'_{ent} + \dot{m}'_{det} \quad (3-5)$$

$$\frac{\partial}{\partial t}(\rho_a u_a) + \frac{\partial}{\partial x}(\rho_a u_a^2) = K'_{a,s} \quad (3-6)$$

$$\frac{\partial}{\partial t}(\rho_a A_a c_{p,a} T_a) + \frac{\partial}{\partial x}(\rho_a A_a c_{p,a} T_a u_a) = \dot{Q}'_{a,s} - \dot{Q}'_{cw} - \dot{Q}'_{ent} + \dot{Q}'_{det} \quad (3-7)$$

$$\frac{\partial}{\partial t}(\rho_a A_a \gamma_a) + \frac{\partial}{\partial x}(\rho_a A_a \gamma_a u_a) = \dot{Y}'_{a,s} - \dot{Y}'_{ent} + \dot{Y}'_{det} \quad (3-8)$$

The formulae below express the mass (3-9), momentum (3-10), energy (3-11), and specie balance (3-12) of the hot smoke layer.

$$\frac{\partial}{\partial t}(\rho_{sm} A_{sm}) + \frac{\partial}{\partial x}(\rho_{sm} A_{sm} u_{sm}) = \dot{m}'_{sm,s} + \dot{m}'_{pl} + \dot{m}'_{ent} - \dot{m}'_{det} \quad (3-9)$$

$$\frac{\partial}{\partial t}(\rho_{sm} u_{sm}) + \frac{\partial}{\partial x}(\rho_{sm} u_{sm}^2) = K'_{sm,s} \quad (3-10)$$

$$\frac{\partial}{\partial t}(\rho_{sm} A_{sm} c_{p,sm} T_{sm}) + \frac{\partial}{\partial x}(\rho_{sm} A_{sm} c_{p,sm} T_{sm} u_{sm}) = \dot{Q}'_{sm,s} + \dot{Q}'_f - \dot{Q}'_{hw} - \dot{Q}'_r + \dot{Q}'_{ent} - \dot{Q}'_{det} \quad (3-11)$$

$$\frac{\partial}{\partial t}(\rho_{sm} A_{sm} \gamma_{sm}) + \frac{\partial}{\partial x}(\rho_{sm} A_{sm} \gamma_{sm} u_{sm}) = \dot{Y}'_{sm,s} + \dot{Y}'_f + \dot{Y}'_{ent} - \dot{Y}'_{det} \quad (3-12)$$

Solving the set of governing equations for the two-layer model is considerably more complex than for the one-layer model:

- Eight coupled equations need to be solved instead of four.
- Conduction through the walls requires at least two separate meshes in the submodel for heat losses.
- The sections A_a and A_{sm} of the layers vary in time, since the smoke height can increase or decrease over time. As a result, the volumes of the discretized cells would not be constant in time.

- The mass flow rate of the smoke plume \dot{m}'_{pl} , as well as the mass entrainment and detrainment flow rates, require a correlation.
- The division of the pressure gradients over the two layers is not straightforward.

To overcome these complications, some simplifications are made in the proposed model. Amongst others, they include inert walls to replace the conduction model and a velocity correlation to replace the momentum balance. The solution scheme, together with the assumptions and employed correlations are discussed in the next chapter.

3.4 Existing one-dimensional models

One-dimensional models were first developed mid-last century for application in the mining industry [61], [62]. Since the nineties, multiple models have also been developed for application in road tunnels and rail tunnels. A short list of common models is provided in Table 4.

Table 4: Overview of one-dimensional models of tunnel fires

Model and year of publication (first version)	Authors, companies, and institutions	Features (latest versions)	Reference
1977: MFire	Authors: Zhou, Yuan & Cole Institution: US Bureau of Mines	<ul style="list-style-type: none"> • Tunnel networks • Steady-state ventilation flow 	[61], [63]
1975: Subway Environmental Simulation Code (SES)	Author: Kennedy Company: Parsons Brinckerhoff Quade and Douglas, for the US Department of Transportation	<ul style="list-style-type: none"> • Tunnel networks • Steady-state ventilation flow • Occurrence of back-layering (*) 	[61], [64]
1999: Rabbit 2000: Smoke Propagation IN Tunnels (SPRINT) 2010: One-Dimensional Egress Model (ODEM) 2017: SpitFire (SPRINT + ODEM)	Authors: Riess, Bettelini & Brandt Company: HBI Haerter	<ul style="list-style-type: none"> • Transient ventilation flow • Back-layering (see below) 	[65], [66]
2003: Calcul Monodimensionnel Anisotherme Transitoire en Tunnel (CAMATT)	Institution: Centre d'Études des Tunnels (CETU)	<ul style="list-style-type: none"> • Tunnel networks • Transient ventilation flow 	[67], [68]

(*) Correlation for critical velocity by Danziger and Kennedy, see section 2.4.

As far as the author of this dissertation is aware, all existing models but SPRINT are one-layer models and none of them can predict stratification or back-layering. SPRINT employs empirical correlations to estimate the smoke propagation velocity and superposes this velocity on the main ventilation flow. These correlations are discussed in the next chapter.

SPRINT can predict the position of the smoke front and the temperature profiles of the cold and hot layer [65], [66]. However, it does not calculate the smoke layer height and therefore, species concentrations cannot be calculated accurately. CAMATT employs similar correlations to determine the velocity of the smoke front downstream [68] but does not consider smoke propagation upstream of the seat of the fire.

4 METHODOLOGY

In this chapter, the methodology of the proposed model is explained. First, the overall concept is clarified. Next, the employed correlations are thoroughly discussed and last, the solution schemes of the three main parts of the model are described. The code of the model (written in Python 3.9) can be found in [Appendix C](#).

4.1 Concept of the proposed model

As explained in the previous chapter, several one-dimensional models have already been developed, but the incorporation of stratification and back-layering has not yet been discussed openly in the literature. Therefore, the proposed method assumes a one-layer model to be accomplished and focuses on stratification and back-layering. As a result, the main velocity flow u_0 , upstream of the smoke, is assumed to be known and considered as input data.

Simplifications and assumptions

To simplify the model, some assumptions have been made and are listed below. Many of those simplifications can easily be reversed later to make the model more accurate.

- The heat release rate is predefined.
- The mass of combustion products is negligible.
- The fresh air and the smoke behave as incompressible ideal gases.
- The tunnel section is rectangular (and constant among the tunnels axis).
- No transverse ventilation is implemented. The tunnel is strictly ventilated longitudinally.
- The tunnel walls and ceiling are thermally inert. They maintain their initial temperature.
- The slope of the tunnel is not taken into account.
- The entrainment and detrainment of smoke are negligible.
- The main ventilation velocity is known. It is assumed that an overall momentum balance is solved by the already accomplished one-layer model. This main velocity depends on the pressure gradient, caused by the meteorological pressure difference between the two portals, the stack effect of the slope, the piston effect of the traffic, the jet fans, and the wall friction.
- The proposed model provides a steady-state solution. Later, a semi-steady state method can be employed, or the transient balances can be solved.

The model consists of three main parts: a first part, in which the properties at the seat of the fire are obtained, and two separate parts, which obtain how the smoke spreads upstream and downstream from the seat of the fire. The concept is represented in the flowchart ([Figure 8](#)). Some clarification is given below.

Solver of the fire plume

The smoke will rise up from the seat of the fire and deflect underneath the ceiling to spread (upstream and) downstream. The plume mass flow rate and the plume temperature are required to assess the properties of those two flows.

The mass flow rate can be calculated from three perspectives: (1) a plume correlation, (2) a mass flow through the smoke section with a certain velocity and (3) a mass flow that relates the heat release to the plume temperature rise. Those three mass flow rates can be combined into two equations and solved simultaneously for the plume height and density. Subsequently, the flow velocity and mass flow rate can be calculated.

Solver of the upstream flow (back-layering flow)

A certain fraction of the plume mass flow rate might flow upstream. If this is the case, back-layering occurs. The properties of the smoke layer in a mesh cell can be calculated from the neighbour, closer to the seat of the fire. Therefore, the mass balance and the heat balance need to be solved together.

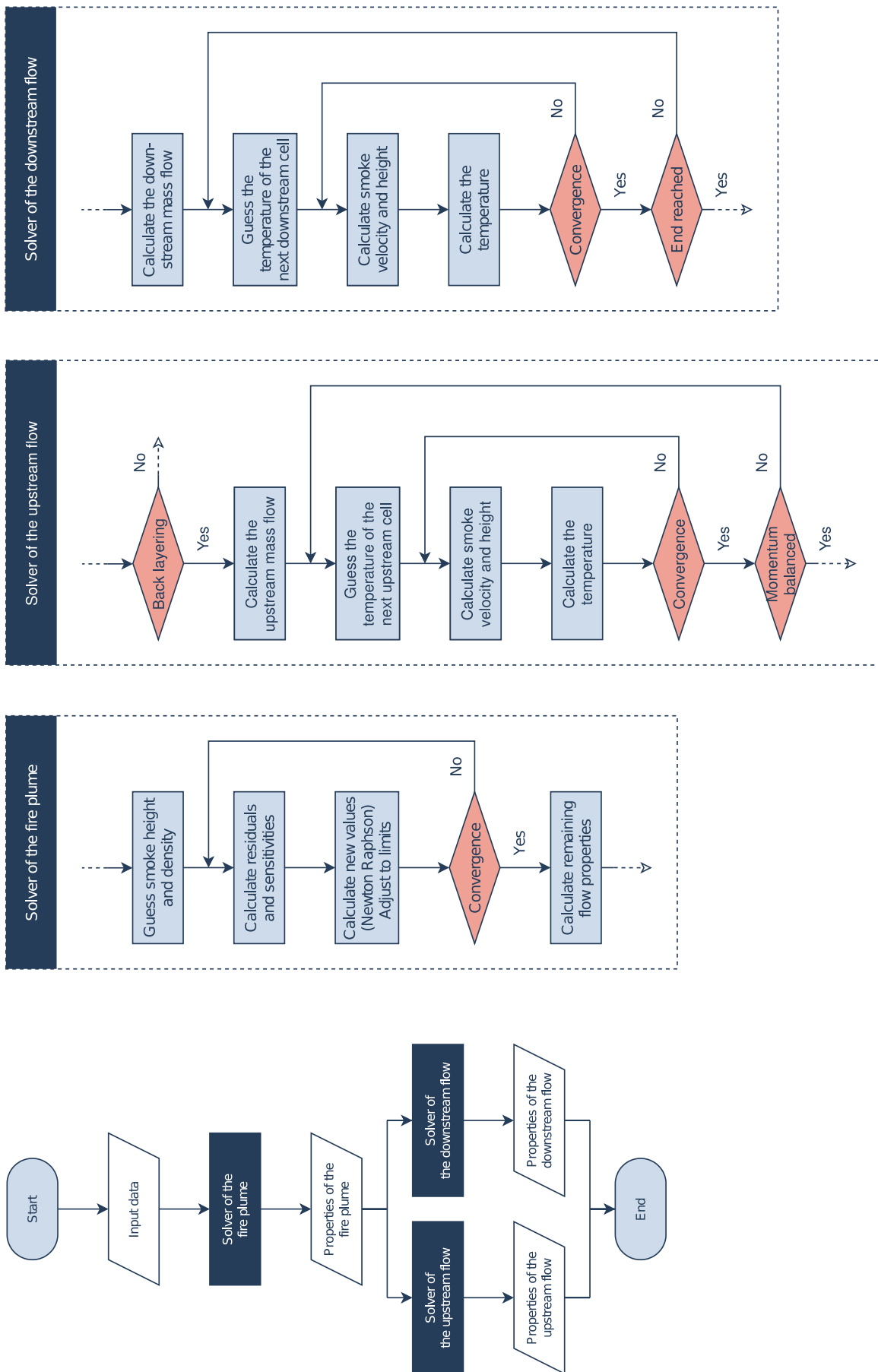


Figure 8: Flowchart of the proposed methodology

Due to the complex nature of the heat balance, a simple iteration process is employed in which both balances are solved sequential, rather than simultaneously. The momentum balance is replaced by a simple smoke propagation velocity correlation (see section 4.4). After convergence is reached, the properties of the upstream neighbour can be determined. This process is continued until the momentum of the back-layering front is in equilibrium with the ventilation flow.

Solver of the downstream flow

The flow properties downstream can be calculated analogue to the properties upstream. No initial check needs to be performed as there will always be a fraction of the plume mass flow rate flowing downstream. Moreover, as the downstream flow is unbalanced, the calculation can be stopped at a predefined point of interest (usually, at the portal).

4.2 Plume mass flow

Just as the two-zone models for enclosures, fresh air of the lower layer is entrained in the plume and enters the upper layer as smoke. An empirical correlation is required to assess the mass flow rate of this plume. In this subsection, four different correlations are briefly discussed and compared.

For all correlations below, SI units should be used, with exception of the heat release rate (kW) and the specific heat capacity (kJ/kg/K). For the simplified correlations which only manifest the heat release rate and the height, the same conditions are assumed as for EX1 (see Table 3). Fresh air and smoke are assumed to behave as ideal gases with a molar mass of 28.97 g/mol.

Plume correlation by Zukoski, Kubota & Cetegen (1980) [69]

In 1980, Zukoski, Kubota and Cetegen performed experiments on free plumes and found a good agreement with the ideal plume theory. The result is the correlation below [69].

$$\dot{m}_{pl} = 0.21 \left(\frac{\rho_0^2 g}{c_p T_0} \right)^{\frac{1}{3}} \dot{Q}^{\frac{1}{3}} z_{eff}^{\frac{5}{3}} \approx 0.078 \dot{Q}^{\frac{1}{3}} z_{eff}^{\frac{5}{3}} \quad (4-1)$$

The correlation has the following limitations:

- The correlation has been derived only from methane fires up to 200 kW and heights in between 1 and 2.3 m. Naturally, relevant tunnel fires lie beyond these limitations: accuracy is not guaranteed.
- The Zukoski plume employs the Boussinesq approximation and will not lead to accurate results in the flaming region of the plume. Here, this is when the flames attach to the ceiling of the tunnel.
- The correlation is developed for free plumes and therefore, the influence of the enclosing walls and ceiling are not considered. Strictly spoken, a distance of $(5/6)\alpha H_{eff} \approx 0.18 H_{eff}$ from the wall suffices to prevent the plume to reach the walls. However, entrainment can be expected to be affected even when the seat of the fire has a greater distance.
- The effect of ventilation flows is not taken into account.

Plume correlation derived from Alpert (1975) [70]

As the smoke in enclosures deflects horizontally after it reaches the ceiling, correlations for ceiling jets might be more appropriate than those for free plumes. In 1975, Alpert published the empirical correlations for unconfined ceilings. The maximum temperature inside the plume ($r < 0.18 H_{eff}$) can be written as follows [70]:

$$\Delta T_{max} = 16.9 \frac{\dot{Q}^{\frac{2}{3}}}{z_{eff}^{\frac{5}{3}}} \quad (4-2)$$

From this formula, the mass flow rate can be calculated, considering that the convective heat of the fire is divided over the entire mass flow rate:

$$\chi_c \dot{Q} = \dot{m}_{pl} c_p \Delta T_{pl} \quad (4-3)$$

Equation (4-2) and (4-3) cannot easily be united since (4-2) is written in terms of the maximum temperature and (4-3) in terms of the average plume temperature. In a first crude approximation, a triangular temperature profile along the radius can be assumed for the temperature ($\Delta T_{max} = 2\Delta T_{pl}$). This results in the correlation below:

$$\rightarrow \dot{m}_{pl} = \frac{2}{16.9} \frac{\chi_c}{c_p} \dot{Q}^{\frac{1}{3}} z_{eff}^{\frac{5}{3}} \approx 0.088 \dot{Q}^{\frac{1}{3}} z_{eff}^{\frac{5}{3}} \quad (4-4)$$

The correlation has the following limitations:

- The correlation has been derived from methane fires test ranging from 500 kW to 100 MW and for ceiling heights that range from 2.4 m to 15.9 m.
- In all those tests, the flames do not reach the ceiling. The correlation will not lead to accurate results when the flames do attach to the ceiling.
- The correlation is developed for unconfined ceilings: the influence of the enclosing walls is not considered.
- The assumption of the triangular temperature profile is crude.
- The effect of the ventilation flow is not taken into account.

Plume correlation by Kunsch (2002) [71]

In 2002, Kunsch published a model to describe the smoke spread in tunnels. In the model, he balances the mass of the smoke flow with the mass at the turning point (e) [71], which implies a plume mass flow rate. This flow rate can be obtained using the following formula:

$$\dot{m}_{pl} = \rho_e (2\pi r_e d_e) u_e \quad (4-5)$$

Kunsch adopts the ceiling jet geometry at this turning point from Alpert [70]:

- The plume radius r_e is assumed equal to $0.20H$
- The smoke layer thickness d_e is assumed equal to $0.05H$
- The radial propagation velocity u_e is assumed to be given by the following equation:

$$u_e = 0.963 \sqrt{gH \frac{\rho_0 - \rho_e}{\rho_0}} \quad (4-6)$$

To determine the temperature at the turning point, Kunsch employs the correlation by Heskestad and Delichatsios [72]. The result is the following correlation:

$$\Delta T_e = \Delta T^* \left(\frac{T_0^{\frac{1}{3}}}{\rho_0^{\frac{2}{3}} c_p^{\frac{2}{3}} g^{\frac{1}{3}}} \right) \frac{\dot{Q}^{\frac{2}{3}}}{H^{\frac{5}{3}}} \approx 16.5 \frac{\dot{Q}^{\frac{2}{3}}}{H^{\frac{5}{3}}} \quad (4-7)$$

Since he assumes that the temperature of the smoke at the turning point is equal to the temperature at the axis of the plume, the empirical parameter ΔT^* is equal to 6.13. More accurate would have been an integration over the plume axis (from $r/H = 0$ till $r/H = 0.20$). However, the difference is minor. Note the agreement with the correlation by Alpert (4-2) for reasonable ambient conditions.

The implied mass flow rate in Kunsch's model is defined by equations (4-5), (4-6) and (4-7) and by the ideal gas law. Since Kunsch relies on the empirical correlations by Heskestad and Delichatsios and by Alpert, similar limitations apply as mentioned above. However, the mass flow rate can be expected to be less accurate since the geometry and the temperature of the plume are taken from different correlations and are therefore not consistent. Note that, with equation (4-3), Kunsch could have omitted the correlations of Heskestad and Delichatsios [72].

Plume correlation by Li, Lei & Ingason (2010) [73], [74]

Li, Lei & Ingason developed a correlation that considers the effect of the ventilation flow on the plume entrainment. They performed small-scale experiments which indicated that a low ventilation velocity ($V^* \leq 0.19$) does not influence the entrainment, while entrainment increases linearly with the higher levels of ventilation ($V^* > 0.19$). The authors propose the following equation, based on the ideal plume theory [73]:

$$\dot{m}_{pl}(z_{eff}) = \begin{cases} 0.071 \dot{Q}_c^{1/3} z_{eff}^{5/3}, & V^* \leq 0.19 \\ 0.3735 \dot{Q}_c^{1/3} z_{eff}^{5/3} V^*, & V^* > 0.19 \end{cases} \quad (4-8)$$

with

$$V^* = \frac{u_0}{w^*}, \quad w^* = \left(\frac{g\dot{Q}}{b_{fo}\rho_0 c_p T_0} \right)^{1/3}$$

The correlation has also been validated by Zhen and Ingason with large-scale experimental data [74]. However, for large fires, the flames impinge on the ceiling and the correlation is no longer accurate. For these fires, the smoke temperature rise ($T_{pl} - T_0$) tops off around 1350 K. Therefore, just as the other correlations mentioned above, this one is limited to relatively small fires.

Comparison of different plume correlations

The different plume correlations are compared by means of an example (EX1, see Table 3). The results are given in Figure 9. All correlations have similar tendencies. However, the formula of Kunsch leads to significantly lower plume mass flow rates.

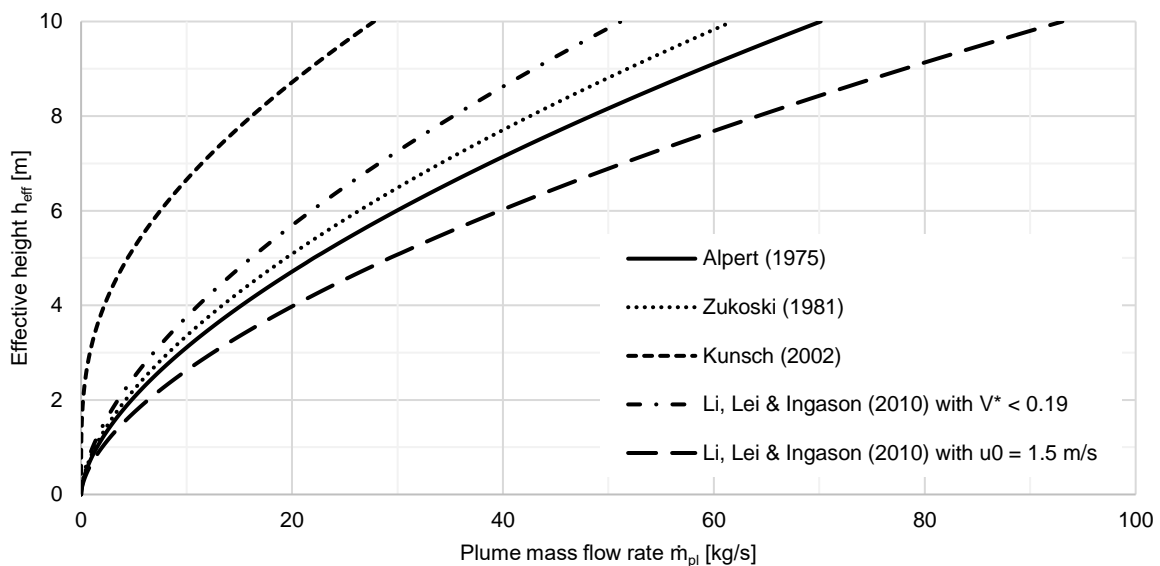


Figure 9: Comparison of different plume mass flow correlations

The proposed model will incorporate the correlation by Li, Lei & Ingason, as it includes the effect of the ventilation flow and it has shown to agree with large-scale tunnel fire tests. Moreover, the validity range is expressed in terms of the temperature rise, which is easy to verify.

Of all correlations, the one by Li, Lei & Ingason leads to the highest mass flow rate when the dimensionless ventilation velocity V^* is equal to or greater than 0.26. Nevertheless, higher mass flow rates are not necessarily conservative, as they also implicate lower smoke temperatures.

4.3 Upstream and downstream distribution of the mass flow

In this section, the distribution of the plume flow over the upstream and the downstream flow is discussed. First, the upstream mass flow is treated. Afterwards, the consequences for the downstream flow are explained.

Upstream mass flow

Not only the total plume mass flow rate is important, but its distribution of the upstream and downstream flow also has a significant influence on the flow properties. Research on this matter has been performed by Wang, Fang, Tang and Yuan. They derived the following formula for the upstream ratio δ [75]:

$$\delta = \frac{\dot{m}_{up}}{\dot{m}_{pl}} = \begin{cases} 0.5, & 0 \leq u_0 \leq 0.5u_{cr} \\ \frac{2(u_{cr} - u_0)}{3u_{cr} - 2u_0}, & 0.5u_{cr} \leq u_0 \leq u_{cr} \\ 0, & u_{cr} \leq u_0 \end{cases} \quad (4-9)$$

It has been shown by Raj and Moussa [76] that the ventilation starts to deflect the plume at ventilation velocities of about $0.19w^*$. This threshold has also been validated by Li, Lei and Ingason [73], as well as the linear increase that follows for higher ventilation velocities. Therefore, the linear influence in the ratio δ is unsurprising. However, the combination of this plume correlation and the upstream ratio leads to counterintuitive results. This is because, for real fires, the ventilation velocity $0.19w^*$ ($V^* = 0.19$) is typically smaller than half of the critically velocity. Therefore, with increasing velocity, the upstream mass flow rate will initially remain constant, then increase and eventually decrease.

Figure 10 illustrates the problematic mass flow rates for EX1 (see Table 3). Note that the total mass flow rates do not appear to be perfectly linear, because the smoke layer height is slightly affected as well. The system is explained in its entirety in section 4.6.

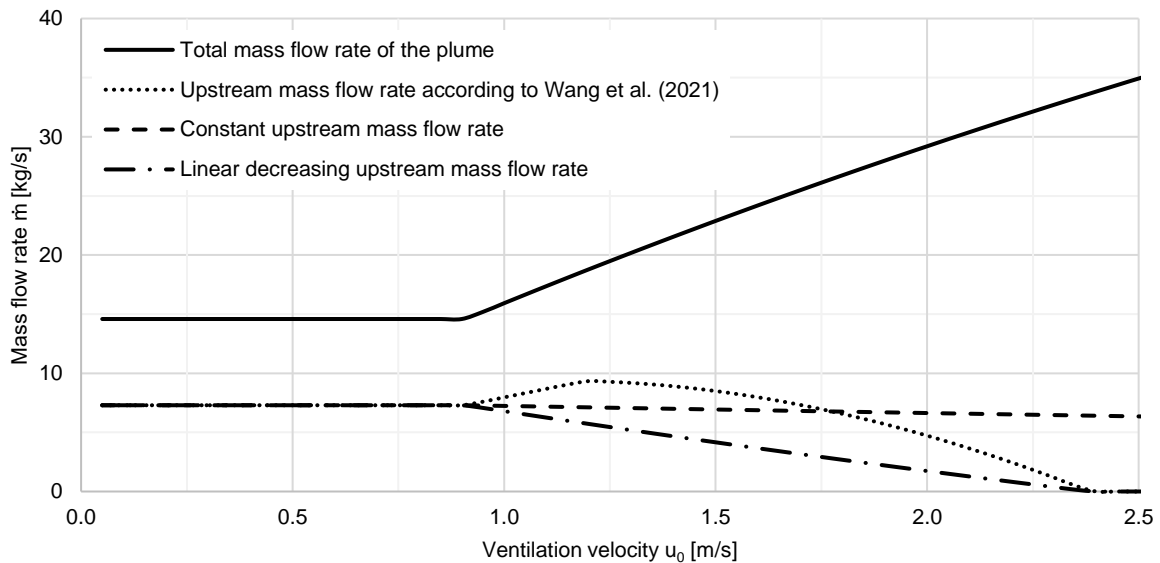


Figure 10: Total mass flow rate and upstream mass flow rate for different distributions

To prevent the counterintuitive result, two different distributions are proposed. The result of the proposed distributions is shown in Figure 10 as well.

- For small ventilation flows ($V^* < 0.19$), the plume mass flow rate $\dot{m}_{pl,0}$ is divided equally. For greater ventilation flows, the ratio of the upstream mass flow rate over the wind still plume mass flow rate $\delta_0 = \dot{m}_{up}/\dot{m}_{pl,0}$ decays linearly until the critical ventilation velocity is reached, as shown in equation (4-10).

$$\delta_0 = \frac{\dot{m}_{up}}{\dot{m}_{pl,0}} = \begin{cases} 0.5, & 0 \leq u_0 \leq 0.19w^* \\ \frac{u_{cr} - u_0}{2u_{cr} - 0.38w^*}, & 0.19w^* \leq u_0 \leq u_{cr} \\ 0, & u_{cr} \leq u_0 \end{cases} \quad (4-10)$$

- The upstream mass flow is not affected by the ventilation flow, as formulated in equation (4-11). The linear increase that occurs for higher ventilation flows allocated to the downstream mass flow rate.

$$\delta_0 = \frac{\dot{m}_{up}}{\dot{m}_{pl,0}} = 0.5 \quad (4-11)$$

To illustrate the effect on the outcome of the model, the back-layering length is shown in [Figure 11](#). Both the distribution of Wang and the proposed linear decrease result in a less continuous curve than expected (considering the prediction by Li et al. [45], [52]). The second proposed distribution, in which the effect of the ventilation is not taken into account for the upstream mass flow rate, seems to correspond better to the prediction by Li et al. (especially for ventilation velocities close to the critical ventilation velocity). Therefore, it is this distribution, described by equation (4-11), that is employed in the proposed model. Note that the back-layering length prediction by Li et al. also has significant model uncertainties and that more research should be performed to gain confidence about the distribution's precision.

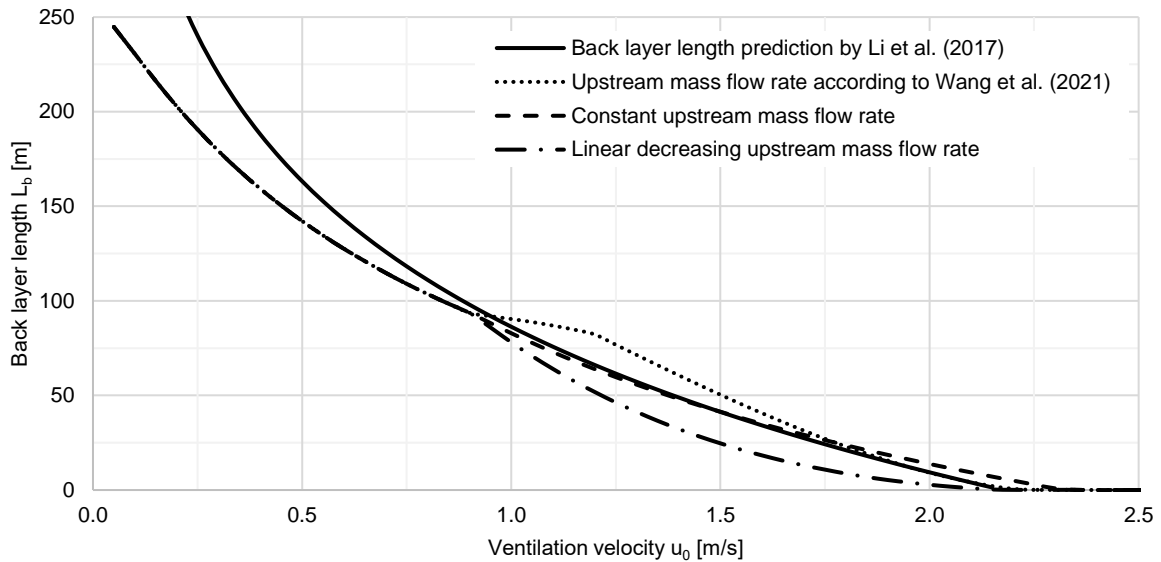


Figure 11: Back-layering length, employing different mass flow rate distributions

Downstream mass flow

When the back-layering flow arrives at the upstream tunnel portal, the smoke will exit the tunnel. In this case, the downstream flow will be the remainder of the plume flow:

$$\dot{m}_{down} = \dot{m}_{pl} - \dot{m}_{up} \quad (4-12)$$

However, when the upstream portal is not reached, the back-layering flow does not exit the tunnel but deflects and flows back downstream. For long back-layering lengths, this deflected flow can be assumed to mix with the fresh air and cool down before the seat of the fire is reached. In this case, equation (4-12) is still applicable. However, for life safety analyses, the smoke contamination of the fresh air should be accounted for.

For short back-layering lengths, the back-layering front will still hot. Therefore, the smoke layer stays buoyant after its deflection and join in the downstream upper layer. In this case, the entire plume mass smoke rate will flow downstream:

$$\dot{m}_{down} = \dot{m}_{pl} \quad (4-13)$$

Naturally, all real back-layering lengths can be considered to be of intermediate length, and the downstream mass flow rate should be somewhere in between (4-12) and (4-13). A more correct approximation could be made when a third layer is taken into account: the deflected back-layering flow. This layer moves at the same velocity as the fresh air layer underneath the upper layer and cools down on its way.

In the proposed model, the back-layering flow is assumed to reach the portal or to be long enough for the deflected flow to cool down before it arrives back at the seat of the fire. Therefore, equation (4-12) is applied for all subcritical ventilation velocities. For critical and supercritical ventilation velocities, equation (4-13) is applied. A more precise downstream flow rate could be implemented later, following the philosophy described above.

4.4 Smoke propagation velocity

To simplify the model, the momentum balance of the smoke layer can be omitted and a correlation can be used instead. In this section, different theoretical and empirical correlations are discussed. Although they are derived from different theories, a reasonable agreement between the correlations can be found.

Some of the correlations are derived from gravity (buoyancy) driven flows. These correlations have many applications, such as leaking oil tankers [77], atmospheric flows, oceanic flows and powder avalanches [68]. They have also been used by NIST to estimate the filling time for the corridor model in CFAST [78] and by Rabbit (later renamed SPRINT and SpitFIRE) [65], [66] and CAMATT [68] to describe the propagation of the smoke front in tunnel fires. Other correlations are derived from ceiling jet models. All of them are first described separately and afterwards compared with each other through an example problem.

Smoke propagation velocity derived from Alpert (1975) [70]

In 1975, Alpert published empirical correlations for the maximum temperature and smoke velocity underneath an unconfined ceiling in the neighbourhood of a jet flow [70]. The correlation for the velocity is given by the equations below:

$$u_{max} = \begin{cases} 0.96 \frac{\dot{Q}^{\frac{1}{3}}}{H^{\frac{1}{3}}}, & \frac{r}{H} < 0.15 \\ 0.195 \frac{\dot{Q}^{\frac{1}{3}} H^{\frac{1}{2}}}{r^{\frac{5}{6}}}, & \frac{r}{H} \geq 0.15 \end{cases} \quad (4-14)$$

The details of the correlations and their limits are described above. Here, only three important limitations are repeated: (1) In tunnels, the walls do restrict the smoke flow to a one-dimensional flow. Moreover, (2) the correlations can only be used for fires for which the flames do not reach the ceiling. Last (3), no external ventilation flow was applied during the experiment.

Kunsch worked around the first limitation (see [below](#)). He assumed that the smoke flow behaves entirely one-dimensional at a distance $x = W/2$ from the point source of the fire. Using the mass and momentum balance, he related the properties of this one-dimensional flow to the properties at the turning point at which the vertical flow deflects horizontally underneath the ceiling [71]. The relation is given as follows:

$$u_h = \frac{2}{\pi} u_{r_{TP}} \quad (4-15)$$

The formula of Alpert can be rewritten in terms of density difference to allow easy comparison with the correlations discussed below. This requires the following assumptions:

- All the convective heat is contained in the smoke layer, see equation (4-3).
- The tunnel is wide enough for the deflection underneath the ceiling to occur radially and transition to a one-dimensional flow later. This also requires the seat of the fire to have a distance r_{TP} of $0.20H$ from the wall.
- The mass flow rate can therefore be written as in equation (4-5).

- The geometry of the ceiling jet at the turning point is adopted from Alpert's correlations: the turning point is located at a horizontal distance r_{TP} of $0.20H$ from the seat of the fire and the smoke layer has a thickness of $d_{TP} = 0.05H$ [70].
- The smoke behaves as an ideal gas.

Moreover, the values of the specific heat capacity, the molar mass, the ideal gas constant, the ambient pressure, and the convective fraction can be assumed as stated in Table 3. Consequently, the velocity can be written as follows:

$$u_{h,max} = \frac{2}{\pi} \left(\frac{0.195}{0.206} \right)^{\frac{3}{2}} \sqrt{2 \cdot 2\pi \cdot 0.20 \cdot 0.05 \left(\frac{c_p p M}{g R \chi_c} \right) g H \frac{\rho_c - \rho_h}{2\rho_c}} \approx 1.009 \sqrt{g H \frac{\rho_c - \rho_h}{2\rho_c}} \quad (4-16)$$

Since equation (4-14) does not describe the average, but the maximum velocity in the ceiling jet, correlation (4-16) is likely to overestimate the average velocity of the smoke front.

Smoke propagation velocity by Kunsch (2002) [71]

In 2002, Kunsch derived the average smoke velocity of the smoke propagation in tunnels. As explained above, he obtained the one-dimensional velocity from the radial velocity at the turning point employing a mass balance, a momentum balance, and a buoyancy balance. In combination with empirical correlations by Alpert and by Heskestad and Delichatsios [70], [72]. This results in the formula given below [71]:

$$u_h = 0.867 \sqrt{g H \frac{\rho_c - \rho_h}{2\rho_c}} \quad (4-17)$$

The difference between 1.009 (4-16) and 0.867 (4-17) should not be seen as a discrepancy, bearing in mind the remark above.

Kunsch used this velocity correlation in a momentum balance close to the seat of the fire, to find the critical velocity and validated his theory with small-scale and large-scale physical. The correlation has not been validated for back-layering.

Gravity-driven (buoyancy-driven) flow

From another perspective, the hot smoke layer can be regarded as a buoyancy-driven flow. The propagation velocity of the smoke front that intrudes in the cold air can be derived by equating the difference in gravitational potential energy and kinematic energy of both fluids (hot smoke and cold air). This section discusses the derivation for a tunnel without a ventilation flow.

The propagation velocity of buoyancy flows and gravity flows has barely been studied in the field of fire safety but is a well-discussed topic in the field of fluid dynamics [77], [79]. To study the flows, the lock-exchange problem has been set up: two fluids with a different density are divided from each other by a vertical lock. Once the lock is removed, the low-density fluid will spread underneath the ceiling of the duct (buoyancy flow) and the high-density fluid will spread above the floor of the duct (gravity flow). The experiment set-up is shown in the figure below. Since the problem is applied on tunnel fires, low-density and high-density fluids will be called hot smoke and cold air in this section.

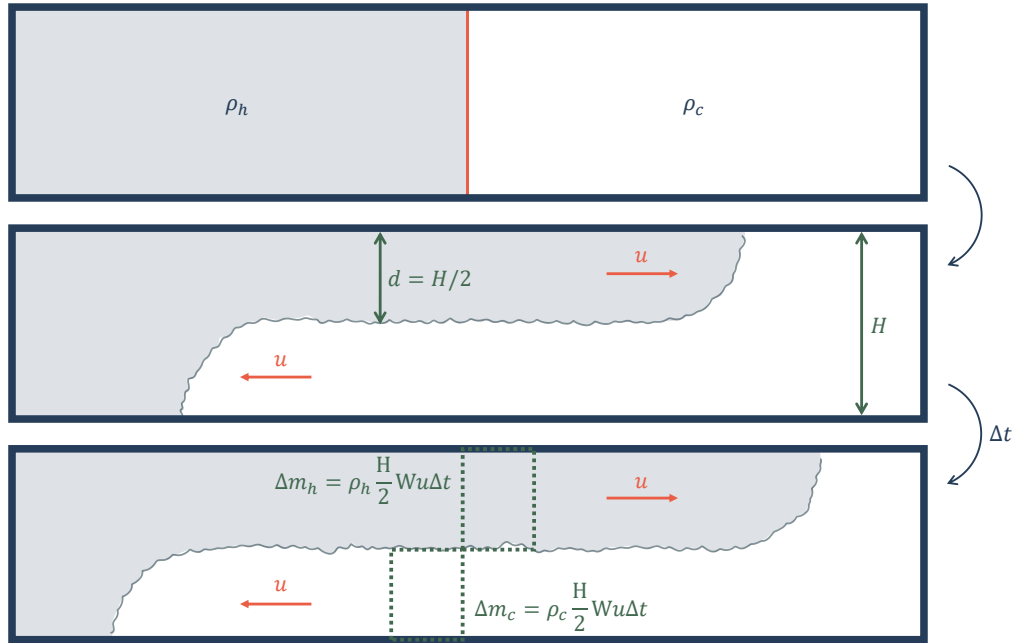


Figure 12: Lock-exchange problem

To derive the propagation velocity, some simplifications can be made:

1. The section of the duct is rectangular.
2. Due to the symmetry of the experiment set-up, the smoke layer height is predefined as half of the total height.
3. The viscosity of the gases and the friction of the gasses with the boundaries can be neglected. Consequently, the exchange of heat or mass at the interface of the gasses and at the boundaries of the duct is negligible as well.

Due to the last simplification, only gravitational potential energy and kinetic energy are considered. As the hot smoke spreads over the ceiling, the mass centre of the smoke gains height. Simultaneously, the mass centre of the cold air drops. The change in gravitational potential energy during the timestep δt is given by formula (4-18). Since the cold air has a higher density than the hot smoke, the total gravitational potential energy decreases ($\delta E_{gra} < 0$).

$$\delta E_{gra} = \frac{1}{8} g \rho_h u H^2 W \delta t - \frac{1}{8} g \rho_c u H^2 W \delta t = \frac{1}{8} g (\rho_h - \rho_c) u H^2 W \delta t < 0 \quad (4-18)$$

Both the hot smoke and the cold air are originally at rest. The gain in kinetic energy during the timestep δt is given by formula (4-19):

$$\delta E_{kin} = \frac{1}{4} \rho_c u^3 H W \delta t + \frac{1}{4} \rho_h u^3 H W \delta t = \frac{1}{4} (\rho_c + \rho_h) u^3 H W \delta t > 0 \quad (4-19)$$

The propagation velocity can be derived by conserving the total energy:

$$\delta E_{kin} + \delta E_{gra} = 0 \rightarrow u_h = u = k \sqrt{gH \frac{\rho_c - \rho_h}{\rho_c + \rho_h}} \quad (4-20)$$

The factor k in this equation is equal to $1/\sqrt{2} \approx 0.707$. Many authors have performed the experiment to verify this theory and establish a factor k that reflects reality better, amongst them Yih [80] and Barr [81]. However, both authors made the Boussinesq approximation:

$$u_h = k \sqrt{gH \frac{\rho_c - \rho_h}{2\rho_c}} \quad (4-21)$$

Yih performed a set of experiments for his master thesis and found that a k -factor equal to 0.67 [79]. This shows a good agreement with the theory above. Unfortunately, information about this experiment (geometry, fluid properties etc.) is no longer accessible. Barr derived a set of factors from experiments, depending on the shape of the duct section. [79]

Due to the high difference in temperature between the fresh air and the smoke layer. This approximation is only appropriate for smoke front sufficiently far from the seat of the fire. Nevertheless, this approach is generally applied in the one-dimensional model SPRINT. The model first obtains a density ρ_h from the average layer temperature and then applies formula (4-21) to calculate the average velocity [66]. The two-zone model CFAST by the NIST includes a submodel, which takes into account the travelling time of smoke through corridors. This submodel applies the formula above as well (k equal to 0.70) [78].

In real fires, the smoke layer height is unknown. In this case, the height H can be seen as a virtual height, analogue to the virtual origin in the free plume model that Heskestad published in 1983. Consequently, equation (4-20) can be reformulated as follows:

$$u_h = \sqrt{gd \frac{\rho_c - \rho_h}{\rho_c + \rho_h}} \quad (4-22)$$

Shin, Dalziel and Linden [79] made an analogue derivation for lock-exchange problems for which only fluid is released from a partial depth d , as shown in the figure below.

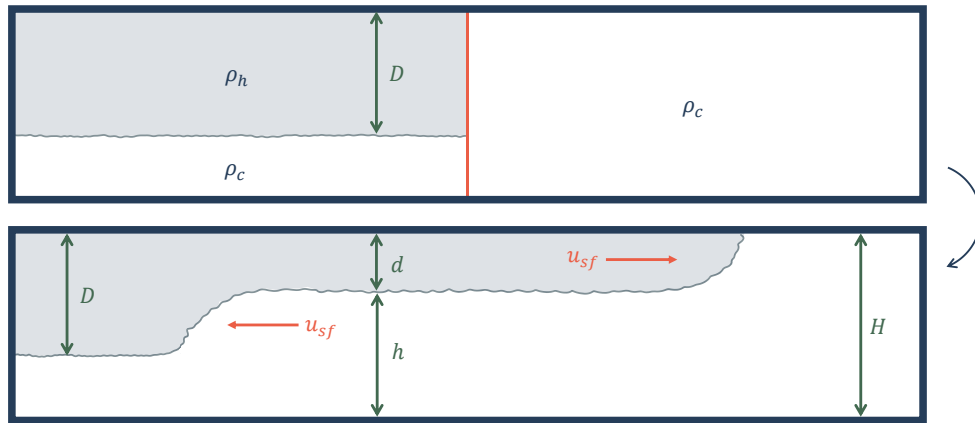


Figure 13: Modified lock-exchange problem with the low-density fluid released from a partial depth

They derived a formula that related the propagation velocity to the densities of the fluids, the total height of the duct, and the partial depth D . In this formula, the partial depth can be replaced by the smoke layer thickness d or the smoke layer height h , as shown below:

$$u_h = \sqrt{g \frac{(\rho_c - \rho_h)d(H-d)}{\rho_c(H-d) + \rho_h d}} = \sqrt{g \frac{(\rho_c - \rho_h)(H-h)h}{\rho_c h + \rho_h(H-h)}} \quad (4-23)$$

Shin, Dalziel and Linden also performed 140 experiments that agreed with their theoretical formula. The experiments took place in a 2-meter-long and a 0.20-meter-high tank. The fluids in the experiment were fresh water and a sodium chloride solution and, therefore, they were miscible fluids, just like smoke and air. Yet, they only have a small density difference ($\rho_h/\rho_c < 0.90$)[79]. In most tunnel fires, the high temperature difference between the hot smoke and the cold air causes a greater difference in density.

The next comments can be made about the previously mentioned simplification.

1. The formula is, strictly speaking, only valid for rectangular cross-sections. In further research, a correction factor could be established to take into account other typical tunnel shapes.
2. No viscosities and frictions are neglected. This simplification is justified since the buoyancy and the inertia dominate over the viscous forces. It has been experimentally demonstrated that for currents with a Reynolds number $Re_H = u_h H / 2\nu$ greater than 1000, the viscous effects on the propagation speed are negligible [79]. Due to the low dynamic viscosity of air and smoke and the great

dimensions of tunnels, the Reynolds number will be practically always above 1000 in case of a tunnel fire, even for very low velocities.

Constant Froude number

When the Boussinesq approximation is made, equation (4-22) result in a constant densimetric Froude number Fr_ρ equal to $1/\sqrt{2}$ ($Ri = 2$). CAMATT, the model of CETU (see Table 4) employs this constant Froude number to describe the downstream smoke propagation [68].

Comparison of different smoke propagation velocities

In the table below, all discussed correlations are summarized to facilitate the comparison.

Table 5: Overview of different smoke propagation correlations

Author of correlation/model	Theory	Formula	Asymptotic value	Reference
1947: Yih	gravity-driven flows	$0.670 \sqrt{gH \frac{\rho_c - \rho_h}{2\rho_c}}$	$0.474\sqrt{gH}$	[80]
1975: Alpert	ceiling-jet	$1.009 \sqrt{gH \frac{\rho_c - \rho_h}{2\rho_c}}$	$0.713\sqrt{gH}$	[70]
2000: SPRINT (HBI Haerter)	Gravity driven flows	$0.5 \dots 0.67 \sqrt{gH \frac{\rho_c - \rho_h}{2\rho_c}}$	$0.35 \dots 0.47\sqrt{gH}$	[66]
2002: Kunsch	ceiling-jet	$0.867 \sqrt{gH \frac{\rho_c - \rho_h}{2\rho_c}}$	$0.613\sqrt{gH}$	[71]
2003: CAMATT (CETU)	constant Froude number	$\sqrt{gd \frac{\rho_c - \rho_h}{2\rho_c}}$	$0.707\sqrt{gd}$	[68]
2004: Shin, Dalziel, Linden	gravity-driven flows	$\sqrt{g \frac{(\rho_c - \rho_h)(H - h)h}{\rho_c h + \rho_h(H - h)}}$	\sqrt{gd}	[79]

All discussed correlations have one limitation in common: they have been derived for flat ceilings. They also have existing asymptotes for intense fires ($\rho_h \rightarrow 0$). The asymptotic values for the correlations of Yih, Kunsch, SPRINT and CAMATT are close to, yet slightly higher than the asymptotic values of the critical velocity (see section 2.4). This is to be expected, as the momentum of the smoke layer will be similar to the momentum of the slower but denser ventilation flow when the critical ventilation velocity is applied.

Figure 14 shows the correlations for the six-meter-high tunnel of the example EX1 (see Table 3). The correlation derived from Alpert's correlations (4-5) leads to higher velocities since it represents the maximum velocity, rather than the average velocity of the smoke layer.

The correlation by Kunsch agrees fairly well with the theoretical equation (4-20) for which no Boussinesq approximation is made. The latter one is shown in the graph as the correlation by Shin et al. for a h/H -ratio of 50%. Kunsch applied the propagation velocity directly on the flow, without taking into account the effect of the ventilation. He validated his model for upstream flows close to the seat of the fire, at critical ventilation velocities. For this validation, he compared the results of his model with fire tests in the tunnel or gallery of the HSL in Buxton ($H = 2.5m$) and laboratory-scale tests by Megret, Vauquelin and Casale [82].

In SPRINT, lower propagation velocities are applied ($k = 0.5 \dots 0.67$) with an upper limit equal to the correlation by Yih. In contrast to Kunsch's model, these velocities are superposed to the ventilation velocity. Consequently, the critical velocity is the ventilation velocity which equals the velocity of the smoke propagation: the momentum equilibrium is not taken into account and neither is the lower layer velocity (which is higher than the main ventilation velocity, as the cold air is forced to flow underneath the smoke, through a smaller section). The validation is achieved by the comparison of a single fire test in the Memorial tunnel.

In the proposed model, the correlation by Kunsch is chosen, as it has a more physical background.

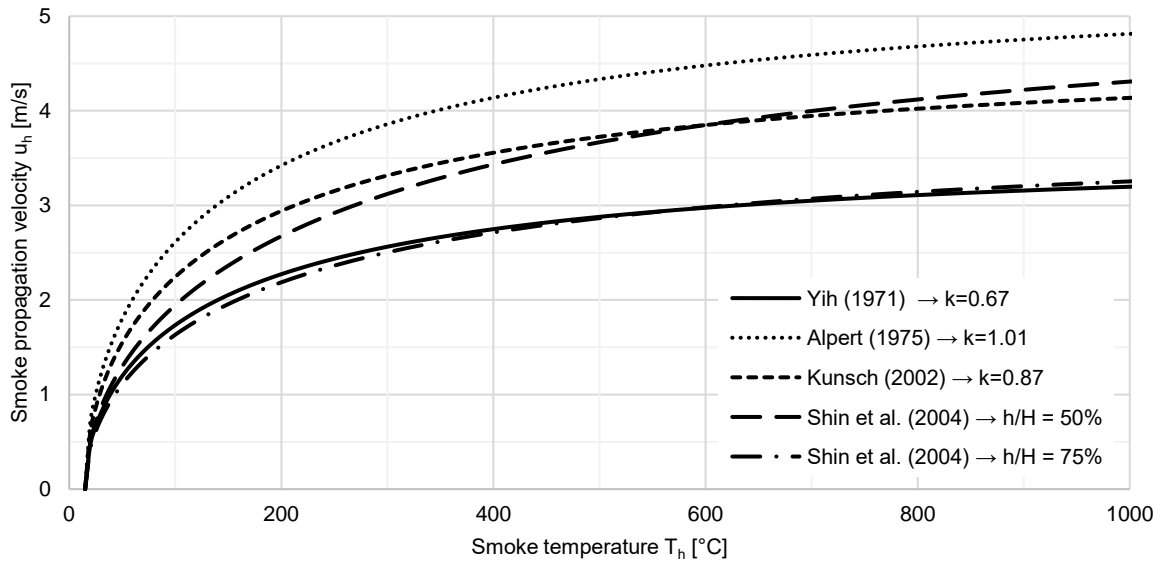


Figure 14: The smoke propagation velocity as a function of the hot gas layer temperature

4.5 Heat loss rates

As the smoke spreads through the tunnel, it loses heat towards the walls and the lower air layer. In this section, the sub-model that assesses the heat loss rate is described. First, it is described how heat is transferred by convection, radiation, and conduction. Afterwards, the choices for the proposed model are clarified.

Convection

The hot smoke layer is assumed to travel longitudinally through the tunnel. Therefore, forced convection will take place between the smoke layer and the flanking walls. No theoretical model exists to assess the convective heat transfer, with exception of direct numerical simulations (DNS) by computational fluid dynamics (CFD) simulators. Therefore, in practical applications, the convective heat transfer coefficient h_c is always estimated from empirical correlations.

Many correlations can be found in the literature. Here, the correlation of Gnielinski [83] is applied (4-24), which described the convection of turbulent flows through circular tubes. The correlation is also employed in CAMATT and in the current one-layer model of FESG. The same correlation can be used in the two-layer model by using the hydraulic diameter \bar{H} of the flow section, rather than the entire tunnel section.

$$h_c = \frac{\lambda Nu}{\bar{H}}, \quad Nu = \frac{\lambda_l}{8} \frac{Re - 1000Pr}{1 + 12.7 \left(\frac{\lambda_l}{8}\right)^{\frac{1}{2}} \left(Pr^{\frac{2}{3}} - 1\right)}, \quad Re = \frac{u\bar{H}}{\nu}, \quad \lambda_l = 0.02, \quad Pr = 0.7, \quad \bar{H} = \frac{4A}{P} \quad (4-24)$$

Note that the convection coefficient is a function of the flow velocity u and the flow temperature T through the Reynolds number Re and the dynamic viscosity ν .

For the example EX1 (see Table 3), the convective heat coefficient varies from 11.9 to 6.1 W/m²/K and for EX2 from 19.8 to 9.4 W/m²/K. The complete profile is presented in Figure 24.

Radiation

In the one-layer model, opaque smoke is typically assumed to fill the whole tunnel section. Therefore, the radiation can be calculated using a simple equation:

$$\dot{q}'' = \varepsilon\sigma(T_s^4 - T_w^4) \quad (4-25)$$

With

\dot{q}''	the heat flux per unit wall area [kW/m ²]
ε	the emissivity of the smoke layer [-]
σ	the Stefan-Boltzmann constant, which equals $5.670 \cdot 10^{-8}$ W/m ² /K ⁴
T_{sm}, T_w	the smoke temperature and the wall surface temperature [K]

In the two-layer model, the smoke will exchange convective heat with the adjacent walls, along the wet perimeter P_c of the smoke layer. In addition, the smoke layer also exchanges thermal radiation with the cold and with the hot walls, along the smoke perimeter P_r . The concept is illustrated in the figure below.

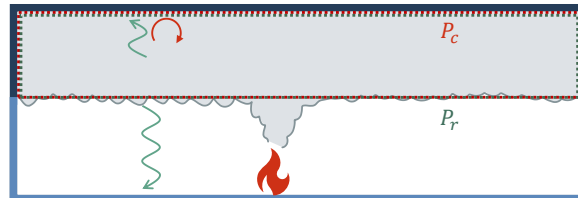


Figure 15: Radiative and convective heat transfer among two different perimeters

Conduction

The conduction through the walls can be simplified by assuming a one-dimensional (4-26) or a cylindrical heating problem (4-27). The first is more appropriate for rectangular cross-section and small thermal penetration depths. The latter is more appropriate for circular sections, horseshoe section or any section when the thermal penetration is deep.

The heat equation can then be simplified further by assuming that no heat generation will take place inside the walls and by assuming that the material properties (k, ρ, c) are homogenous, isentropic, and independent of the temperature. Consequently, the heat equations can be rewritten as the following partial derivatives [84].

$$\frac{\partial T}{\partial t} = \alpha \frac{\partial^2 T}{\partial x^2} \quad (4-26)$$

$$\frac{\partial T}{\partial t} = \alpha \frac{1}{r} \frac{\partial}{\partial r} \left(r \frac{\partial T}{\partial r} \right) \quad (4-27)$$

This derivative can be solved numerically. In the one-layer model, this requires one mesh for every cell of the flow domain. In the two-layer model, it requires at least two meshes for every cell (one for the 'cold walls', and one for the 'hot walls'). As a result, the conduction model does have a large contribution to the computational cost of the complete model.

As briefly mentioned in section 4.1, the proposed model assumes inert walls. The walls are assumed to maintain their initial temperature and therefore, only convection and radiation are accounted for. This simplification has been made to avoid the complex submodel for conduction. However, in later work, the simplification can easily be undone.

4.6 Solution schemes

In this section, the applied schemes are explained, and more details are given about the numerical techniques. Figure 8 provides visual support.

Solver of the fire plume

As mentioned briefly in section 4.1, the flow properties at the seat of the fire ($h_{pl}, \rho_{pl}, T_{pl}, \dot{m}_{pl}$) are derived by formulating the mass flow rate from three different perspectives. The concept is visualized in Figure 16.

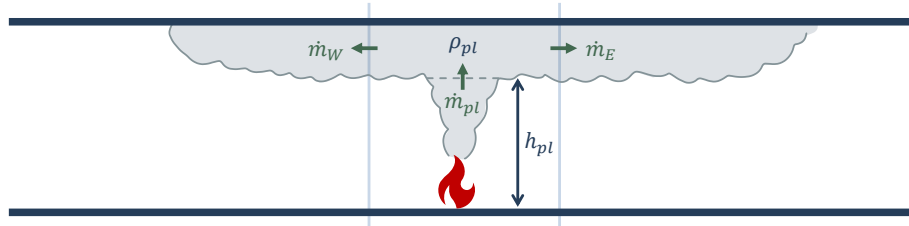


Figure 16: Mass flow at the seat of the fire

The first mass flow rate is the plume correlation by Ingason and Li (2010), the second is calculated from the convective heat and the third from the velocity through the section of the layer. Note that the effect of the ventilation flow is accounted for in the plume correlation. For the third mass flow rate, the smoke velocity can be considered superposed on the ventilation flow. However, this velocity is eliminated in the sum of the flow upstream (\dot{m}_W) and downstream (\dot{m}_E). The set of equations is as follows:

$$\begin{cases} \dot{m}_1 = \dot{m}_{pl} = 0.3735 \dot{Q}_c^{\frac{1}{3}} (h_{pl} - h_f)^{\frac{5}{3}} V^* \\ \dot{m}_2 = \frac{\dot{Q}_c}{c_p (T_{pl} - T_0)} = \frac{\dot{Q}_c R}{c_p p_{atm} M \left(\frac{1}{\rho_{pl}} - \frac{1}{\rho_0} \right)} \\ \dot{m}_3 = \dot{m}_W + \dot{m}_E = 2(H - h_{pl}) W \rho_{pl} u_{pl} \end{cases} \quad (4-28)$$

with

$$V^* = \max \left(0.19, \frac{u_0}{w^*} \right), \quad w^* = \left(\frac{g \dot{Q}}{b_f \rho_0 c_p T_0} \right)^{\frac{1}{3}}, \quad u_{pl} = k \sqrt{gH \frac{\rho_0 - \rho_{pl}}{2\rho_0}}$$

The three mass flow rates combine into two equations, which are solved for the smoke height and smoke density with a multivariate Newton Raphson scheme. In order to improve the efficiency of the Newton Raphson scheme, the partial derivatives are also calculated analytically. Those partial derivatives are presented in [Appendix A](#). Their implementation is verified numerically. The multivariate Newton Raphson scheme is given by equation (4-29) [85]:

$$\mathbf{x}_{k+1} = \mathbf{x}_k - \mathbf{J}_k^{-1} \mathbf{F}(\mathbf{x}_k) \quad (4-29)$$

with

$$\mathbf{x} = \begin{Bmatrix} h_{pl} \\ \rho_{pl} \end{Bmatrix}, \quad \mathbf{F}(\mathbf{x}) = \begin{cases} f_1(\mathbf{x}) = \dot{m}_1 - \dot{m}_2 = 0 \\ f_2(\mathbf{x}) = \dot{m}_1 - \dot{m}_3 = 0 \end{cases}, \quad \mathbf{J} = \begin{bmatrix} \frac{\partial f_1}{\partial h_{pl}} & \frac{\partial f_1}{\partial \rho_{pl}} \\ \frac{\partial f_2}{\partial h_{pl}} & \frac{\partial f_2}{\partial \rho_{pl}} \end{bmatrix}$$

Here, \mathbf{x}_k represents the unknowns of a certain timestep at iteration k . The iteration process is repeated until convergence is reached. After convergence, the temperature T_{pl} , the mass flow rate \dot{m}_{pl} and the velocity u_{pl} are obtained from the height h_{pl} and the density ρ_{pl} .

Solver of the upstream flow

The upstream mass flow rate is determined as discussed in section 4.2: the influence of the ventilation velocity is not taken into account. Therefore, the mass flow rate can be written as follows:

$$\dot{m}_{up} = \frac{1}{2} \dot{m}_{pl,0} = 0.03548 \dot{Q}_c^{\frac{1}{3}} (h_{pl} - h_f)^{\frac{5}{3}} \quad (4-30)$$

Before the properties of the upstream mass flow are calculated, it is verified if an upstream mass flow would occur. This is done with the same criterium as for the back-layering front (4-34). If the ventilation flow has sufficient momentum to counter the smoke flow at the seat of the fire, no back-layering will occur, and the calculations are stopped.

If not, the smoke layer height, velocity, and temperature (or density) need to be calculated. Since the complex nature of the heat equation, this process is done iteratively, according to the following scheme:

1. The temperature is estimated to equal the temperature of the neighbouring cell downstream. For the first cell, this is the plume temperature. The density follows from the ideal gas law.
2. The velocity is calculated from the smoke propagation correlation by Kunsch [71]. Here, no influence of the ventilation velocity is modelled.

$$u_{h,P0} = k \sqrt{gH \frac{\rho_0 - \rho_{h,P0}}{2\rho_0}} \quad (4-31)$$

Note that in SPRINT, a superposition of a similar correlation with the ventilation velocity is applied. However, this superposition does not allow to balance the momentum of the involved flows (as it balances the velocity instead).

3. The height of the smoke layer is calculated from the mass balance:

$$\dot{m}_{up} = \rho_{h,P0}(H - h_{P0})Wu_{h,P0} \rightarrow h_{P0} = H - \frac{\dot{m}_{up}}{\rho_{h,P0}Wu_{h,P0}} \quad (4-32)$$

4. Next, the heat balance is employed to make a new temperature approximation T_{P0} for cell P0 (Figure 17). A simple finite volume method is employed. The walls and lower air layer are assumed to maintain their initial temperature and therefore, the heat losses of the smoke layer can be calculated as explained in section 4.5. For the ease of implementation, a simple upwind interpolation scheme is used ($T_{h,E0} = T_{h,E1}$, $T_{h,W0} = T_{h,P0}$) to assess the inflowing and outflowing heat rates ($\dot{Q}_{in} = \dot{m}_{up}c_pT_{h,E0} = \dot{m}_{up}c_pT_{h,E1}$, $\dot{Q}_{out,P0} = \dot{m}_{up}c_pT_{h,W0} = \dot{m}_{up}c_pT_{h,P0}$). Therefore, the new temperature approximation of $T_{h,P0}$ is calculated from the equation below.

$$\dot{Q}_{out,P0} = \dot{Q}_{in,P0} - \dot{Q}_{loss,P0} \rightarrow T_{h,P0} = \frac{\dot{Q}_{in,P0} - \dot{Q}_{loss,P0}}{\dot{m}_{up}c_p} \quad (4-33)$$

Step 2 is resumed with the new temperature approximation.

The process is repeated until convergence is reached. The simple upwind scheme requires small cells and therefore, neighbouring cells have similar temperatures. Consequently, convergence is reached after a couple of iteration. More advanced interpolation schemes, such as parabolic upwind schemes, can be applied later to create a more stable finite volume method that allows for bigger mesh cells and are therefore less computational costly.

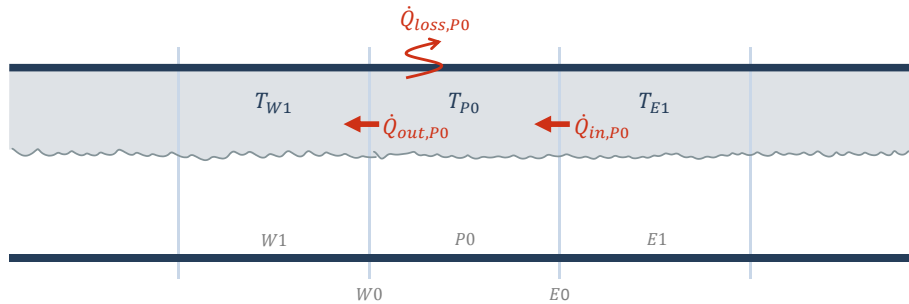


Figure 17: Heat balance of cell P0

After convergence, the overall momentum balance of the cell is verified. Kunsch [71] derived a formula to verify if the momentum of the main velocity balances out the momentum of the back-layering flow. In his derivation, he assumes that the back-layering front deflects and flows downstream at the same speed as the cold air flow below it. This cold air flow increases velocity once it flows underneath the smoke layer, as the section of the flow is reduced. The confinement ventilation velocity that is required to halt the smoke layer propagation ($u_{0,r,P0}$) is given by the following equation [71]:

$$u_{conf,P0}^2 = \frac{H - 2d_{P0}}{H + 2d_{P0}} \left[4 \left(1 - \frac{\rho_{P0}}{\rho_0} \right) g \frac{d_{P0}(H - d_{P0})}{H} + \left(\frac{\rho_{P0}}{\rho_0} \right) u_{P0}^2 \frac{H - 4d_{P0}}{H} \right] \quad (4-34)$$

Therefore, the condition $u_0^2 \geq u_{conf,P0}^2$ is checked for every cell. Once the condition is true, the momentum is in equilibrium and the back-layering front is reached.

Solver of the downstream flow

The solver of the downstream flow is conceptionally identical to the solver of the upstream flow. Only three differences are present:

- As the upstream flow is always present, there is no need to verify this.
- When the flow loses buoyancy, it is carried with the ventilation flow. Therefore, the ventilation velocity defines the minimum smoke propagation velocity.
- As the upstream flow is unbalanced, the iterations are stopped when a predefined length (instead of a momentum equilibrium) is reached. This is typically the downstream portal of the tunnel.

5 DISCUSSION OF THE RESULTS

In this chapter, the outcome of the model is presented by means of examples EX1 and EX2 (Table 3). The first example corresponds to the peak heat release rate of a single passenger car [53], the second of two busses, a small lorry or a metro carriage [53]. The effect of the prescribed heat release rate and ventilation velocity are discussed, and the comparison has been made with empirical correlations and experimental data.

The first section discussed the critical velocity, and the second section elaborates on the flow properties. Next, the back-layering length is examined. Last, the effect of an elevated fire seat is treated.

5.1 Critical velocity

The model that is proposed in chapter 4 does not require the explicit assessment of the critical velocity. However, this velocity can be calculated easily in an iterative process:

1. An initial guess is made for the critical ventilation velocity.
2. The properties at the seat of the fire are calculated by ‘the solver of the fire plume’ (see section 4.1).
3. The critical ventilation velocity is calculated as the confinement velocity (4-31), considering the properties at the fire plume as the properties at the back-layering front.
4. Step two is repeated with the new ventilation velocity until convergence occurs.

Figure 18 shows the critical velocity for EX1 (see Table 3). The radius of the seat of the fire varies with the total heat release rate to maintain the prescribed heat release rate per unit area of 1 MW/m^2 .

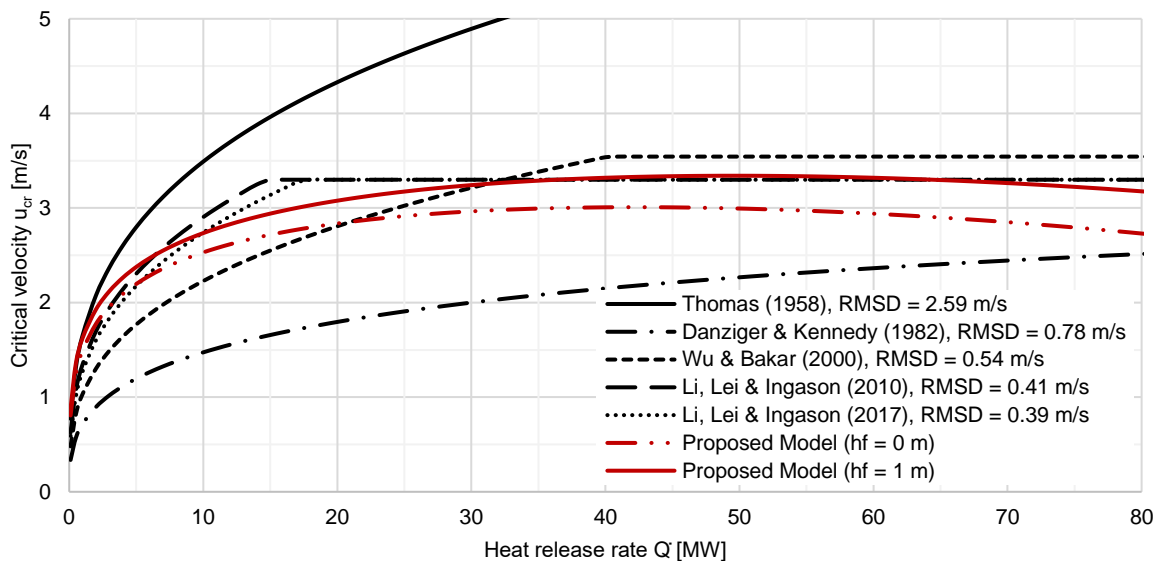


Figure 18: Critical velocity as a function of the total heat release rate for EX1
The RMSD is calculated for a heat release rates up to 87.8 MW (validity domain)

The employed plume mass flow rate is derived from a free plume model and, therefore, loses accuracy when the flames reach the ceiling. The average height of the flames can be estimated with the empirical correlation by Heskestad [86]:

$$H_f = 0.235Q^{2/5} - 2.04b_f \quad (5-1)$$

Although this flame length correlation itself is derived for free plumes of round pool fires, it can offer a rough approximation for flame lengths in tunnels. For EX1, the flames touch the ceiling for heat releases of 6.7 MW and larger (11.4 MW when h_f equals 0). However, the plume correlation has been validated by Li, Lei and Ingason for tunnel fires with small-scale and large-scale experimental data and seem to

agree with this data till a temperature rise ΔT_{pl} equal to 1350 K occurs. This occurs for heat releases of 73.2 MW and larger (87.8 MW when h_f equals 0).

The critical velocity reaches a maximum value for heat releases rates of 45 MW (42 MW when h_f equals 0 m) and slowly decreases for more intense fires. This is contractionary to the constant critical velocity, generally assumed in literature for high heat release rates. This effect is related to the lowering mass flow rate: the decreasing smoke layer height leads to less air entrainment, despite the rising heat release rate and rising fire radius, as shown in Figure 19.

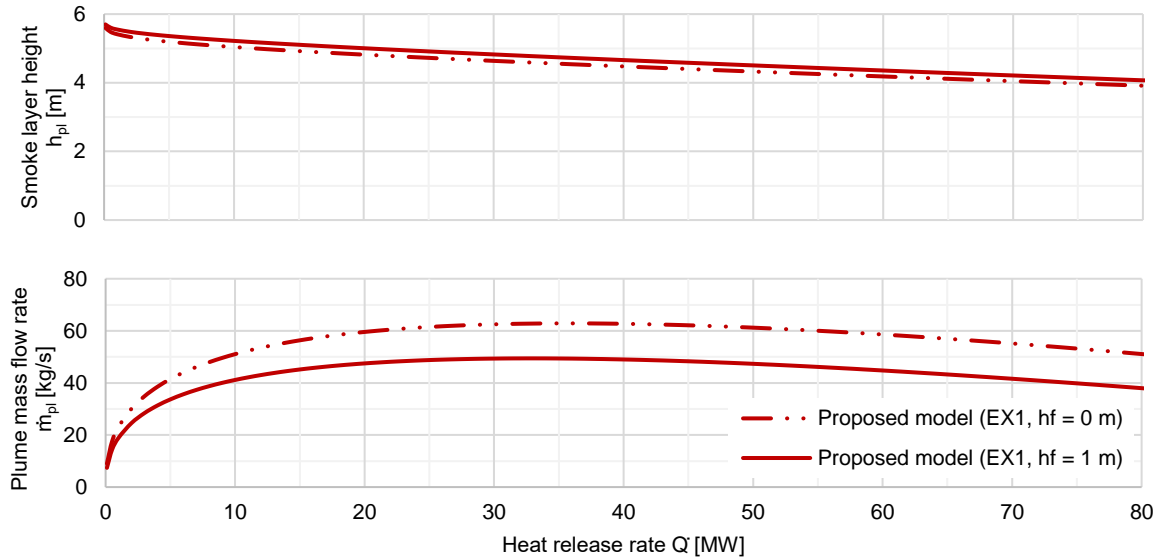


Figure 19: Smoke layer height and plume mass flow rate in function of the heat release rate (EX1)

Regardless of this slight decay, this outcome of the proposed model agrees well with the correlations. Note that the correlation of Li, Lei and Ingason [52] is obtained from small-scale tests for which the methane burner was placed in the floor of the model. Therefore, the results should be primary compared to a similar problem (h_f equal to 0 m). The agreement is qualified by the root mean squared deviations (RMSD) of the correlations and the model (h_f equalling 0) over the validity domain (0 – 87.8 MW). The RMSDs are listed in Figure 18.

The critical velocity of the proposed model can also be compared directly to experimental data. For this purpose, the example above has been presented on a dimensionless graph (Figure 20). The dimensionless parameters are scaled with the tunnel height (2-9), even though some of the correlations employ different scales.

Figure 20 shows the critical velocity of the proposed model as well as experimental data. The large-scale experimental data is gathered by Li, Lei and Ingason [45] from different fire tests in the Memorial tunnel, the Runehamar tunnel, the Yuanjiang tunnel and the Repparfjord tunnel. The values are corrected for short back-layering lengths and slopes by Li, Lei and Ingason. A more detailed description of the tests can be found in [87], [88]. The small-scale experiments were conducted by Li, Lei and Ingason themselves [45].

Figure 20 reveals that the experimental data is well scattered and that the outcome of the correlations and models should always be treated carefully, as the uncertainties are high. Nevertheless, the experimental data and the outcome of the proposed model are considered to have a satisfactory agreement.

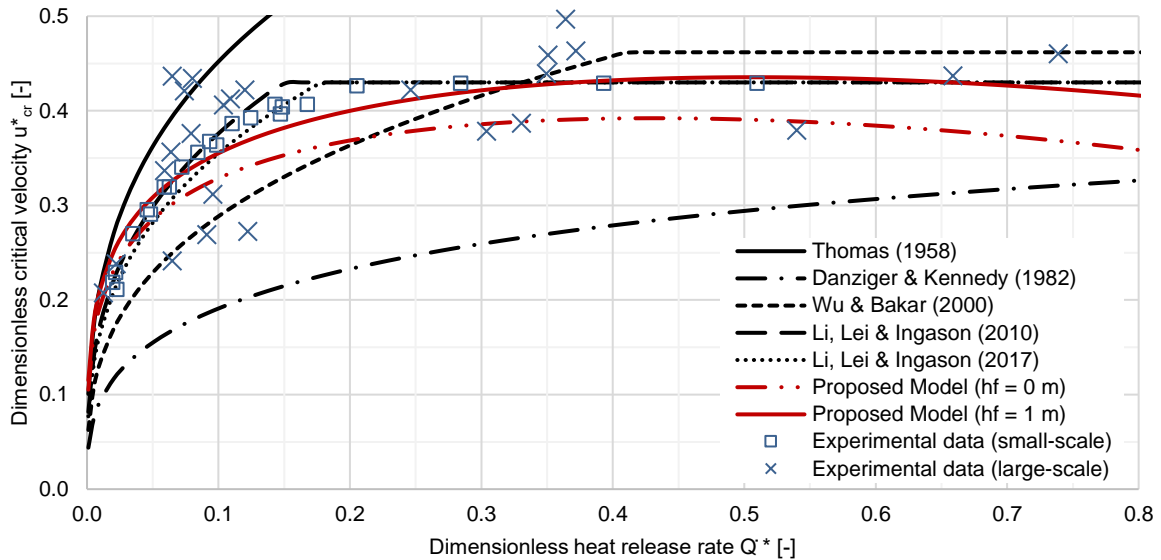


Figure 20: Dimensionless critical velocity, presented with experimental data from Li, Lei & Ingason [45]

For EX1 and EX2, the critical velocity is equal to 2.39 m/s and 3.24 m/s respectively (according to the proposed model). The sensitivity of this outcome to the input values is represented in the tornado diagram below, which shows the effect on the critical velocity when the input values are increased or decreased by 10%. Note that sensitivities do depend on the chosen base case. Moreover, the sensitivity also depends on the chosen unit of the input parameter. Here, the initial temperatures increase and decrease is expressed in degrees Celsius ($\pm 1.5^{\circ}\text{C}$) and not in degrees Kelvin (which would lead to $\pm 29\text{K}$). Naturally, the choice of parameter does also influence the result ($H_{eff} = H - h_f$ and not h_f , W and not $\varphi = W/H$, \dot{q}'' and not $b_f \dots$).

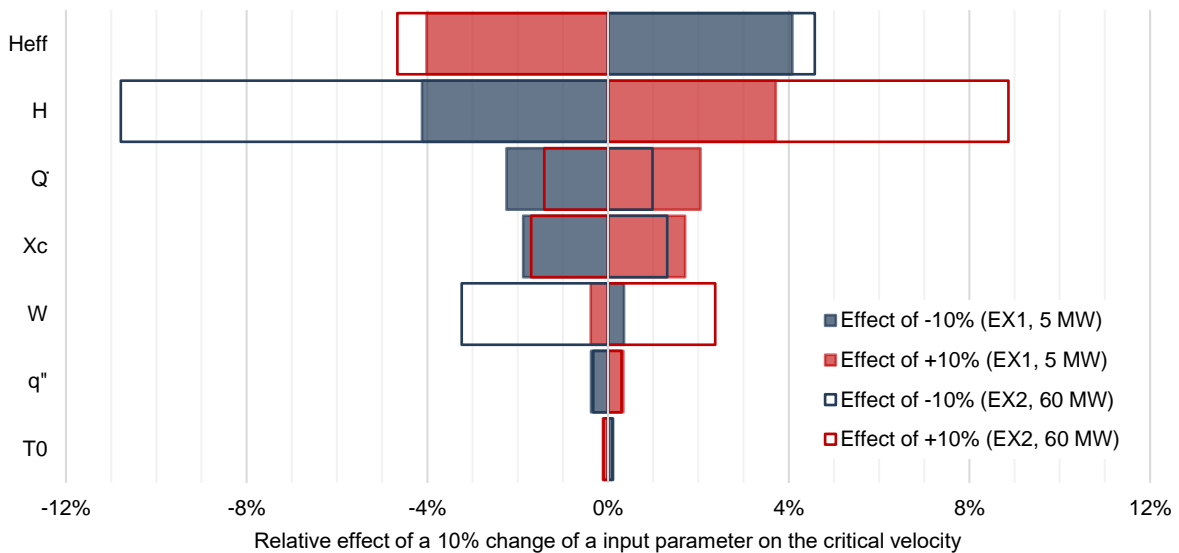


Figure 21: Sensitivity of the critical velocity for EX1 and EX2

The critical velocity is not very sensitive to the input values, because a 10% change in input values leads to smaller changes (with exception of the height for EX2). The two most important sensitivities are the effective height and the total height. For EX1, the outcome is also sensitive to \dot{Q} and χ_c . Due to the decreasing critical velocities for higher heat releases (discussed above), these sensitivities reverse for EX2. Note that they are more significant than what would be expected from Figure 19. This is because the absolute increase of heat is much higher in EX2 (10% of 60 MW compared to 10% of 5 MW), while for all other parameters, the increase and the decrease are identical for both problems.

5.2 Flow profiles

The proposed model provides the flow properties as a function of the distance to the seat of the fire. This is illustrated with EX1 and EX2 in [Figure 22](#) and [Figure 23](#). The negative distances represent locations upstream of the seat of the fire, and the positive distances represent downstream locations.

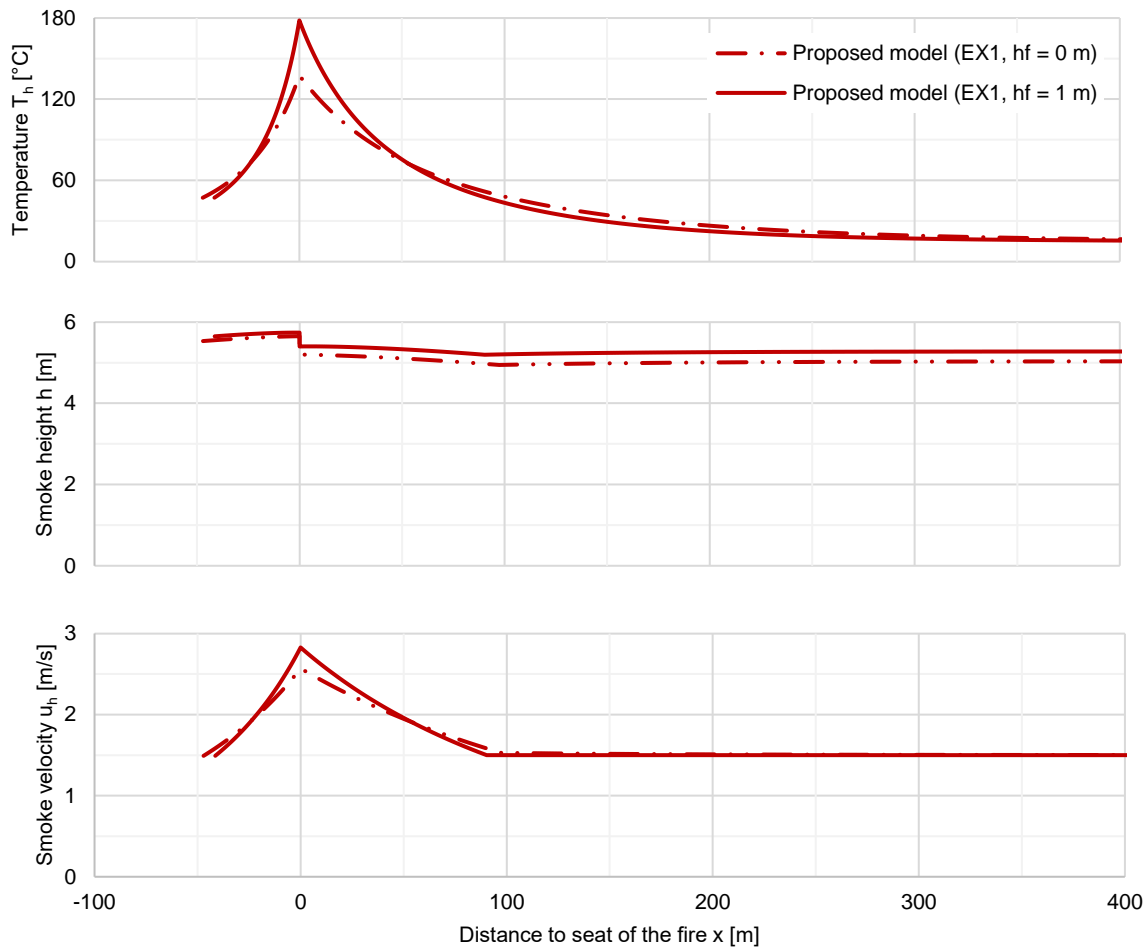


Figure 22: Temperature, height, and velocity profiles of the smoke layer of EX1

The smoke temperatures of EX1 are the highest close to the seat of the fire and decrease with distance, due to the heat loss. Further away from the seat of the fire, the temperature gradient is lower, as the heat loss is driven by a lower temperature difference between the smoke and the walls. A similar profile occurs for the smoke velocity, as the smoke propagation is driven by buoyancy. At a certain distance downstream from the seat of the fire (here 90.3 m), the smoke layer has cooled down sufficiently and the smoke propagates at the main ventilation velocity. Since the temperature decrease (density increase) comes with a decrease in velocity, the smoke layer heights remain quite constant in the downstream and the upstream flow.

The same trends are visible for EX2 ([Figure 23](#)). The more intense fire results in higher temperatures and higher smoke layer velocities. Due to the higher temperature gradients, the smoke layer height changes significantly, close to the seat of the fire.

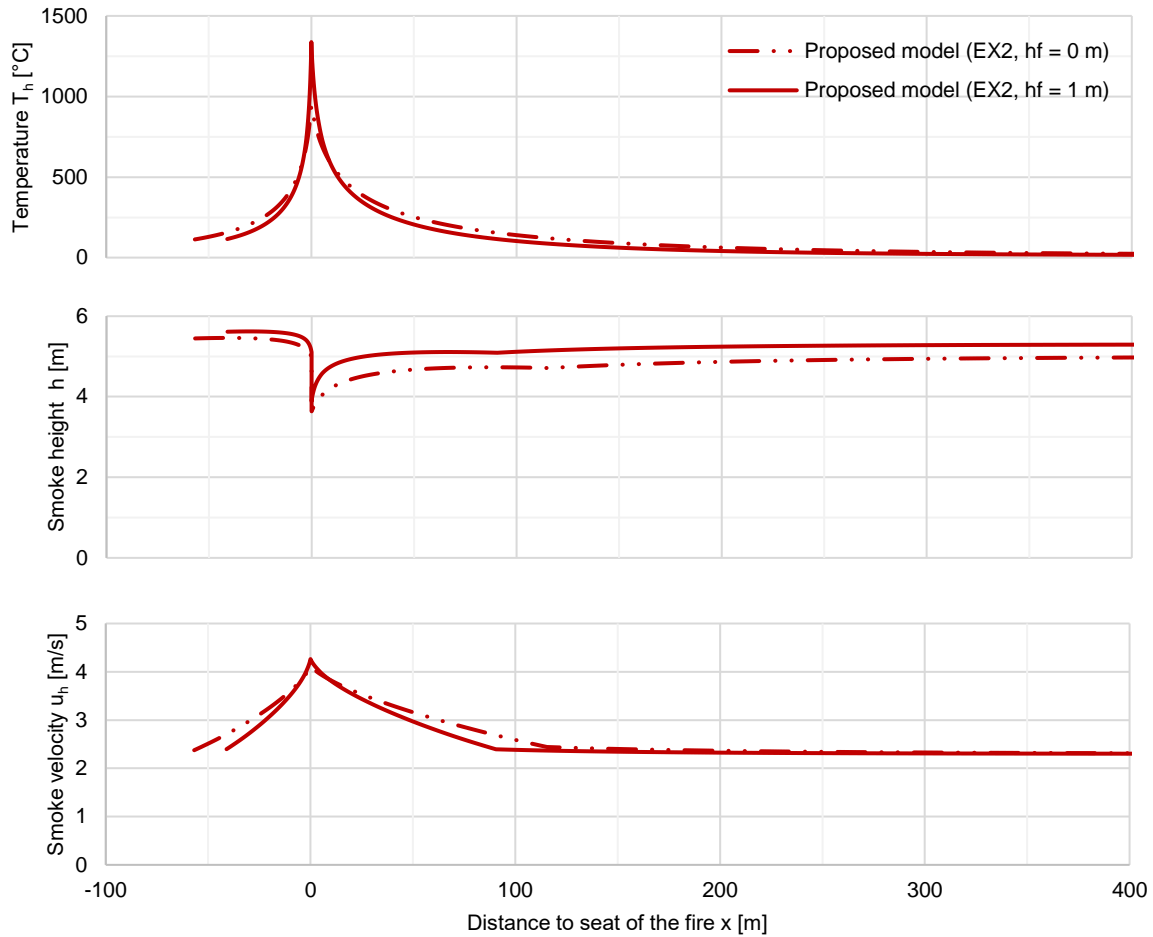


Figure 23: Temperature, height, and velocity profiles of the smoke layer of EX2

The temperature profile can be compared with the analytical steady-state formula, derived by Ingason, Li and Lönnemark for longitudinal ventilated tunnels [89]:

$$\frac{\Delta T(x)}{\Delta T_{max}} = \exp\left(-\frac{h_t(W + 2d)}{\dot{m}c_p}x\right) \quad (5-2)$$

To derive this formula, three assumptions are made: (1) entrainment can be neglected, (2) the smoke height is constant and (3) the heat losses can be presented by a constant heat coefficient h_t . The latter assumption is the most problematic, especially for fires with high smoke temperatures for which radiation is dominant. Consequently, the value of h_t should be chosen wisely. The value 25 W/m²/K is suggested [89], and therefore also applied here to compare the model with the formula.

Figure 24 shows the total heat coefficient h_t , which correspond to the heat loss calculations of the proposed model. For EX1, 25 W/m²/K is a reasonable assumption. For EX2, the high temperatures lead to dominating radiative losses (fourth power in (4-25)). Consequently, the heat loss coefficient is far less constant.

Despite the assumptions, Ingason, Li and Lönnemark found that the temperature profiles in small-scale and large-scale tunnel fires relates well with an exponential formula (5-3). The large-scale experimental data originates from fire tests in the Memorial tunnel and the Runehamar tunnel, mentioned before.

$$\frac{\Delta T(x)}{\Delta T_{max}} = 0.55 \exp\left(-0.143 \frac{x}{H}\right) + 0.45 \exp\left(-0.024 \frac{x}{H}\right) \quad (5-3)$$

The empirical formula (5-3) does not take into account the temperature rise at the seat of the fire ΔT_{max} , nor does it take into account the ventilation velocity. Note that, despite the numerous data points, the formula is based on a limited number of fire scenarios and tunnels and that it should be treated critically.

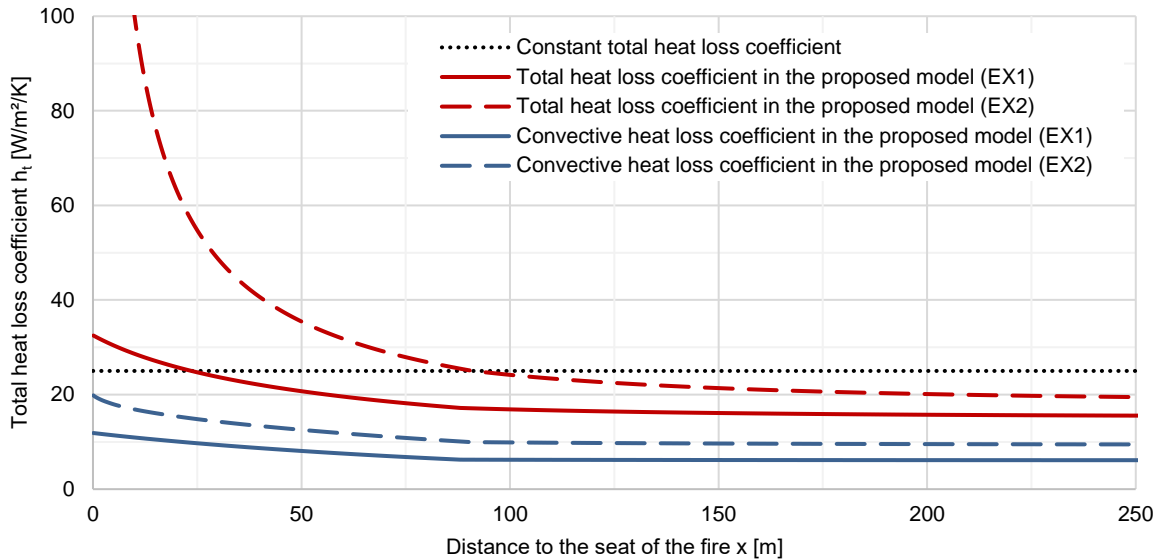


Figure 24: Comparison between the constant heat loss coefficient and the proposed model (for EX1 and EX2)

Figure 25 shows the dimensionless temperature rise $\Delta T/\Delta T_{max}$ as a function of the dimensionless distance to the seat of the fire x/H . For the theoretical formula (5-2), the average height h and the downstream smoke mass flow rate \dot{m} are adopted from the proposed model.

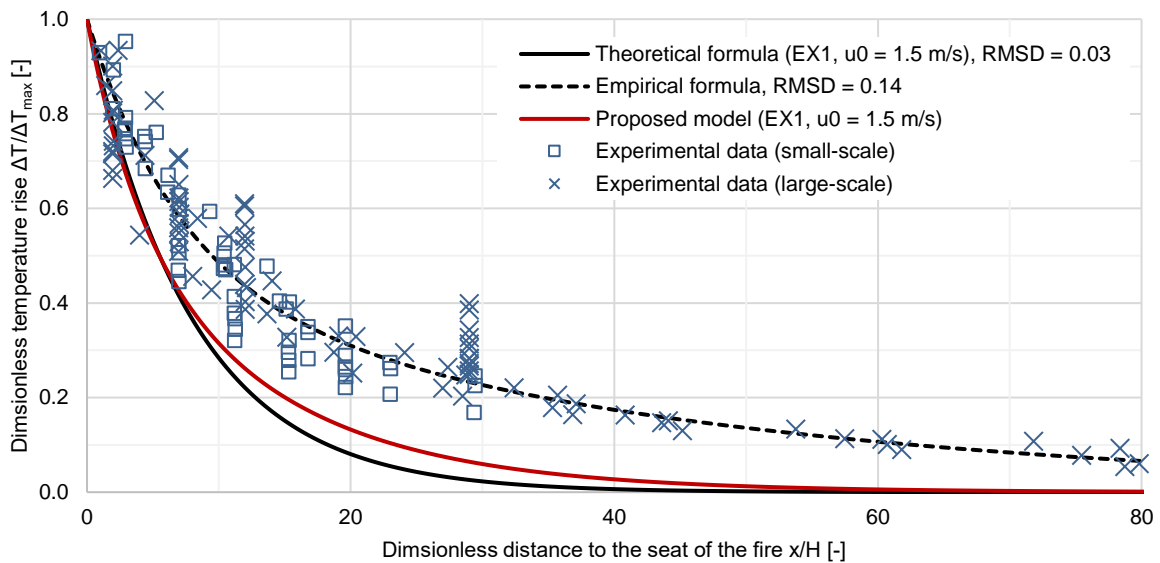


Figure 25: Downstream temperature profile for EX1, with a ventilation velocity of 1.5 m/s. The theoretical and empirical formula, as well as the experimental data, are adopted from [89].

The theoretical formula shows a good agreement (RMSD = 0.03), as expected due to the reasonable heat loss coefficient (Figure 24). The empirical formula does not show a good agreement. This is probably caused by two inaccurate assumptions: (1) the mass distribution upstream and downstream and (2) the inert walls. Appendix B elaborates on this matter. The disagreement is even higher for EX2 (also presented in Appendix B).

5.3 Level of stratification

The model does not consider entrainment or mixing of the two layers. In reality, the stratification of smoke flow over fresh air disappears at a certain distance, where the buoyancy forces become weak, as explained in section 2.2. It is at the beginning of the second region (RII) that the stratification becomes less distinct. At the end of the region, stratification is entirely absent. Table 6 shows the position of this region. To calculate the temperature difference of the Froude number Fr_N , the difference between the

two layers is used. Therefore, the Froude number might be slightly overestimated, resulting in shorter distances to the seat of the fire.

Table 6: Position of destratification (region RII) for EX1

Source	Froude number	Limits of RII [-]	Position of RII [m]
Newman (1984) [42]	Fr_N	0.90 10.0	154.1 527.3
Nyman and Ingason (2012) [34], [43]	Fr_N	0.90 3.20	154.1 350.4
Zeng, Xiong et al. (2018) [44]	Correlation for length, see equation (2-5)		108.6

This position varies significantly (from 109 to 527m), depending on the author and consequently, no strong conclusion can be drawn without further research.

Note that the densimetric Froude number reaches 0 where the downstream velocity is assumed to equal the velocity of the fresh air below (for this example, this occurs at 90 m). Therefore, this number is of no use for the model. However, the densimetric Froude number can be calculated when other modelling assumptions are made, such as the superposition of the ventilation velocity and the smoke propagation (as in SPRINT). In this case, the number cannot be considered a pure 'measurement', as it is partly defined by the chosen smoke propagation velocity:

$$Fr_\rho = \frac{u_r}{\sqrt{gd \frac{\rho_c - \rho_h}{\rho_c}}} = \frac{k \sqrt{gH \frac{\rho_c - \rho_h}{2\rho_c}}}{\sqrt{gd \frac{\rho_c - \rho_h}{\rho_c}}} = k \sqrt{\frac{H}{2d}} \quad (5-4)$$

Therefore, the Froude number is dictated by the velocity correlation (k) and the layer thickness (d), which remains rather constant. In CAMATT, a constant Froude number is even predefined for the downstream flow.

5.4 Back-layering length

One of the most important features of the proposed model is its prediction of the back-layering length. This length is a crucial parameter for risk assessment concerning life safety. Figure 26 shows the results of the proposed model for EX1 and Figure 27 for EX2, for varying ventilation velocities. Figure 28 shows the results for varying heat release rates.

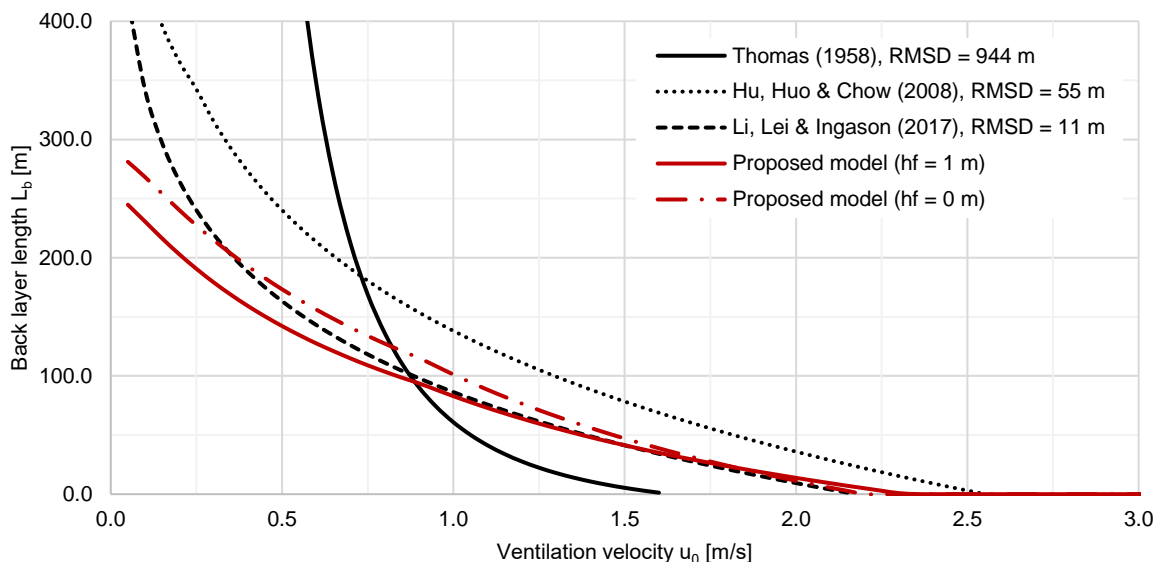


Figure 26: Back-layering length as a function of the ventilation velocity for EX1 ($\dot{Q} = 5 \text{ MW}$)
The RMSD is calculated for a ventilation velocity in between 0.25 and 2.19 m/s (critical velocity) for $h_f = 0 \text{ m}$

The proposed model shows a good agreement with the back-layering length predictions, found in the literature, especially with the correlation by Li, Lei and Ingason. However, for particularly low ventilation velocities, the model does not reveal asymptotic behaviour. Nevertheless, this asymptotic behaviour is

expected, as the back-layering flow can propagate unrestrained for tunnels without ventilation flow. This might be related to the confinement velocity (4-32): for low ventilation velocities, the first term in between the brackets does not tend towards zero. Nevertheless, further research is required to make eloquent statements. When small ventilation velocities are applied (smaller than 10% of the critical velocity), it is advisable to consider unrestrained back-layering lengths. This is true even when the correlation of Li et al. is employed since the obtained length is extremely sensitive to the velocity.

Note that for EX2, the low ventilation velocity and the corresponding low plume entrainment lead to high plume temperatures. The temperature rise ΔT_{pl} is below 1350 K for ventilation velocities equal to and above 2.25 m/s. For lower velocities, the plume mass correlation might become inaccurate. However, Figure 27 shows that good agreements are found for much lower ventilation velocities, despite the correlation's limitations.

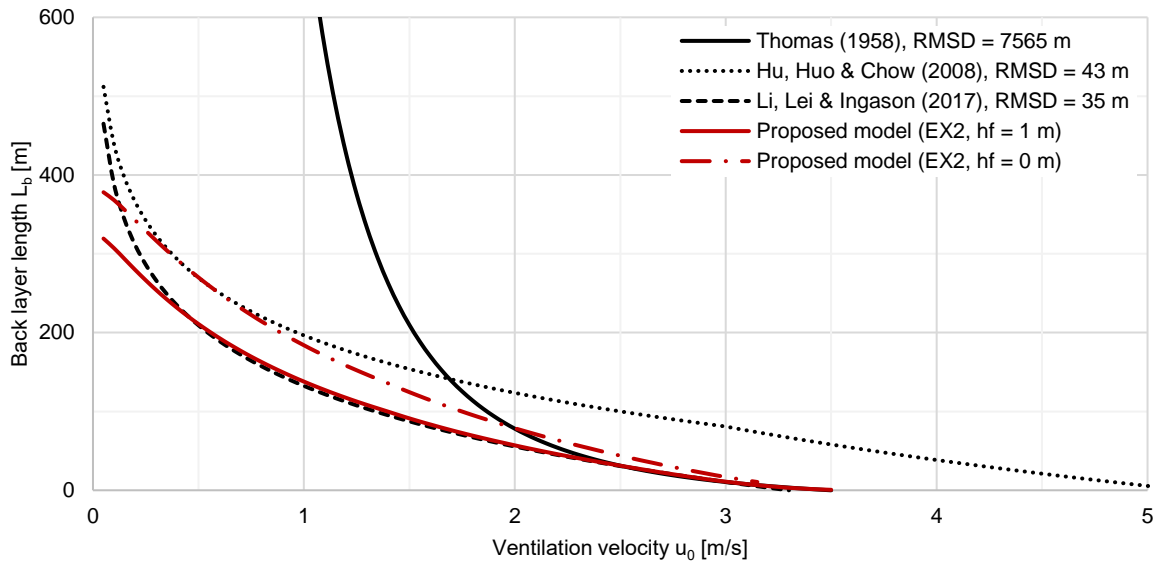


Figure 27: Back-layering length as a function of the ventilation velocity for EX2 ($\dot{Q} = 60 \text{ MW}$)
The RMSD is calculated for a ventilation velocity in between 0.25 and 3.50 (critical velocity) for $h_f = 0 \text{ m}$

The outcome of the proposed model can be compared to the experimental data of Li, Lei and Ingason [45], used to obtain the empirical correlation. In order to compare the small-scale fire test with the example problem, the data is expressed in the dimensionless confinement velocity u/u_{cr} and the dimensionless back-layering length L_b/H . The result is given in Figure 29.

The proposed model fits almost perfectly with the experimental data points. The slight discrepancies between the empirical correlation by Li, Lei and Ingason and the model, visible in Figure 26, Figure 27 and Figure 28 are therefore mainly caused by the discrepancies in the critical velocity. This is confirmed by Figure 18 and Figure 26: as the problem with h_f equal to 1 m correspond better to the correlation for the critical velocity by Li et al, it also corresponds better to the correlation for the back-layering length.

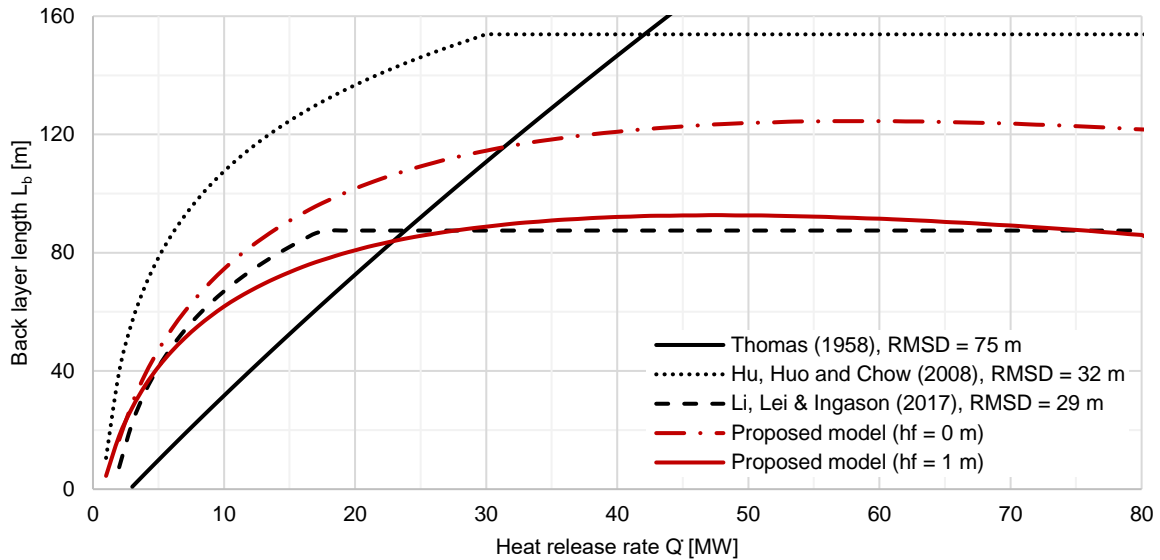


Figure 28: Back-layering length as a function of the heat release rate, for EX1 ($u_0 = 1.5\text{m/s}$)
The RMSD is calculated for heat release rates up to 87.8 MW (validity domain) for $h_f = 0\text{ m}$

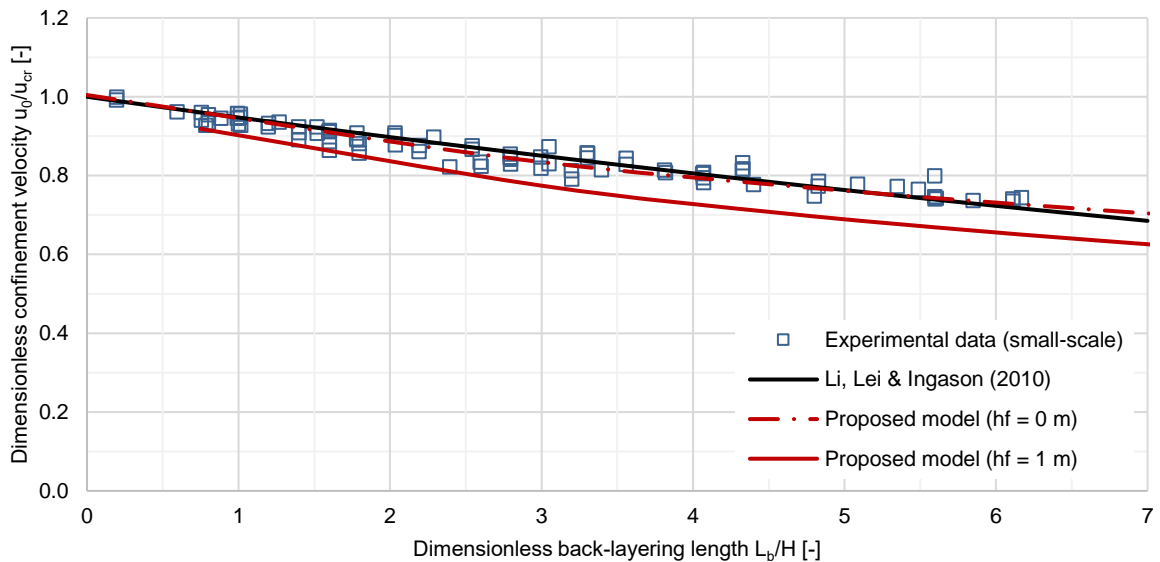


Figure 29: Dimensionless back-layering length as a function of the dimensionless confinement velocity presented with experimental data obtained by Li, Lei and Ingason [45]

For EX1 (5 MW, Table 3), the back-layering length is equal to 41m (according to the proposed model). The sensitivity of this outcome to the input values is represented in a tornado diagram (Figure 30), which shows the effect on the back-layering length when the input value is decreased or increased by 10%. This figure also presents the sensitivities of EX2 (60 MW, Table 3).

The back-layering length is very sensitive to the input values, as a 10% change in input value leads to changes up to 30% for EX2. The sensitivities to the ventilation flow and the tunnel geometry are the highest. For EX1, the next important parameter is the heat release rate and convective heat release rate (\dot{Q} and χ_c). For EX2, the back-layering length is less much sensitive to the heat release.

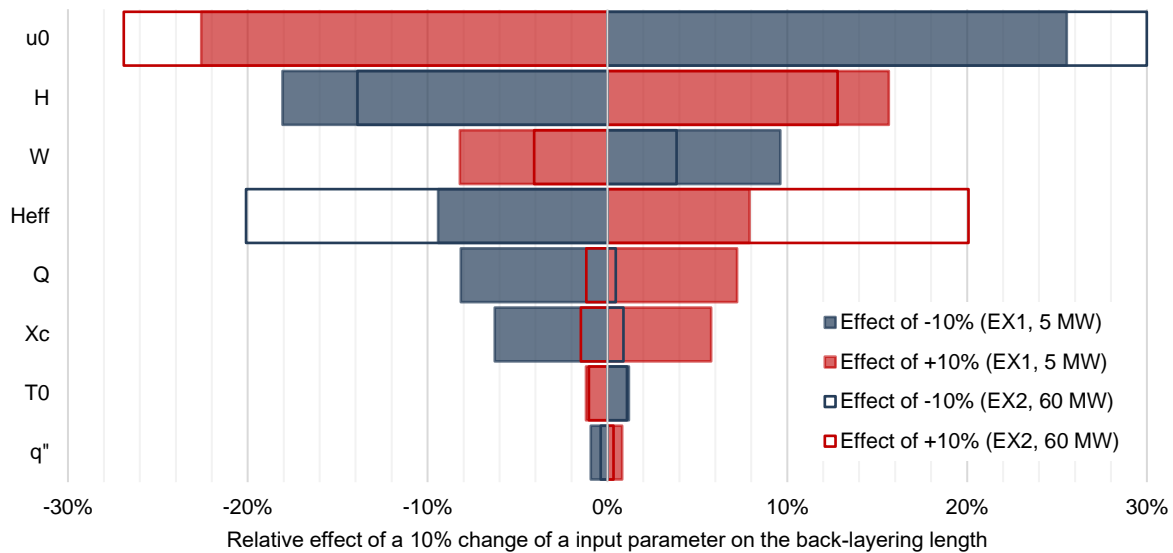


Figure 30: Sensitivity of the back-layering length for EX1 and EX2

5.5 Effective height and total height

Most small-scale fire tests are performed with a gas burner at ground level. For large-scale tests, liquid pool fires are often positioned on the floor. As a result, the effective height H_{eff} and total height H are identical and the elevation of the fire source h_f is often disregarded. However, the importance of this parameter has been reflected by the model, as shown in Figure 18 till Figure 30.

Despite the sensitivity of the result to this parameter, it might not be desirable to consider the height of the seat of the fire, as it is a difficult parameter to define for three-dimensional fires, such as vehicle fires. Above, it has been shown that assuming the seat of the fire to be levelled with the floor ($h_f = 0$), leads to conservative values, regarding the back-layering length. However, when the seat of the fire is positioned closer to the ceiling, the smoke temperature is higher and the smoke spreads faster (Figure 23). This is to be expected, as the heat is divided over less entrained air and therefore, the buoyancy is higher. Similar trends were noticed from experiments in recent research by Liu, Fang, Tang, Beji and Merci [90].

Consequently, the effect of h_f should always be studied for structural stability and for life safety of occupants located underneath the back-layering flow.

5.6 Calculation time

The objective of the model is to predict back-layering and stratification in a fast and reliable manner. A low calculation time is important for probabilistic risk assessments that employ sampling techniques and therefore require the simulation of thousands of scenarios.

The calculation time is presented in Figure 31 for varying simulated length. The varying simulated lengths are established by varying the downstream length of the tunnel. The tests are performed on a conventional laptop (HP ENVY x360, Intel Core i5 8265U 1.6 GHz - 3.9 GHz, 8 GB DDR4-2400 SDRAM). Three tests are performed per example and additional efforts are taken to minimize the inevitable influence of background processes. Nevertheless, the reader should keep in mind that the calculation time is only a rough approximation of the computational cost.

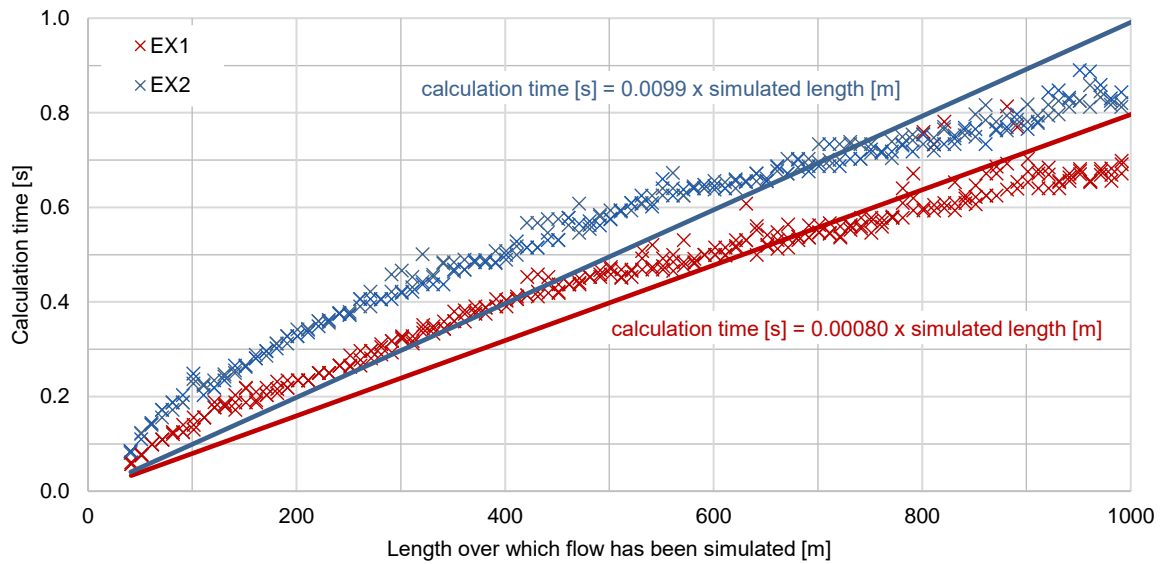


Figure 31: Calculation time in function of the simulated length for examples EX1 and EX2

From Figure 31, it can be concluded that it takes about 1 second to simulate the steady-state flow over 1 km. This calculation time is found to be satisfactory, as it allows for a thousand simulations of short tunnels (< 1 km) in less than a quarter of an hour. Note that, once conduction through the walls is implemented, the calculation time will increase significantly and should be re-evaluated.

6 CONCLUSION

Fires in tunnels can have severe consequences. Examples are the BAKU metro tunnel fire of 1995 (289 fatalities and 265 injuries), the Mont Blanc road tunnel fire of 1999 (all 39 occupants died) and the Daegu subway tunnel fire of 2003 (over 192 fatalities) [1]. Life safety is not naturally guaranteed in tunnels, neither is structural stability or traffic continuation. Therefore, a comprehensive risk assessment of existing and new designs is indispensable. Such a risk assessment requires a reasonably fast and accurate smoke behaviour model. One-dimensional, one-layer models provide fast simulations but are not able to predict stratification or back-layering phenomena.

A model is developed in Python 3.9. It considers the separation of a hot smoke layer and a cold fresh air layer, analogue to the two-zone model for enclosures. Unlike simple empirical correlations, the model is not only able to predict the back-layering length, but also the temperature, velocity, and layer thickness variations along the length of the tunnel. The model considers the tunnel's geometry, applied ventilation strategies and fire parameters. Unlike complex three-dimensional CFD calculations, the simulations are obtained almost instantaneously.

The concept is visualized in [Figure 8](#). It consists of three main parts. First (1), a system of equations is solved numerically to obtain the smoke layer properties at the seat of the fire (temperature, density, velocity, mass flow and layer thickness). The system includes empirical correlations to assess the plume entrainment and the smoke velocity. The mass flow rate is divided over the upstream and the downstream flow. Next (2), the flow properties are calculated cell by cell in an upstream direction. For every cell, an iteration process solves the mass balance and the heat balance, as well as a velocity correlation that replaces the momentum balance. When convergence within a cell is reached, the properties are calculated for the upstream neighbour and so on, until the momentum of the back-layering front is in equilibrium with the ventilation flow. Last (3), a similar calculation is made for the downstream flow. However, in contrast to the upstream flow, the downstream flow is unbalanced, and the calculations are stopped when a predefined length is reached.

The proposed model comes with some important simplifications (elaborated upon in [section 4.1](#)), which can be reversed in later research. The most important simplifications are the steady-state conditions, inert walls, strictly longitudinal ventilation, and constant rectangular cross-sections.

Despite these simplifications, the outcome of the model corresponds well to the correlations and experimental data found in the literature and the objective is achieved: the back-layering effect and stratification are predicted in a fast and reliable manner. This is presented by means of two example problems ([Table 3](#)), which represent a fire involving a single passenger car (EX1) and a fire involving two busses, a small lorry, or a metro carriage (EX2).

For the six-meter-high and twelve-meter-wide tunnel of the examples, the model can calculate critical velocities for fires up to 73.2 MW when the source is elevated with one meter, up to 87.8 MW for fire sources without elevation. The outcome is in good agreement with the correlation of Li, Lei and Ingason [45] (although slightly lower) and is congruent with the scattered experimental data.

The temperature profiles agree reasonably well with the theoretical and empirical formulae accomplished by Ingason, Li and Lönnemark [89] for supercritical ventilation flows and low heat release rates (like EX1). The implementation of a more elaborate heat loss model, including the conduction through the walls, would improve the accuracy. This is especially true when the heat release rate is high. Moreover, for subcritical velocities, more research should be performed to investigate the influence of the deflected back-layering flow, as discussed in [Appendix B](#).

The back-layering lengths agree well with the correlation by Hu, Huo and Chow and the correlation by Li, Lei and Ingason (although slightly higher). When analysing the dimensionless back-layering length as a function of the dimensionless velocity, a high level of congruence can be noticed with the small-scale experiments of Li, Lei and Ingason. Therefore, it can be concluded that the slight deviation of the back-layering length is due to the deviation in critical velocity.

Notwithstanding the adequate agreement of the proposed model with the experimental data, some improvements can be realized in further research to enhance the accuracy and expand the domain of validity of the model. Below, a few potential topics are listed:

- Implementation of a plume entrainment model for high heat release rates.
- Implementation of a more elaborate heat loss model, including conduction through the walls.
- Research concerning the influence of the deflected back-layering flow on the flow properties downstream from the seat of the fire.
- Research concerning the confinement criterium to increase accuracy for low ventilation velocities.
- Implementation of entrainment and detrainment between the upper and lower layer.
- Adjustment of the balances and correlations to deal with non-rectangular, varying cross-sections.
- Research concerning destratification downstream.
- Adjustments of the balances to simulate the transient conditions.
- Implementation of an overall momentum balance as replacement of the predefined ventilation flow.

REFERENCES

- [1] R. Carvel and G. Marlair, 'Chapter 1: A history of fire incidents in Tunnels', in *Handbook of Tunnel Fire Safety, 2nd edition*, 2012, pp. 1–25. DOI: [10.1680/hfts.41530.003](https://doi.org/10.1680/hfts.41530.003), ISBN: 978-0-7277-4153-0.
- [2] Wikipedia, 'List of long tunnels by type', 2020. URL: https://en.wikipedia.org/wiki/List_of_long_tunnels_by_type (accessed Jan. 21, 2021).
- [3] G. Grant and S. Jagger, 'Chapter 10: The use of tunnel ventilation for fire safety', in *Handbook of Tunnel Fire Safety, 2nd edition*, 2012, pp. 176–216. DOI: [10.1680/hfts.41530.003](https://doi.org/10.1680/hfts.41530.003), ISBN: 978-0-7277-4153-0.
- [4] A. H. Tullo, 'Plastics makers plot the future of the carle', *Chemical & Engineering News*, vol. 95, no. 45, 2017. URL: <https://cen.acs.org/articles/95/i45/Plastics-makers-plot-future-car.html>.
- [5] Vlaams netwerk van ondernemingen, 'Waarom kiezen ondernemers en kmo's voor elektrische mobiliteit? | Voka', Feb. 08, 2021. URL: <https://www.voka.be/nieuws/waarom-kiezen-ondernemers-en-kmos-voor-elektrische-mobiliteit> (accessed Feb. 09, 2021).
- [6] Milieurapport Vlaanderen (MIRA), 'Aantal wegvoertuigen', Jun. 2020. URL: <https://www.milieurapport.be/sectoren/transport/sectorkenmerken/aantal-wegvoertuigen> (accessed Feb. 09, 2021).
- [7] Magdalena Dugdale, 'European countries banning fossil fuel cars and switching to electric', *Road Traffic Technology*, Aug. 2018. URL: <https://www.roadtraffic-technology.com/features/european-countries-banning-fossil-fuel-cars/>.
- [8] Le Monde, 'Réouverture du tunnel du Mont-Blanc', Mar. 09, 2002. URL: https://www.lemonde.fr/archives/article/2002/03/09/reouverture-du-tunnel-du-mont-blanc_265936_1819218.html.
- [9] L. Y. Siang, F. E. M. Ghazali, N. Y. Zainun, and R. Ali, 'General risks for tunnelling projects: An overview', in *AIP Conference Proceedings*, 2017, vol. 1892, p. 080004. DOI: [10.1063/1.5005730](https://doi.org/10.1063/1.5005730).
- [10] European Economic Community, 'Directive 2004/54/EC of the European Parliament and of the Council of 29 April 2004 on minimum safety requirements for tunnels in the Trans-European Road Network', Apr. 2004. URL: <https://eur-lex.europa.eu/legal-content/EN/ALL/?uri=CELEX%3A32004L0054>.
- [11] P. Ntzeremes and K. Kirytopoulos, 'Evaluating the role of risk assessment for road tunnel fire safety: A comparative review within the EU', *Journal of Traffic and Transportation Engineering (English Edition)*, vol. 6, no. 3, pp. 282–296, 2019. DOI: [10.1016/j.jtte.2018.10.008](https://doi.org/10.1016/j.jtte.2018.10.008).
- [12] NTUA, 'Upgrading Road Transport Safety by Improving the Behaviour of Tunnel Users with New Training Technologies', *National Technical University of Athens, School of Mechanical Engineering*, 2013.
- [13] FESG, '[draft] FIERCE Project description', 2020.
- [14] A. N. Beard, 'Tunnel safety, risk assessment and decision-making', *Tunnelling and Underground Space Technology*, vol. 25, no. 1, pp. 91–94, Jan. 2010. DOI: [10.1016/j.tust.2009.07.006](https://doi.org/10.1016/j.tust.2009.07.006).
- [15] P. Ntzeremes and K. Kirytopoulos, 'A stochastic-based evacuation model for risk assessment in road tunnel fire accidents and the importance of educating users', in *Safety and Reliability - Safe Societies in a Changing World - Proceedings of the 28th International European Safety and Reliability Conference, ESREL 2018*, 2018, pp. 2185–2192. DOI: [10.1016/j.safrel.2018.07.006](https://doi.org/10.1016/j.safrel.2018.07.006).

- 10.1201/9781351174664-274, ISBN: 9780815386827.
- [16] P. Ntzeremes, K. Kirytopoulos, and V. Leopoulos, 'Discussing the Need to Manage Uncertainty Relating to Users in Road Tunnel Fire Risk Assessment', *Journal of Risk Analysis and Crisis Response*, 2020. DOI: [10.2991/jracr.k.200507.002](https://doi.org/10.2991/jracr.k.200507.002).
- [17] H. Bjelland, 'Engineering Safety With applications to fire safety design of buildings and road tunnels', 2013. DOI: [10.2307/j.ctt1f89r3q.8](https://doi.org/10.2307/j.ctt1f89r3q.8), ISBN: 9788276445497.
- [18] Rijkswaterstaat - Ministerie van Infrastructuur en Milieu, 'QRA-tunnels 2.0 Achtergrondduccement', 2012. URL: https://puc.overheid.nl/rijkswaterstaat/doc/PUC_159718_31/.
- [19] S. Frey, N. Riklin, R. Brandt, O. Heger, and B. Kohl, 'Modelling of tunnel ventilation' s influence on fire risk – a detailed comparison of model assumptions and their potential influence', *BHR Group*, no. 53, pp. 1–15, 2019. URL: <https://www.researchgate.net/project/Risk-assessment-of-longitudinal-ventilation-strategies>.
- [20] C. Zulauf *et al.*, *Risk evaluation, current practice for risk evaluation for road tunnels*. Comité technique AIPCR C.4 Exploitation des tunnels routiers / PIARC Technical Committee C.4 Road Tunnel Operation, 2013. ISBN: 978-2-84060-290-3.
- [21] ILF Consulting Engineers, 'Capability Statement - Safety Management and Civil Security of Transport Infrastructure Capability Statement', Linz, 2020. URL: http://www.tunnelriskmodel.at/wp-content/uploads/2015/10/ILF_CapabState_E.pdf.
- [22] 'TuRisMo - Tunnel Risk Model', 2020. URL: <http://www.tunnelriskmodel.at/>.
- [23] Kohl B, Forster C, and Wiesholzer S, 'Upgrading Of The Austrian Tunnel Risk Model Turismo-Methodical And Practical Aspects', 2014, pp. 90–99. URL: https://lampx.tugraz.at/~tunnel2016/history/Tunnel_2014_CD/Dateien/24_Kohl_2014_neu.pdf.
- [24] Hörhan R, Forster C, and Kohl B, 'Upgrading Of The Austrian Tunnel Risk Model Turismo', *6th International Conference 'Tunnel Safety and Ventilation' 2012, Graz*, pp. 66–73, 2012. URL: https://lampx.tugraz.at/~tunnel2016/history/Tunnel_2012_CD/PDF/10_Hoerhan.pdf.
- [25] N. Goncalves *et al.*, *Risk Analysis For Road Tunnels*. Management of Road Tunnel Safety” of the Technical Committee C3.3 Road Tunnel Operation of the World Road Association PIARC, 2008. ISBN: 2-84060-202-4.
- [26] G. Christian *et al.*, *ASTRA 19004: Risikoanalyse Für Tunnel Der Nationalstrassen*. Bundesamt für Strassen ASTRA, 2014. URL: <https://www.astra.admin.ch/astra/de/home/fachleute/dokumente-nationalstrassen/standards/risiko-sicherheitsmanagement.html>.
- [27] L. Uusitalo, 'Advantages and challenges of Bayesian networks in environmental modelling', *Ecological Modelling*, vol. 203, pp. 312–318, 2007. DOI: [10.1016/j.ecolmodel.2006.11.033](https://doi.org/10.1016/j.ecolmodel.2006.11.033).
- [28] G. Christian *et al.*, *ASTRA 89005: Risikokonzzept Für Tunnel Der Nationalstrassen*. Bundesamt für Strassen ASTRA, 2014. URL: <https://www.astra.admin.ch/astra/de/home/fachleute/dokumente-nationalstrassen/standards/risiko-sicherheitsmanagement.html>.
- [29] Rijkswaterstaat - Ministerie van Infrastructuur en Milieu, 'Gebruikshandleiding QRA-tunnels 2.0', 2012. URL: https://puc.overheid.nl/rijkswaterstaat/doc/PUC_159718_31/.
- [30] R. M. L. Nelisse and A. C. W. M. Vrouwenvelder, 'De statistische kans op brand in tunnels', Organistatie voor Toegepast Natuurwetenschappelijk onderzoek, 2013. URL: https://puc.overheid.nl/rijkswaterstaat/doc/PUC_146949_31/.
- [31] J. Reinders and C. C. Domingo, 'Consequenties voor QRA-tunnels van het vervoer van nieuwe

- stoffen', 2013. URL: <https://www.cob.nl/document/consequenties-voor-gra-tunnels-van-het-vervoer-van-nieuwe-stoffen/>.
- [32] M. Schubert, N. P. Høj, A. Ragnøy, and H. Buvik, 'Risk Assessment of Road Tunnels using Bayesian Networks', *Procedia - Social and Behavioral Sciences*, vol. 48, pp. 2697–2706, 2012. DOI: [10.1016/j.sbspro.2012.06.1239](https://doi.org/10.1016/j.sbspro.2012.06.1239).
- [33] M. J. Hurley *et al.*, *SFPE handbook of fire protection engineering, fifth edition*. Springer New York, 2016. ISBN: [9781493925650](https://www.isbn-international.org/product/9781493925650).
- [34] H. Ingason, Y. Z. Li, and A. Lönnemark, 'Chapter 12: Smoke Stratification', in *Tunnel Fire Dynamics*, 2014, pp. 321–329. DOI: [10.1007/978-1-4939-2199-7](https://doi.org/10.1007/978-1-4939-2199-7), ISBN: [978-1-4939-2199-7](https://www.isbn-international.org/product/978-1-4939-2199-7).
- [35] H. Ingason, 'Chapter 13: Fire Dynamics in Tunnels', *Handbook of Tunnel Fire Safety, 2nd edition*, pp. 272–307, 2012. DOI: [10.1680/htfs.41530.273](https://doi.org/10.1680/htfs.41530.273).
- [36] I. Riess, 'Simple Smoke Stratification Model', 2018. URL: <https://www.researchgate.net/project/SpitFIRE>.
- [37] J. C. R. Hunt, 'Lewis Fry Richardson and his contributions to mathematics, meteorology and models of conflict', *Annual Review of Fluid Mechanics*, vol. 30, no. 1, pp. xiii–xxxvi, Jan. 1998. DOI: [10.1146/annurev.fluid.30.1.0](https://doi.org/10.1146/annurev.fluid.30.1.0).
- [38] D. Yang, L. H. Hu, R. Huo, Y. Q. Jiang, S. Liu, and F. Tang, 'Experimental study on buoyant flow stratification induced by a fire in a horizontal channel', *Applied Thermal Engineering*, vol. 30, no. 8–9, pp. 872–878, Jun. 2010. DOI: [10.1016/j.applthermaleng.2009.12.019](https://doi.org/10.1016/j.applthermaleng.2009.12.019).
- [39] F. Tang, L. J. Li, M. S. Dong, Q. Wang, F. Z. Mei, and L. H. Hu, 'Characterization of buoyant flow stratification behaviors by Richardson (Froude) number in a tunnel fire with complex combination of longitudinal ventilation and ceiling extraction', *Applied Thermal Engineering*, vol. 110, pp. 1021–1028, Jan. 2017. DOI: [10.1016/j.applthermaleng.2016.08.224](https://doi.org/10.1016/j.applthermaleng.2016.08.224).
- [40] F. Tang, Z. Zhao, and K. Zhao, 'Experimental investigation on carriage fires hazards in the longitudinal ventilated tunnels: Assessment of the smoke stratification features', *Safety Science*, vol. 130, no. December 2019, 2020. DOI: [10.1016/j.ssci.2020.104901](https://doi.org/10.1016/j.ssci.2020.104901).
- [41] W. H. Hager and O. Castro-Orgaz, 'William Froude and the Froude Number', *Journal of Hydraulic Engineering*, vol. 143, no. 4, p. 02516005, Apr. 2017. DOI: [10.1061/\(ASCE\)HY.1943-7900.0001213](https://doi.org/10.1061/(ASCE)HY.1943-7900.0001213).
- [42] J. S. Newman, 'Experimental evaluation of fire-induced stratification', *Combustion and Flame*, vol. 57, no. 1, pp. 33–39, Jul. 1984. DOI: [10.1016/0010-2180\(84\)90135-4](https://doi.org/10.1016/0010-2180(84)90135-4).
- [43] H. Nyman and H. Ingason, 'Temperature stratification in tunnels', *Fire Safety Journal*, vol. 48, pp. 30–37, Feb. 2012. DOI: [10.1016/j.firesaf.2011.11.002](https://doi.org/10.1016/j.firesaf.2011.11.002).
- [44] Z. Zeng, K. Xiong, X. Lu, M. Weng, and F. Liu, 'Study on the smoke stratification length under longitudinal ventilation in tunnel fires', *International Journal of Thermal Sciences*, vol. 132, no. May, pp. 285–295, Oct. 2018. DOI: [10.1016/j.ijthermalsci.2018.05.038](https://doi.org/10.1016/j.ijthermalsci.2018.05.038).
- [45] Y. Z. Li, B. Lei, and H. Ingason, 'Study of critical velocity and backlayering length in longitudinally ventilated tunnel fires', *Fire Safety Journal*, vol. 45, no. 6–8, pp. 361–370, Nov. 2010. DOI: [10.1016/j.firesaf.2010.07.003](https://doi.org/10.1016/j.firesaf.2010.07.003).
- [46] P. H. Thomas, 'The movement of buoyant fluid against a stream and the venting of underground fires', *Fire safety science*, vol. 351, p. 1, 1958. URL: https://www.iafss.org/publications/frn/351/-1/view/frn_351.pdf.
- [47] N. H. Danziger and W. D. Kennedy, 'Longitudinal ventilation analysis for the glenwood canyon tunnels', in *Proceedings of the Fourth International Symposium Aerodynamics and Ventilation of Vehicle Tunnels*, 1982, pp. 169–186.

- [48] C. Lee, R. F. Chaiken, and J. M. Singer, 'Interaction Between Duct Fires and Ventilation Flow: An Experimental Study', *Combustion Science and Technology*, vol. 20, no. 1–2, pp. 59–72, Jul. 1979. DOI: [10.1080/00102207908946897](https://doi.org/10.1080/00102207908946897).
- [49] H. Ingason, Y. Z. Li, and A. Lönnemark, 'Chapter 13: Tunnel Fire Ventilation', in *Tunnel Fire Dynamics*, 2014, pp. 333–370. DOI: [10.1007/978-1-4939-2199-7](https://doi.org/10.1007/978-1-4939-2199-7), ISBN: 978-1-4939-2199-7.
- [50] Y. Wu and M. Z. Bakar, 'Control of smoke flow in tunnel fires using longitudinal ventilation systems – a study of the critical velocity', *Fire Safety Journal*, vol. 35, no. 4, pp. 363–390, Nov. 2000. DOI: [10.1016/S0379-7112\(00\)00031-X](https://doi.org/10.1016/S0379-7112(00)00031-X).
- [51] Y. Oka and G. T. Atkinson, 'Control of smoke flow in tunnel fires', *Fire Safety Journal*, vol. 25, no. 4, pp. 305–322, Nov. 1995. DOI: [10.1016/0379-7112\(96\)00007-0](https://doi.org/10.1016/0379-7112(96)00007-0).
- [52] Y. Z. Li and H. Ingason, 'Effect of cross section on critical velocity in longitudinally ventilated tunnel fires', *Fire Safety Journal*, vol. 91, no. May, pp. 303–311, Jul. 2017. DOI: [10.1016/j.firesaf.2017.03.069](https://doi.org/10.1016/j.firesaf.2017.03.069).
- [53] Y. Z. Li and H. Ingason, 'Overview of research on fire safety in underground road and railway tunnels', *Tunnelling and Underground Space Technology*, vol. 81, pp. 568–589, Nov. 2018. DOI: [10.1016/j.tust.2018.08.013](https://doi.org/10.1016/j.tust.2018.08.013).
- [54] L. H. Hu, R. Huo, and W. K. Chow, 'Studies on buoyancy-driven back-layering flow in tunnel fires', *Experimental Thermal and Fluid Science*, vol. 32, no. 8, pp. 1468–1483, Sep. 2008. DOI: [10.1016/j.expthermflusci.2008.03.005](https://doi.org/10.1016/j.expthermflusci.2008.03.005).
- [55] N. Tilley, X. Deckers, and B. Merci, 'CFD study of relation between ventilation velocity and smoke backlayering distance in large closed car parks', *Fire Safety Journal*, vol. 48, pp. 11–20, Feb. 2012. DOI: [10.1016/j.firesaf.2011.12.005](https://doi.org/10.1016/j.firesaf.2011.12.005).
- [56] S. Gannouni and R. Ben Maad, 'Numerical study of the effect of blockage on critical velocity and backlayering length in longitudinally ventilated tunnel fires', *Tunnelling and Underground Space Technology*, vol. 48, pp. 147–155, Apr. 2015. DOI: [10.1016/j.tust.2015.03.003](https://doi.org/10.1016/j.tust.2015.03.003).
- [57] S. Zhang *et al.*, 'Prediction of smoke back-layering length under different longitudinal ventilations in the subway tunnel with metro train', *Tunnelling and Underground Space Technology*, vol. 53, pp. 13–21, Mar. 2016. DOI: [10.1016/j.tust.2015.12.013](https://doi.org/10.1016/j.tust.2015.12.013).
- [58] Gwon Hyun Ko, Seung Ryul Kim, and Hong Sun Ryou, 'An Experimental Study on the Effect of Slope on the Critical Velocity in Tunnel Fires', *Journal of Fire Sciences*, vol. 28, no. 1, pp. 27–47, Jan. 2010. DOI: [10.1177/0734904109106547](https://doi.org/10.1177/0734904109106547).
- [59] F. Wang, M. Wang, R. Carvel, and Y. Wang, 'Numerical study on fire smoke movement and control in curved road tunnels', vol. 67, no. March, pp. 1–7, 2017. DOI: [10.1016/j.tust.2017.04.015](https://doi.org/10.1016/j.tust.2017.04.015).
- [60] A. Haerter, 'Theoretische und experimentelle Untersuchungen über die Lüftungsanlagen von Strassentunneln', ETH Zürich, 1961. DOI: [10.3929/ethz-a-000088598](https://doi.org/10.3929/ethz-a-000088598).
- [61] F. Colella, 'Chapter 2: One-dimensional modelling', Multiscale Modelling of Tunnel Ventilation Flows and Fires, PhD Thesis, Politecnico di Torino, 2010. URL: <http://hdl.handle.net/1842/3528>.
- [62] R. E. Greuer, 'Chapter 2: Review of existing programs for ventilation network calculations', in *USBM SO241032 - Study of mine fires and mine ventilation, Part I*, Michigan Technological University. U.S. Department of the Interior, Bureau of Mines, 1977, pp. 8–10.
- [63] The National Institute for Occupational Safety and Health (NIOSH), 'Mining Product: MFIRE', 2020. URL: <https://www.cdc.gov/niosh/mining/works/cover-sheet1816.html>.
- [64] J. A. Volpe, *Subway Environmental Design Handbook, Subway Environmental Simulation*

- Computer Program, Version 4*. Cambridge: U.S. Department of Transportation, 1997. URL: <https://trid.trb.org/view/42724>.
- [65] M. Riess, I. & Bettelini, 'The prediction of smoke propagation due to tunnel fires', *ITC Conference Tunnel Fires and Escape from Tunnels*, Lyon, 1999. URL: <https://www.researchgate.net/project/Tunnel-Ventilation-Safety-Air-Quality>.
- [66] R. Riess, I., Bettelini, M. & Brandt, 'Sprint – a design tool for fire ventilation', *10th Int. Symp. on Aerodynamics and Ventilation of Vehicle Tunnels*, no. November, 2000. URL: <https://www.researchgate.net/project/SpitFIRE>.
- [67] Centre d'Études des Tunnels (CETU), 'La modélisation aéraulique pour les tunnels, Fascicule 1 : outils et critères de choix', 2011. URL: http://www.cetu.developpement-durable.gouv.fr/IMG/pdf/CETU_Guide_Mod_Aer_F1_2011.pdf.
- [68] Centre d'Études des Tunnels (CETU), 'La modélisation aéraulique pour les tunnels, Fascicule 2 : la modélisation monodimensionnelle', pp. 1–32, 2013. URL: http://www.cetu.developpement-durable.gouv.fr/IMG/pdf/Guide_modelisation_f2_2013-03-06_BD.pdf.
- [69] E. E. Zukoski, T. Kubota, and B. Cetegen, 'Entrainment in fire plumes', *Fire safety journal*, vol. 3, no. 2, pp. 107–121, 1981. DOI: [10.1016/0379-7112\(81\)90037-0](https://doi.org/10.1016/0379-7112(81)90037-0).
- [70] R. L. Alpert, 'Turbulent Ceiling-Jet Induced by Large-Scale Fires', *Combustion Science and Technology*, vol. 11, no. 5–6, pp. 197–213, Nov. 1975. DOI: [10.1080/00102207508946699](https://doi.org/10.1080/00102207508946699).
- [71] J. P. Kunsch, 'Simple model for control of fire gases in a ventilated tunnel', *Fire Safety Journal*, vol. 37, no. 1, pp. 67–81, Feb. 2002. DOI: [10.1016/S0379-7112\(01\)00020-0](https://doi.org/10.1016/S0379-7112(01)00020-0).
- [72] G. Heskestad and M. A. Delichatsios, 'The initial convective flow in fire', *Symposium (International) on Combustion*, vol. 17, no. 1, pp. 1113–1123, Jan. 1979. DOI: [10.1016/S0082-0784\(79\)80106-X](https://doi.org/10.1016/S0082-0784(79)80106-X).
- [73] Y. Z. Li, B. Lei, and H. Ingason, 'The maximum temperature of buoyancy-driven smoke flow beneath the ceiling in tunnel fires', *Fire Safety Journal*, vol. 46, no. 4, pp. 204–210, 2011. DOI: <https://doi.org/10.1016/j.firesaf.2011.02.002>.
- [74] Y. Zhen and H. Ingason, 'The maximum ceiling gas temperature in a large tunnel fire', *Fire Safety Journal*, vol. 48, pp. 38–48, 2012. DOI: [10.1016/j.firesaf.2011.12.011](https://doi.org/10.1016/j.firesaf.2011.12.011).
- [75] J. Wang, Z. Fang, Z. Tang, and J. Yuan, 'Influence of longitudinal ventilation on the mass flow rate distribution of fire smoke flow in tunnels', *Tunnelling and Underground Space Technology*, vol. 112, p. 103938, Jun. 2021. DOI: [10.1016/j.tust.2021.103938](https://doi.org/10.1016/j.tust.2021.103938).
- [76] P. Raj, A. Moussa, and K. Aravamudan, 'Experiments involving pool and vapor fires from spills of Liquefied natural gas on water', Prepared for U.S. Dept. of Transportation, U.S. Coast Guard, Rept. No. CG-D-55–79, 1981. URL: <https://apps.dtic.mil/sti/citations/ADA077073>.
- [77] T.K. Flannelop, 'Chapter 4: Unsteady Outflow Driven By Gravity', in *Fluid mechanics for industrial safety and environmental protection*, 1994. DOI: [10.1016/S0304-3894\(96\)90010-2](https://doi.org/10.1016/S0304-3894(96)90010-2), ISBN: [0444898638](https://www.isbn-international.org/product/0444898638).
- [78] J. L. Bailey, G. P. Forney, P. A. Tatem, and W. W. Jones, 'Development and validation of corridor flow submodel for CFAST', *Journal of Fire Protection Engineering*, vol. 12, no. 3, pp. 139–162, 2002. DOI: [10.1177/10423910260620473](https://doi.org/10.1177/10423910260620473).
- [79] J. O. Shin, S. B. Dalziel, and P. F. Linden, 'Gravity currents produced by lock exchange', *Journal of Fluid Mechanics*, vol. 521, pp. 1–34, Dec. 2004. DOI: [10.1017/S002211200400165X](https://doi.org/10.1017/S002211200400165X).
- [80] C. S. Yih, 'A study of the characteristics of gravity waves at a liquid interface', Master thesis,

- State University of Iowa, 1947.
- [81] D. I. H. Barr, 'Densimetric exchange flow in rectangular channels', *La Houille Blanche*, vol. 22, no. 6, pp. 619–632, Oct. 1967. DOI: [10.1051/lhb/1967042](https://doi.org/10.1051/lhb/1967042).
- [82] O. Megret, O. Vauquelin, and E. Casale, 'An experimental study of critical velocity and the influence of source diameter', in *Tunnel Fires and Escape from Tunnels, International Conference, Lyon, France, 5th*, 1999, pp. 429–436.
- [83] V. Gnielinski, 'New equations for heat and mass transfer in turbulent pipe and channel flow', *Int. Chem. Eng.*, vol. 16, no. 2, pp. 359–368, 1976.
- [84] F. P. Incropera, A. S. Lavine, T. L. Bergman, and D. P. DeWitt, 'Chapter 2: Introduction to Conduction', *Fundamentals of heat and mass transfer*, pp. 67–110, 2007. ISBN: [978-0470-50197-9](https://doi.org/10.1007/978-0-470-50197-9).
- [85] A. J. Conejo and L. Baringo, 'Appendix A: Solving Systems of Nonlinear Equations', *Power System Operations*, pp. 271–296, 2018. DOI: [10.1007/978-3-319-69407-8](https://doi.org/10.1007/978-3-319-69407-8), ISBN: [978-3-319-69406-1](https://doi.org/10.1007/978-3-319-69406-1).
- [86] G. Heskestad, 'Chapter 12: Fire Plumes, Flame Height, and Air Entrainment', in *SFPE Handbook of Fire Protection Engineering*, New York, NY: Springer New York, 2016, pp. 396–428. DOI: [10.1007/978-1-4939-2565-0_13](https://doi.org/10.1007/978-1-4939-2565-0_13), ISBN: [978-1-4939-2564-3](https://doi.org/10.1007/978-1-4939-2564-3).
- [87] H. Ingason, Y. Z. Li, and A. Lönnemark, 'Chapter 3: Tunnel Fire Tests', in *Tunnel Fire Dynamics*, New York, NY: Springer New York, 2015, pp. 45–88. DOI: [10.1007/978-1-4939-2199-7](https://doi.org/10.1007/978-1-4939-2199-7), ISBN: [978-1-4939-2198-0](https://doi.org/10.1007/978-1-4939-2198-0).
- [88] R. Carvel and G. Marlair, 'Chapter 12: A history of experimental tunnel fires', in *Handbook of Tunnel Fire Safety, 2nd edition*, R. Carvel and A. Beard, Eds. Thomas Telford Ltd, 2011, pp. 239–272. DOI: [10.1680/htfs.41530](https://doi.org/10.1680/htfs.41530), ISBN: [978-0-7277-4153-0](https://doi.org/10.1680/htfs.41530).
- [89] H. Ingason, Y. Z. Li, and A. Lönnemark, 'Chapter 8: Gas Temperatures', in *Tunnel Fire Dynamics*, 2014, pp. 207–231. DOI: [10.1007/978-1-4939-2199-7](https://doi.org/10.1007/978-1-4939-2199-7), ISBN: [978-1-4939-2199-7](https://doi.org/10.1007/978-1-4939-2199-7).
- [90] Y. Liu, Z. Fang, Z. Tang, T. Beji, and B. Merci, 'Analysis of experimental data on the effect of fire source elevation on fire and smoke dynamics and the critical velocity in a tunnel with longitudinal ventilation', *Fire Safety Journal*, vol. 114, no. April, p. 103002, Jun. 2020. DOI: [10.1016/j.firesaf.2020.103002](https://doi.org/10.1016/j.firesaf.2020.103002).

APPENDIX A: DERIVATIVES OF THE PLUME MASS FLOWS

This appendix deals with the partial derivatives, required to calculate the fluid properties (h_{pl} , ρ_{pl} , T_{pl} , u_{pl} , \dot{m}_{pl}) at the seat of the fire, employing a multivariate Newton Raphson scheme. To obtain these properties, the following three mass flow rates are equated:

$$\begin{cases} \dot{m}_1 = \dot{m}_{pl} = 0.3735 \dot{Q}_c^{\frac{1}{3}} (h_{pl} - h_f)^{\frac{5}{3}} V^* \\ \dot{m}_2 = \frac{\dot{Q}_c}{c_p (T_{pl} - T_0)} = \frac{\dot{Q}_c R}{c_p p_0 M \left(\frac{1}{\rho_{pl}} - \frac{1}{\rho_0} \right)} \\ \dot{m}_3 = \dot{m}_W + \dot{m}_E = 2(H - h_{pl}) W \rho_{pl} u_{pl} \end{cases} \quad (A1)$$

with

$$V^* = \max\left(0.19, \frac{u_0}{w^*}\right), \quad w^* = \left(\frac{g \dot{Q}}{b_f \rho_0 c_p T_0}\right)^{\frac{1}{3}}, \quad u_{pl} = k \sqrt{gH \frac{\rho_0 - \rho_{pl}}{2\rho_0}}$$

The multivariate Newton Raphson scheme is executed in the following form [85]:

$$\mathbf{x}_{k+1} = \mathbf{x}_k - \mathbf{J}_k^{-1} \mathbf{F}(\mathbf{x}_k) \quad (A2)$$

with

$$\mathbf{x} = \begin{Bmatrix} h_{pl} \\ \rho_{pl} \end{Bmatrix}, \quad \mathbf{F}(\mathbf{x}) = \begin{cases} f_1(\mathbf{x}) = \dot{m}_1 - \dot{m}_2 = 0 \\ f_2(\mathbf{x}) = \dot{m}_1 - \dot{m}_3 = 0 \end{cases}, \quad \mathbf{J} = \begin{bmatrix} \frac{\partial f_1}{\partial h_{pl}} & \frac{\partial f_1}{\partial \rho_{pl}} \\ \frac{\partial f_2}{\partial h_{pl}} & \frac{\partial f_2}{\partial \rho_{pl}} \end{bmatrix}$$

The partial derivatives are calculated analytically, as this is the most efficient and accurate manner. However, the specific heat capacity c_p is assumed to be independent of ρ_{pl} (or T_{pl}). The dependency is so weak that the required number of iterations will not be influenced by this simplification.

The partial derivatives of the mass flow rates are given below. The implementation is verified numerically (through a simple forward finite difference method).

$$\frac{\partial \dot{m}_1}{\partial h_{pl}} = 0.6225 \dot{Q}_c^{\frac{1}{3}} (h_{pl} - h_f)^{\frac{2}{3}} V^* \quad (A3)$$

$$\frac{\partial \dot{m}_1}{\partial \rho_{pl}} = 0 \quad (A4)$$

$$\frac{\partial \dot{m}_2}{\partial h_{pl}} = 0 \quad (A5)$$

$$\frac{\partial \dot{m}_2}{\partial \rho_{pl}} = \frac{\dot{Q}_c R}{c_p p_0 M \left(\frac{\rho_{pl}}{\rho_0} - 1 \right)^2} \quad (A6)$$

$$\frac{\partial \dot{m}_3}{\partial h_{pl}} = -2W \rho_{pl} u_{pl} \quad (A7)$$

$$\frac{\partial \dot{m}_3}{\partial \rho_{pl}} = 2(H - h_{pl}) W u_{pl} + 2(H - h_{pl}) W \rho_{pl} \frac{\partial u_{pl}}{\partial \rho_{pl}} \quad (A8)$$

with

$$\frac{\partial u_{pl}}{\partial h_{pl}} = 0, \quad \frac{\partial u_{pl}}{\partial \rho_{pl}} = -\frac{k}{2} \sqrt{\frac{gH}{2\rho_0(\rho_0 - \rho_{pl})}}$$

APPENDIX B: TEMPERATURES PROFILES DOWNSTREAM

As discussed in section 5.2, there is a mismatch between the temperature profile downstream as a result of the proposed model and derived from correlations found in the literature. In this appendix, three probable causes (inaccurate simplifications) are discussed.

- For low heat release rates, the theoretical formula and the proposed model are reasonably congruent. This is visible for example EX1 with ventilation velocities equal to 1.5 m/s and 2.5 m/s in Figure 32. Small differences could be caused by the simplification of the theoretical formula (the constant heat loss coefficient). For high heat release rates, this assumption is less accurate (Figure 24) and produces a higher level of disagreement between the formula and the model (Figure 33).
- However, the disagreement with the experimental formula also increases for high heat release rates. This is likely to be caused by the inert wall assumption of the proposed model. To fully assess the consequences of this assumption, conduction through walls should be implemented in the model.
- Figure 32 and Figure 33 also uncover a second assumption of the proposed model that contribute to the discrepancies. Both figures show that the temperature profiles of supercritical ventilation velocities (2.5 m/s and 3.6 m/s) have a better agreement with the empirical formula, which indicates that there might be a problem with disregarding the deflected back-layering flow for subcritical ventilation velocities. The upstream mass flow rate is assumed to leave the tunnel through a portal or to deflect at the back-layering front and mix with the ventilation flow. The stored heat in this layer is not taken into account. This assumption is less accurate for short back-layering lengths (see the discussion in section 4.3). The reader is reminded that the back-layering length equals 41.2 m for EX1 and 40.7 m for EX2.

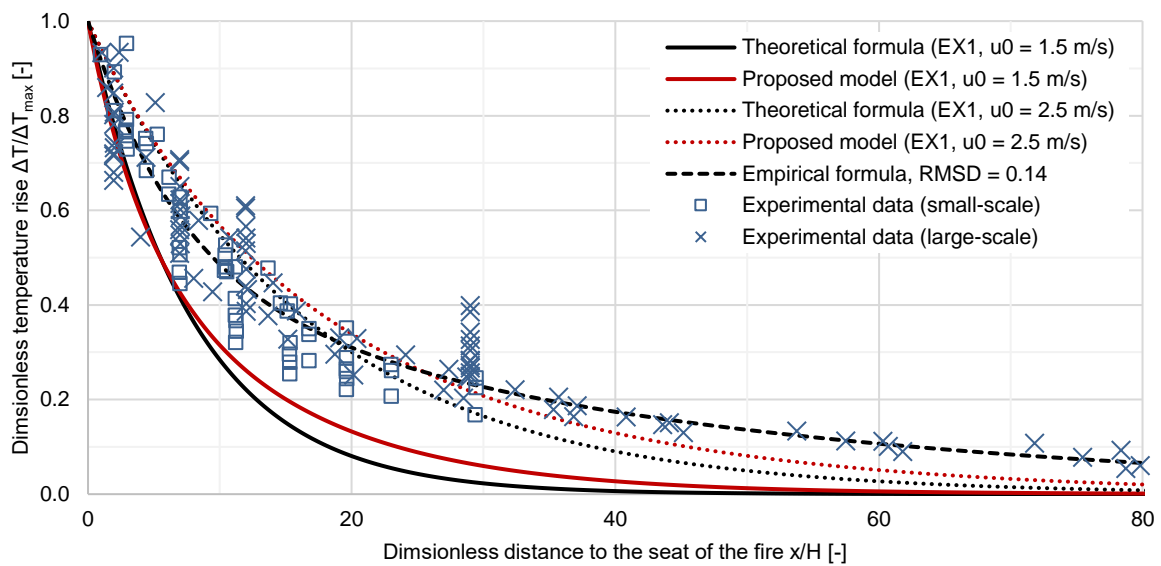


Figure 32: Downstream temperature profile for EX1 with subcritical and supercritical ventilation flows. The theoretical and empirical formula, as well as the experimental data, are adopted from [89].

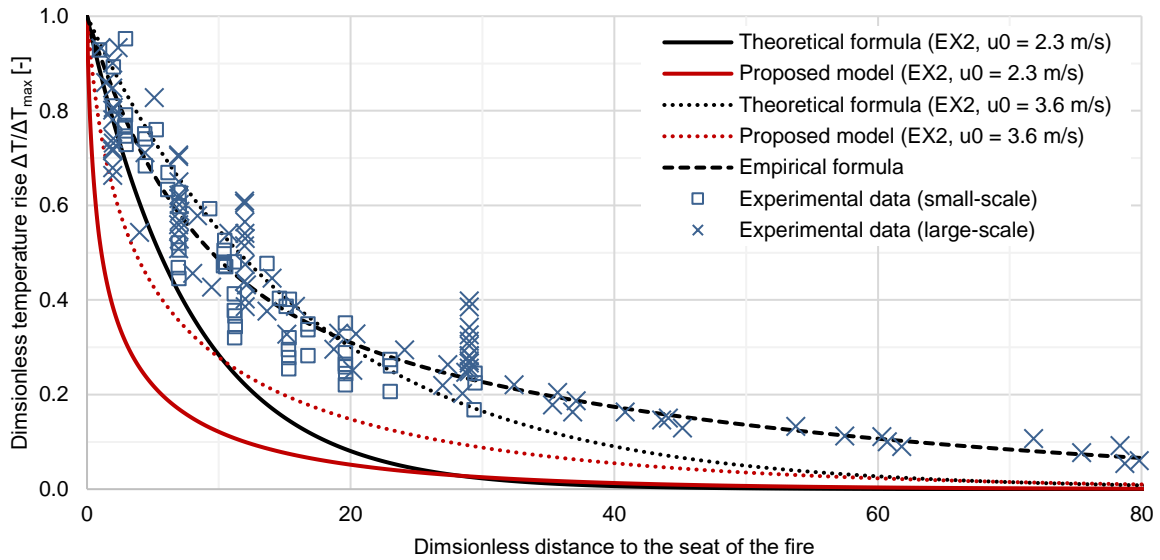


Figure 33: Downstream temperature profile for EX2 with subcritical and supercritical ventilation flows. The theoretical and empirical formula, as well as the experimental data, are adopted from [89].

To examine the effect of this last simplification, a comparison is made with another assumption: the deflected back-layering flow is assumed to stay buoyant and join the smoke of the fire plume in the downstream smoke layer. This concept is illustrated in Figure 34.

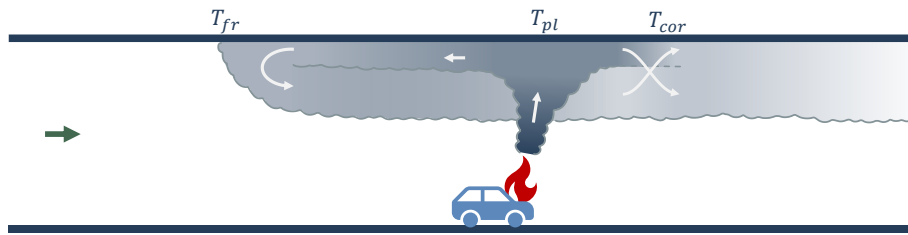


Figure 34: Different assumption regarding the downstream mass flow rate and temperature

The implementation of this different assumption, introducing a third layer, has some more profound implications. Among others, there is the implication that the back-layering flow no longer radiates heat towards the floor and lower walls, but exchanges heat with the deflected back-layering flow. Therefore, the properties of the flow are coupled to the properties further upstream.

However, in the following calculations, the following assumptions are made:

- The properties of the back-layering flow are calculated as described before. Heat is exchanged as described in chapter 4.
- The deflected back-layering flow does not exchange net heat (the heat loss towards the walls and the air below are assumed to equal the gains from the hotter layer above). Therefore, the flow arrives back at the seat of the fire with a temperature equal to the temperature at the back-layering front.
- The two layers mix perfectly at the seat of the fire. The mass flow rate of the downstream flow equals the entire plume entrainment \dot{m}_{pl} . The temperature is averaged over the mass rates of the two layers:

$$T_{cor} = \frac{T_{fr}\dot{m}_{up} + T_{fr}(\dot{m}_{pl} - \dot{m}_{up})}{\dot{m}_{pl}} \quad (C1)$$

These assumptions allow an easy implementation but require further research to be justified. They are only made to quickly examine the effect of the deflected back-layer.

The result is given in [Figure 35](#) (EX1) and [Figure 36](#) (EX2). For both examples, the agreement with the empirical formula is improved.

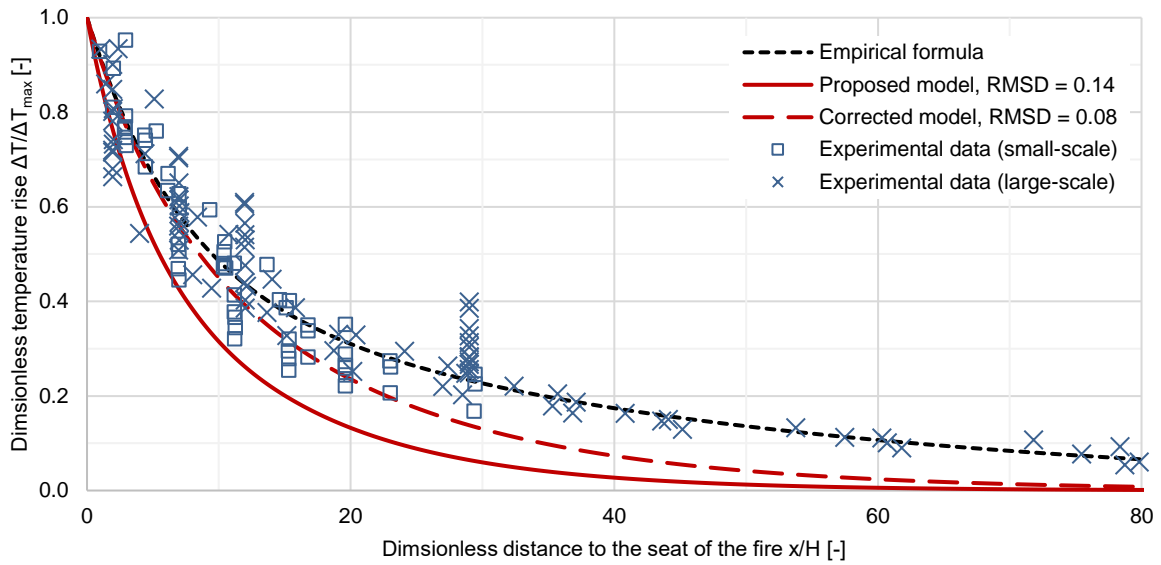


Figure 35: Corrected downstream temperature profile for EX1, considering the deflected back-layering flow

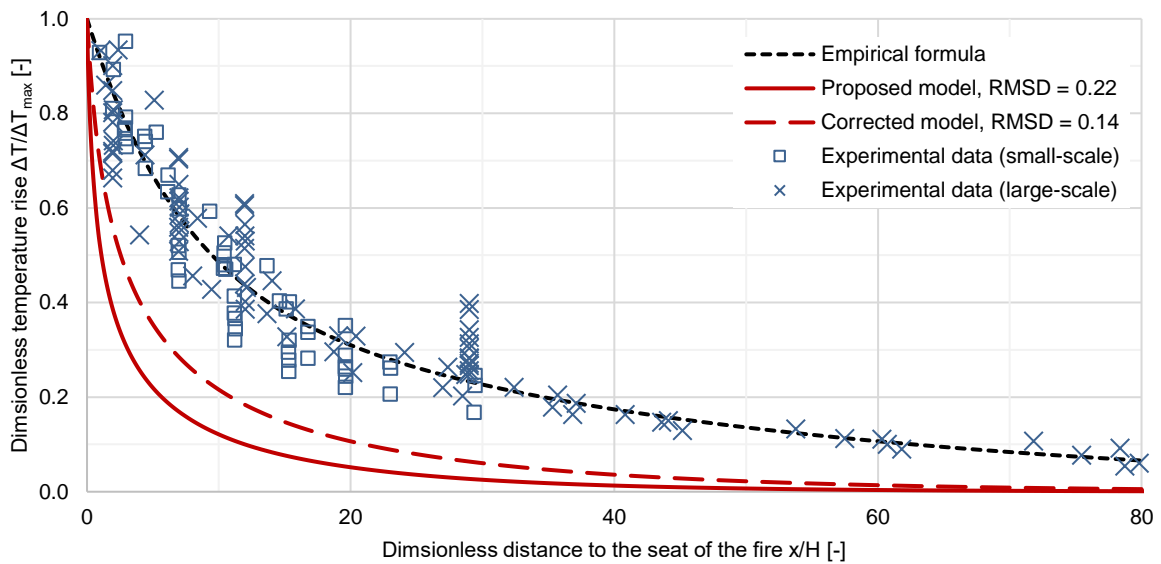


Figure 36: Corrected downstream temperature profile for EX2, considering the deflected back-layering flow

APPENDIX C: CODE OF THE PROPOSED MODEL

```

1  """
2  Arthur Rohaert
3  -----
4  Master dissertation
5  STRATIFICATION AND BACK-LAYERING MODELLING FOR LONGITUDINAL VENTILATED TUNNELS
6
7  January - May
8  2021
9  #####
10 """
11
12 import numpy as np
13 import csv
14
15 #####
16 """ SEAT OF THE FIRE """
17 #####
18
19
20 def density(T=288.15, p=101325, M=0.02897):
21     """ Returns the density of air or smoke, depending on the temperature, in
22     accordance with the ideal gas law. SI units are used. """
23
24     R = 8.31446261815324
25     return p * M / (T * R)
26
27
28 def heat_capacity(T=288.15):
29     """ Returns the specific heat capacity of air or smoke, depending on the
30     temperature. SI units are used, except for heat (kJ or kW).
31     This function is originally written by Matteo Pachera. """
32
33     temperature = [250, 300, 350, 400, 450, 500, 550, 600, 650, 700, 750, 800,
34                   900, 1000, 1100, 1200, 1300, 1400, 1500]
35     capacity = [1.003, 1.005, 1.008, 1.013, 1.020, 1.029, 1.040, 1.051, 1.063,
36               1.075, 1.087, 1.099, 1.121, 1.142, 1.155, 1.173, 1.190, 1.204,
37               1.216]
38     return np.interp(T, temperature, capacity)
39
40
41 def viscosity(T):
42     """ Returns the dynamic viscosity of air, depending on the temperature. SI
43     units are used, except for heat (kJ or kW).
44     This function is originally written by Matteo Pachera. """
45
46     temperature=[175,200,225,250,275,300,325,350,375,400,450,500,550,600,650,
47                700,750,800,850,900,950,1000,1050,1100,1150,1200,1250,1300,
48                1350,1400,1500,1600,1700,1800,1900]
49     viscosity=np.array([1.182,1.329,1.467,1.599,1.725,1.846,1.962,2.075,2.181,
50                        2.286,2.485,2.67,2.849,3.017,3.178,3.332,3.482,3.624,

```

```

51         3.763,3.897,4.026,4.153,4.276,4.396,4.511,4.626,4.736,
52         4.846,4.952,5.057,5.264,5.457,5.646,5.829,6.008])*1E-5
53     return np.interp(T, temperature, viscosity)
54
55
56 def conductivity(T):
57     """ Returns the thermal conductivity of air, depending on the temperature.
58     SI units are used, except for heat (kJ or kW).
59     This function is originally written by Matteo Pachera."""
60
61     temperature=[175,200,225,250,275,300,325,350,375,400,450,500,550,600,650,
62                 700,750,800,850,900,950,1000,1050,1100,1150,1200,1250,1300,
63                 1350,1400,1500,1600,1700,1800,1900]
64     conductivity=np.array([1.593,1.809,2.02,2.227,2.428,2.624,2.816,3.003,
65                            3.186,3.365,3.71,4.041,4.357,4.661,4.954,5.236,
66                            5.509,5.774,6.03,6.276,6.52,6.754,6.985,7.209,
67                            7.427,7.64,7.849,8.054,8.253,8.45,8.831,9.199,
68                            9.554,9.899,10.233])*1E-2
69     return np.interp(T, temperature, conductivity)
70
71
72 def smoke_velocity(H, rho_0, rho):
73     """ Returns the smoke velocity according to the correlation by Kunsch
74     (2002). SI units are used. """
75
76     g, k = 9.81, 0.867
77     return k * (g*H*(rho_0-rho)/(2*rho_0))**0.5
78
79
80 def mass_balances_plume(H, W, h_f, h_pl, rho_0, rho_pl, Q, Xc, b_f, u_0):
81     """ Returns the function residuals (F) and the inverse of the Jacobian (J)
82     of the set of equations, solved to obtain the smoke height and smoke
83     temperature at the seat of the fire (h_pl and rho_pl). The two equations
84     are constructed by equating the three mass flow rates. SI units are used,
85     except for heat (kJ or kW). """
86
87     # MFR1: Plume correlation
88     g = 9.81
89     T_0 = density(rho_0)
90     cp = heat_capacity(T_0)
91     w_star = (g * Q / (b_f * rho_0 * cp * T_0)) ** (1 / 3)
92     V_star = max(u_0 / w_star, 0.19)
93     Qc = Xc * Q
94     m1 = 0.3735 * Qc ** (1 / 3) * (h_pl-h_f) ** (5 / 3) * V_star
95     dm1dh = 0.6225 * Qc ** (1 / 3) * (h_pl-h_f) ** (2 / 3) * V_star
96     dm1dr = 0
97
98     # MFR2: Convective heat
99     Qc = Q * Xc
100    T_0 = density(rho_0)
101    T_pl = density(rho_pl)
102    m2 = Qc / (cp * (T_pl-T_0))
103    dm2dh = 0

```

```

104 dm2dr = (Qc / (cp * (T_pl-T_0)**2))*(T_pl/rho_pl)
105
106 # MFR3: Velocity through section
107 k = 0.613
108 u = k * (g*H*(rho_0-rho_pl)/(rho_0))**0.5
109 dudh = 0
110 dudr = -0.5*k*(g*H/((rho_0-rho_pl)*(rho_0)))**0.5
111 m3 = 2*rho_pl*(H-h_pl)*W*u
112 dm3dh = - 2 * rho_pl * W * u + 2 * rho_pl * (H - h_pl) * W * dudh
113 dm3dr = 2 * (H - h_pl) * W * u + 2 * rho_pl * (H - h_pl) * W * dudr
114
115 # Residuals and Jacobian
116 F = np.array([m1-m2, m1-m3])
117 J = np.array([[dm1dh-dm2dh, dm1dr-dm2dr], [dm1dh-dm3dh, dm1dr-dm3dr]])
118 detJ = J[0, 0] * J[1, 1] - J[0, 1] * J[1, 0]
119 invJ = (1 / detJ) * np.array([[J[1, 1], -J[0][1]], [-J[1][0], J[0][0]]])
120 return F, invJ
121
122
123 def plume(H, W, h_f, T_0, Q, Xc, b_f, u_0):
124     """ Returns the mass flow rate and the temperature of the plume (= of the
125     smoke layer at the seat of the fire). This MFR and temperature are
126     calculated from the two equations that are obtained by equating the three
127     mass flow rates, using a Newton Raphson technique for multiple variables.
128     SI units are used, except for heat (kJ or kW). """
129
130     #1) Initial guess
131     rho_0 = density(T_0)
132     x_old = np.array([h_f + 0.70 * (H - h_f), density(450)])
133     x_min = np.array([h_f + 0.005 * (H - h_f), density(10000)])
134     x_max = np.array([h_f + 0.995 * (H - h_f), rho_0*0.995])
135
136     #2) Loop set-up
137     x_tol, x_diff = 1E-4, np.inf
138     it, it_max = 0, 1E2
139
140     #3) Loop
141     while x_diff > x_tol and it < it_max:
142
143         # Newton Raphson iteration
144         h_pl, rho_pl = x_old
145         F, invJ = mass_balances_plume(H, W, h_f, h_pl, rho_0, rho_pl,
146                                     Q, Xc, b_f, u_0)
147         x_new = x_old - invJ @ F
148
149         # Adjust outcome of iteration
150         x_adj = np.maximum(x_min, np.minimum(x_new, x_max))
151         if np.array_equal(x_new, x_adj):
152             x_diff = max(abs((x_old - x_new) / x_new))
153         else:
154             x_diff = np.inf
155         x_new = x_adj
156

```

```

157     # Prepare for next iteration
158     x_old = x_new
159     it += 1
160     if it == it_max:
161         print('Max iteration reached, no convergence! <Plume>')
162         return np.nan, np.nan, np.nan, np.nan, np.nan
163
164     #4) Plume temperature and mass flow rate
165     h_pl, rho_pl = x_new
166     u_pl = smoke_velocity(H, rho_0, rho_pl)
167     m_pl = 2 * rho_pl * W * (H - h_pl) * u_pl
168     T_pl = density(rho_pl)
169     return h_pl, rho_pl, T_pl, u_pl, m_pl
170
171
172 def confinement_velocity(H, h, rho, rho_0, u):
173     """ Returns the confinement velocity according to the equation by Kunsch
174     (2002). SI units are used. """
175
176     g = 9.81
177     phi = 1 - h/H
178     C1 = (1-2*phi)/(1+2*phi)
179     C2 = (1-rho/rho_0)*g*(H-h)*4*(1-phi)
180     C3 = (rho/rho_0)*u**2*(1-4*phi)
181     return (C1*(C2+C3))**0.5
182
183
184 def critical_velocity(H, W, h_f, T_0, Q, Xc, b_f):
185     """ Returns the critical velocity by equating the ventilation velocity to
186     the confinement velocity (assuming the back-layering front is at the seat
187     of the fire), except for heat (kJ or kW). """
188
189     # First guess
190     g = 9.81
191     rho_0 = density(T_0)
192     cp = heat_capacity(T_0)
193     Q_star = Q / (rho_0 * cp * T_0 * g ** 0.5 * H ** 2.5)
194     u_cr = 0.81 * min(Q_star, 0.15) ** (1 / 3) * np.sqrt(g * H)
195
196     # Loop set-up
197     tol, step = 1E-4, np.inf
198     it, it_max = 0, 1E2
199
200     # Loop
201     while abs(step) > tol and it < it_max:
202         u_0 = u_cr
203         h_pl, rho_pl, _, u_pl, m_pl = plume(H, W, h_f, T_0, Q, Xc, b_f, u_0)
204         u_cr = confinement_velocity(H, h_pl, rho_pl, rho_0, u_pl)
205
206         step = u_cr - u_0
207         it += 1
208     if it == it_max:
209         print('Max iteration reached, no convergence! <Critical velocity>')

```



```

210         return np.nan, np.nan, np.nan, np.nan
211
212     delta_T = density(rho_pl)-T_0
213     return u_cr, delta_T, h_pl, m_pl
214
215
216     #####
217     """ UPSTREAM FLOW """
218     #####
219
220
221 def convection_coefficient(A,P,u,T_h,T_w):
222     """ Returns the convective heat coefficient, employing the correlation by
223     Gnielinski (1976). SI units are used, except for heat (kJ or kW) """
224
225     T = 0.5*T_w + 0.5*T_h
226     D, λ_l, Pr = 4*A/P, 0.02, 0.7
227     v, k = viscosity(T), conductivity(T)
228     Re = u*D/v
229     Nu = 0.125*λ_l*(Re-1000*Pr)/(1+12.7*(λ_l/8)**(1/2)*(Pr**(2/3)-1))
230     return 0.001*(k*Nu)/D
231
232
233 def heat_loss(H, W, dx, h, u_0, u_h, T_h, T_w):
234     """ Returns the convective and radiative heat loss of the smoke layer
235     towards the walls along a segment of length dx. SI units are used, except
236     for heat (kJ or kW). """
237
238     # Convection
239     d = H-h
240     if h==0:
241         A_smoke = H*W
242         P_smoke = 2*H+2*W
243     else:
244         A_smoke = W*d
245         P_smoke = W+2*d
246
247     h_conv = convection_coefficient(A_smoke,P_smoke,u_h,T_h, T_w)
248     Q_conv = P_smoke*dx*h_conv*(T_h-T_w)
249
250     # Radiation
251     P_rad = 2*W+2*d
252     epsilon = 0.9
253     sigma = 5.67037E-8
254     Q_rad = P_rad*dx*epsilon*sigma*(T_h**4-T_w**4)/1000
255
256     # Total heat loss
257     return Q_conv+Q_rad
258
259
260 def next_temperature(H, W, dx, h_out, T_out, T_in, T_w, u_0, u_out, m_up):
261     """ Returns the temperature T_P0 as a result of the heat (and mass) balance
262     of the hot smoke layer upstream in steady state conditions. An upwind

```

```

263     scheme is employed (T_out = T_P0, T_in = T_E1 or T_W1). SI units are used,
264 except for heat rates (kW). """
265
266     Q_in = m_up*heat_capacity(T_in)*T_in
267     Q_det, Q_ext = 0, 0
268     Q_loss = heat_loss(H, W, dx, h_out, -u_0, u_out, T_out, T_w)
269     Q_out = Q_in - Q_det - Q_ext - Q_loss
270     T_out = Q_out / (m_up*heat_capacity(T_out))
271     return T_out, Q_loss
272
273
274 def upstream_properties(H, W, dx, T_E0, T_w, T_0, u_0, m_up, indx):
275     """ Returns the flow properties of the next cell upstream as a result of
276 the heat (and mass) balance of the hot smoke layer upstream in steady state
277 conditions. An upwind scheme is employed (T_W0 = T_P0, T_E0 = T_E1). SI
278 units are used, except for heat rates (kW). """
279
280     # First guess
281     rho_0 = density(T_0)
282     T_P0 = T_E0
283
284     # Loop set-up
285     tol = 1E-3
286     step = tol+1
287     it = 0
288     it_max = 1E2
289
290     # Loop
291     while abs(step) > tol and it < it_max:
292         rho_P0 = density(T_P0)
293         u_P0 = smoke_velocity(H, rho_0, rho_P0)
294         h_P0 = H - m_up/(rho_P0*W*u_P0)
295         T_P0_new, Q_loss = next_temperature(H, W, dx, h_P0, T_P0, T_E0, T_w,
296                                           u_0, u_P0, m_up)
297         step = T_P0_new - T_P0
298         T_P0 = T_P0_new
299         it += 1
300         if it == it_max:
301             print('Max iteration reached, no convergence! <Upstream Prop.>')
302             return [np.nan, np.nan, np.nan, np.nan, np.nan, np.nan, np.nan]
303
304     x_P0 = indx*dx
305     u_conf = confinement_velocity(H, h_P0, rho_P0, rho_0, u_P0)
306     return [x_P0, h_P0, rho_P0, T_P0, u_P0, Q_loss, u_conf]
307
308
309 def upstream_flow(W, H, T_0, T_pl, u_0, m_up, L_up):
310     """ Returns the upstream flow properties: back-layering length, profile of
311 the height, density, temperature, and velocity. SI units are used, except
312 for heat rates (kW)."""
313
314     #1) Boundary conditions
315     T_w, rho_0, rho_pl = T_0, density(T_0), density(T_pl)

```

```

316 u_pl = smoke_velocity(H, rho_0, rho_pl)
317 h_pl = H - m_up/(rho_pl*W*u_pl)
318 Flow_up = [['x', 'h', 'rho', 'T', 'u', 'Q_loss', 'u_conf'],
319            [0, h_pl, rho_pl, T_pl, u_pl, 0, 0]]
320
321 #2) Check if back-layering occurs
322 u_conf = confinement_velocity(H, h_pl, rho_pl, rho_0, u_pl)
323 if u_0 > u_conf:
324     return 0, Flow_up
325
326 #3) Loop set-up
327 dx = 0.1
328 indx = 0
329
330 #4) Loop
331 while indx*dx > -L_up:
332     indx -= 1
333     T_E0 = Flow_up[-1][3]
334     Flow_up.append(upstream_properties(H, W, dx, T_E0, T_w, T_0,
335                                     u_0, m_up, indx))
336
337     u_conf = Flow_up[-1][-1]
338     if u_0 > u_conf:
339         break
340
341 #5) Back-Layering Length
342 L_b = -indx*dx
343 return L_b, Flow_up
344
345
346 #####
347 """ DOWNSTREAM FLOW """
348 #####
349
350
351 def downstream_properties(H, W, dx, T_W0, T_w, T_0, u_0, m_down, indx):
352     """ Returns the flow properties of the next cell upstream as a result of
353     the heat (and mass) balance of the hot smoke layer downstream flow in
354     steady-state conditions. An upwind scheme is employed (T_E0 = T_P0, T_W0 =
355     T_W1). SI units are used, except for heat rates (kW). """
356
357     # First guess
358     T_P0 = T_W0
359     rho_0, rho_P0 = density(T_0), density(T_P0)
360     u_P0 = smoke_velocity(H, rho_0, rho_P0)
361     h_P0 = H - m_down/(rho_P0*W*u_P0)
362
363     # Loop set-up
364     tol = 1E-3
365     step = tol+1
366     it = 0
367     it_max = 1E2
368

```

```

369 # Loop
370 while abs(step) > tol and it < it_max:
371     rho_P0 = density(T_P0)
372     u_min = u_0*(rho_0*H)/(rho_0*h_P0+rho_P0*(H-h_P0))
373     u_P0 = max(smoke_velocity(H, rho_0, rho_P0), u_min)
374     h_P0 = H - m_down/(rho_P0*W*u_P0)
375     T_P0_new, Q_loss = next_temperature(H, W, dx, h_P0, T_P0, T_W0, T_w,
376                                     u_0, u_P0, m_down)
377     step = T_P0_new - T_P0
378     T_P0 = T_P0_new
379     it += 1
380     if it == it_max:
381         print('Max iteration reached, no convergence! <Downstream Prop.>')
382         return np.nan, np.nan, np.nan, np.nan, np.nan, np.nan
383
384     x_P0 = indx*dx
385     return [x_P0, h_P0, rho_P0, T_P0, u_P0, Q_loss]
386
387
388 def downstream_flow(W, H, T_0, T_pl, u_0, m_down, L_down):
389     """ Returns the downstream flow properties: profile of the height, density,
390     temperature and velocity. SI units are used, except for heat rates (kW). """
391
392     #1) Boundary conditions
393     T_w, rho_0, rho_pl = T_0, density(T_0), density(T_pl)
394     u_pl = smoke_velocity(H, rho_0, rho_pl)
395     h_pl = H - m_down/(rho_pl*W*u_pl)
396     Flow_down = [['x', 'h', 'rho', 'T', 'u', 'Q_loss'],
397                 [0, h_pl, rho_pl, T_pl, u_pl, 0]]
398
399     #2) Loop set-up
400     dx = 0.1
401     indx = 0
402
403     #3) Loop
404     while indx*dx < L_down:
405         indx += 1
406         T_W0 = Flow_down[-1][3]
407         Flow_down.append(downstream_properties(H, W, dx, T_W0, T_w, T_0,
408                                             u_0, m_down, indx))
409
410     return Flow_down
411
412
413 #####
414 """ RESULTS AND CURVES """
415 #####
416
417 def critical_velocities_curve():
418     """ Returns the critical velocities of EX1 for different heat release
419     rates. SI units are used, except for heat (kJ or kW). """
420     T_0 = 273.15+15
421     Xc, h_f = 0.75, 1

```

```

422     H, W = 6, 12
423
424     hist = [['Q', 'u_cr', 'delta_T', 'h_pl', 'm_pl']]
425     for Q in np.arange(1, 81, 1):
426         Q *= 1000
427         b_f = (Q/1/np.pi)**0.5
428         u_cr, delta_T, h_pl, m_pl = critical_velocity(H, W, h_f, T_0, Q, Xc, b_f)
429         print('Q: ', "{:4.0f}".format(Q/1000), 'MW -> Crit. velocity: ',
430               "{:4.1f}".format(u_cr), 'm/s, with Tmax-T0 equal to: ',
431               "{:4.0f}".format(delta_T), 'K.')
432         hist.append([Q, u_cr, delta_T, h_pl, m_pl])
433
434     with open('Critical_velocity.csv', 'w', newline='') as csvfile:
435         writer = csv.writer(csvfile)
436         writer.writerows(hist)
437     return
438
439
440 def back_layering_length_curve():
441     """ Returns the back-layering length of EX1 for different ventilation
442     velocities. SI units are used, except for heat (kJ or kW). """
443     T_0, T_w = 273.15+15, 273.15+15
444     H, W = 6, 12
445     Q, Xc, h_f, b_f = 5000, 0.75, 1, (5/np.pi)**0.5
446
447     hist = [['u_0', 'm_pl', 'm_up', 'T_pl', 'T_fr', 'u_fr', 'h_fr', 'L_b']]
448     for u_0 in np.arange(0.05, 4, 0.05):
449         h_pl, rho_pl, T_pl, u_pl, m_pl = plume(H, W, h_f, T_0, Q, Xc, b_f, u_0)
450         m_up = 0.5 * 0.3735 * (Q*Xc) ** (1 / 3) * (h_pl-h_f) ** (5 / 3) * 0.19
451         L_b, Flow_up = upstream_flow(W, H, T_w, T_pl, u_0, m_up, 5000)
452         [, h_fr, rho_fr, T_fr, u_fr, _, _] = Flow_up[-1]
453         print('u_0: ', "{:4.2f}".format(u_0), 'm/s -> Back layer length: ',
454               "{:4.1f}".format(L_b), 'm.')
455         hist.append([u_0, m_pl, m_up, T_pl, T_fr, u_fr, h_fr, L_b])
456         if L_b == 0: break
457
458     with open('Back_layer.csv', 'w', newline='') as csvfile:
459         writer = csv.writer(csvfile)
460         writer.writerows(hist)
461     return
462
463
464 def flow_property_profiles():
465     """ Returns the flow property profiles of EX1. SI units are used, except
466     for heat (kJ or kW). """
467     T_0, T_w, rho_0 = 273.15+15, 273.15+15, density(273.15+15)
468     H, W = 6, 12
469     Q, Xc, h_f, b_f = 5000, 0.75, 1, (5/np.pi)**0.5
470     u_0 = 1.5
471     L_up = 5000 # maximum distance for the back-layering flow [m]
472     L_down = 400 # distance for which the downstream profile is calculated [m]
473
474     h_pl, rho_pl, T_pl, u_pl, m_pl = plume(H, W, h_f, T_0, Q, Xc, b_f, u_0)

```

```
475 u_conf = confinement_velocity(H, h_pl, rho_pl, rho_0, u_pl)
476 m_up = 0.5 * 0.3735 * (Q*Xc) ** (1 / 3) * (h_pl-h_f) ** (5 / 3) * 0.19
477 m_down = m_pl if u_0 > u_conf else m_pl - m_up
478 L_b, Flow_up = upstream_flow(W, H, T_w, T_pl, u_0, m_up, L_up)
479 Flow_down = downstream_flow(W, H, T_0, T_pl, u_0, m_down, L_down)
480
481 with open('Flow_upstream.csv', 'w', newline='') as csvfile:
482     writer = csv.writer(csvfile)
483     writer.writerows(Flow_up)
484
485 with open('Flow_downstream.csv', 'w', newline='') as csvfile:
486     writer = csv.writer(csvfile)
487     writer.writerows(Flow_down)
488 return
```